UNIVERSITAT DE BARCELONA

Control of integrin-mediated mechanoresponse by binding partners and force loading rates

Víctor González Tarragó

Tesi doctoral

Control of integrin-mediated mechanoresponse by binding partners and force loading rates

Memòria per optar al grau de Doctor en el
Programa de Doctorat en Biomedicina

Barcelona, Juliol de 2019

Presentada per Víctor González Tarragó

Dirigida per Dr. Pere Roca-Cusachs Soulere

A tots els que m’heu acompanyat
Els últims 6 anys, 9 mesos, i 11 dies

“Consider fully, act decisively”

Jigoro Kano

Agraïments

Al llarg de la meva estada al laboratori hi han hagut moments molt bons, i moments molt dolents. La tesi ha sigut com una muntanya russa. Gràcies a totes les persones que han estat al meu costat he pogut per una banda disfrutar dels bons moments, i per altra banda superar els dolents. És per això que voldria donar les gràcies a totes les persones que heu compartit aquesta etapa de la meva vida amb mi.

Gràcies Pere, per haver-me donat l'oportunitat de treballar al laboratori, pel problema que no es sabia resoldre a primer, *challenge accepted*, per les tres reunions on et vaig dir que no abans de les pràctiques de grau, per la conversa a l'autobús a Donosti, per acceptar la meva irreverència d'entrar al teu despatx en qualsevol moment, per estar sempre al meu costat, per les converses sobre la vida en general, per l'empenta que m'has donat, gràcies.

Voldria també donar les gràcies al Xavi, per mi has sigut el meu segon group leader, gràcies per donar-me *bon courage*. Gràcies Daniel, perquè has sigut la meva referència des que vaig començar el grau, i Ramon, perquè has sigut la part implacable, no se t'escapa ni una! Moltes gràcies Domènec, et vaig conèixer a tercer i no només em vas mostrar el que és l'estadística sinó que has sigut des de llavors una font de suport molt important.

M'agradaria agraïr també el suport del Jordi Alcaraz, per estar tan segur que podria aconseguir la tesi. Muchas gracias Miguel Ángel. Has hecho posible lo imposible, has diseñado y contruido una ingente cantidad de instrumentos y software para nuestros proyectos, siempre me acordaré de cuando reparamos el sistema de stretch en la India desde tu taller... ¡qué odisea!

Timo, thanks for having me in Münster, and for fixing the optical tweezers in the mornings. And for giving that push to the project when it was so much needed.

Elsa y Alberto, me lo habéis enseñado todo. Tuve el privilegio y el honor de ser vuestro estudiante y sin vosotros no hubiera podido continuar. Me habéis mostrado que la disciplina lo vence todo, que una poyata llena de stainings, y mil máscaras de segmentación de collective cell migration no son razón para desistir. Roger, TUKI! Ets per mi un exemple de superació diària, gràcies. Anita, moltes gràcies per tots els moments de troubleshooting i de no caure en la

desesperació.
The old guard of the lab, Romaric, because there are other important things in life such as climbing. Andrea, thanks for all those discussions with and about pizza. Simon, you showed me that we must go where our heart tells us. Laura, me mostraste que la vida sigue después del phd, Agustí, que no ens hem de rendir mai! Marina, hem compratit un forn a dues temperatures, no tothom pot dir això, gràcies. Dobryna, gracias por todas las conversaciones acerca de microscopía, al final... terminaré instalando estos sistemas, las vueltas que da la vida. Raimon, m'has mostrat que es pot fer PDMS magnètic amb tòner d'impersora, hi ha recursos a tot arreu! Anna, you never truly know someone until you fight, and we fought, even scoring Ippon to me, thanks for sharing judo with me. Jeroen, you showed me that we will persevere, no matter what happens, and Michel, I still remember that day at the lab playing Plague Inc, who wanted to release a lethal virus? Mark, thanks for showing me all the possible outcomes of everything, because we will succeed, maby yes... or maby not haha. Katie, thanks for joining the judo classes, and showing me that you can travel to another country and survive, with limited resources, even if I am not a northener like you. Carlos, mi compañero de viaje, ¡qué decir! El laboratorio, Boston, Nueva York, he compartido contigo toda mi vida en el laboratorio. Vas a ser un gran científico. El día que te den el Nobel, acuérdate de mi. Gracias por estar a mi lado siempre. Existen pocas personas tan maduras como tú, gracias.
Gràcies a les noves generacions del laboratori. Ariadna, que el laboratori no és més que una abstracció del ricochet robot. Ernest, a tirar pel dret, la cadira i tot! Manu, no sé que habríamos hecho sin ti en el laboratorio, eres el rey del Matlab. Laura, thanks for all the conversations about life. Anabel-Lise, todo el sistema de stretch en aluminio es obra tuya, esta tesis nuna habría visto la luz sin tí. Jenny, we will always have tsipouro! Sefora, thanks for helping me relativize the problems, Giordano, you are a much better battlefield teamplayer than me. Juanfra, tienes la mejor libreta de laboratorio de todos, eres increíble, gracias por las conversaciones que hemos tenido. Natalia, gracias por todo el soporte que nos has ofrecido a todos, por todo el peso que recae en tus hombros. Marilena, we shared very nice conversations. I don't know where you are now, but I am sure you will succeed. Macià, cada vegada contractem millors estudiants, segueix així! Sri, I am just an antlavedava, have I written that correctly? Probably

not. Marina Pavlova, you are an example of perseverance. Marija, I don't know you a lot, but so far, I have the impression that we could become good friends, thanks for cheering me up that day at the cafeteria. Nacho, apenas hace dos semanas que nos conocemos, pero vas a ser instrumental en el laboratorio, eres un tío excelente. Captain Tom Didom, recently Dr, du bist mein bester deutscher wissenschaftler freund. Dimitri, la garde meurt, mais ne se rend pas! Malèke, although we haven't shared a lot of time together, it was very nice to have those Islamic discussions. Amy, thanks for all the cheering up since the Edinburgh conference. You are such a good experimentalist, you are incredible. Gerardo, hemos interactuado poco, cierto, pero gracias por aguantarme cuando te he pinchado en el laboratorio. Marc, el primer del pelotón de ciclistes, quin treball en equip! Cada vegada que ho penso, el teu nivell està a anys llum del meu quan vaig començar. Segueix així! Ignasi, ets una màquina, el cell profiler és el futur. I has picat tu tots els scripts, gràcies també per la xocolata i les galetes.

Thanks to all the people in Münster, Jade, Basilio, Phillip, Karolin, and Timo (again), Ina, Alfred, Arne, Matthias, Sebastian, Till, Swetha, Bernhard, Bart, Ce, Sophie, who is Sophie?, Sadhna, Amrita, Zahara, Sargo, Esther, Fabian, Paul, Kim, Anto, Gaby and Isabel.

Nimesh, ab ki baar, Nimesh sarkaar, you analyzed all the optical tweezers data, all the afm data, and sped up my project by at least two years. I owe you one, my communist friend. All our conversations about politics, science, and philosophy. Thanks man. Leone, the physicist, you made me realize the reality, you kept me down to earth when I needed it, thanks for all the philosophical conversations. Ion, el primer día que te conocí me di cuenta que ése podría ser el inicio de una gran amistad. Hemos compartido muchas cosas. Has hecho experimentos para mi proyecto, que yo nunca podría haber realizado. Eres parte de esta tesis. Es difícil para mí encontrar un referente como persona mejor que tú. Incluso me has aguantado cuando te he enchufado el pollo del diskstation. Has sido como mi hermano mayor. Muchas gracias por todo. Xarxa, gracias por estar a mi lado, literalmente, durante la tesis. Por tener las etiquetas de estrella galicia enganchadas en la pared, y por pelearte conmigo por el espacio entre nuestros escritorios. Por todas las *cerves*, y por hacer el troubleshooting de la caja de stretch, de las membranas, por las discusiones sobre el graphpad, y sobre future careers. Por robarme la silla, y por las galletas de trigo inflado. Gracias por ser

la más riquiña.
M'agradaria especialment donar les gràcies a la meva família. M'ho han donat tot, han fet tot i més perquè jo tingués la possibilitat de ser aquí. M'heu donat tot l'amor que teniu i per a mi això ha sigut el més important. Vull donar-te les gràcies a tú, Sílvia, he tingut la sort més gran del món de conèixer-te, gràcies per recolzar-me i donar-me suport en els pitjors moments.
Gràcies a tots els meus amics, especialment al Jordi Peris, que m'està acompanyant ja des de fa 15 anys, i que m'has apoyat sempre, sempre, passés el que passés. Gracias Carlos, por tocar conmigo en el grupo y por todas esas partidas de Bang! Juan, ¡por el fantástico skate! (lo tengo yo, ¿o lo tienes tú?) A ti Joselu, siempre te recordaré, Brescó, que siempre presumo de tener un amigo que tiene una fábrica de chocolate! Muchas gracias a los Sons, Carlos, Héctor, Álvaro y Jona, por vuestro apoyo que siempre me habéis dado sin ningún ápice de duda. També al Dani, el Fran, la Laura Clua, el Pau Viladomiu, el Pau Calderó, l'Àlex Badia, i tots els companys que han seguit al meu costat després de la carrera. Gracias a Fox, Aníbal, Mike, Luna, Cetus, Jaag, Augusto, y todos los compañeros que tantas conversaciones habéis compartido conmigo en discord. Gracias a todos los compañeros de Judo, y especialmente Alberto, que has sido mi mentor, y Nico, mi compañero en esta aventura judoka.

Estic segur que m'he deixat persones, però seria impossible de recordar-les totes, agraeixo a tothom que ha interactuat amb mi aquests anys, aquesta tesi és de tots.

Contents

Preface

It looks to me that life is driven by chance.
I ended up in the laboratory by chance. The sensation that I have is that in this game we only decide the colour of the dice. And the number of times we roll them. Living systems can't determine absolute values.
What now seems a long time ago I was attending a talk by Pere. He posed the following question: How do cells sense rigidity? This prompted me to expand this question globally. So, how do living systems sense? Cells can't determine the absolute temperature of the media. They do not have a reference spot at 273 K. In a similar manner, cells can't determine the stiffness of the extracellular matrix. They do not have a reference spot at 100 Pa. So then, what do they sense? The general objective of this thesis has been to try to increase our knowledge about this topic.

This thesis is the result of 3 and a half years of research at the Institute for Bioengineering of Catalonia. The work is divided in five chapters. In the first chapter, I introduce what mechanobiology is, and what are the molecular components of mechanotransduction pathways. In the second chapter, I set the aims of the thesis: to study the mechanical response of integrin-mediated cell adhesions, in response to both integrin binding partners and force loading rates. In the third chapter, I describe the setups that I used in the laboratory to execute experiments. In the fourth chapter, I delve into the research about ZO-1 binding to integrins, and the mechanical implications of this phenomena. The results obtained in this study were published in Molecular Biology of the Cell (1). In the fifth chapter, I delve into the response of cells to force loading rates, and the implications of this response. The results obtained in this study are currently submitted to a scientific journal. In the sixth chapter I expose the conclusions of the thesis. In the appendix, I discuss about the funding, and other topics not covered in the main chapters of the thesis.

Chapter 1. Introduction

1.1 Cellular mechanobiology

Mechanobiology can be described as the field of science that studies how cells exert forces and how do they respond to the application of these forces (2). It has now become clear that the response of cells to forces is fundamental in multiple processes, including tumour progression and metastasis (3). As an example, the model to study tumour microenvironment has rapidly moved from a purely biochemical based approach to a global approach, including both biochemistry and mechanobiology (3, 4) (Figure 1).

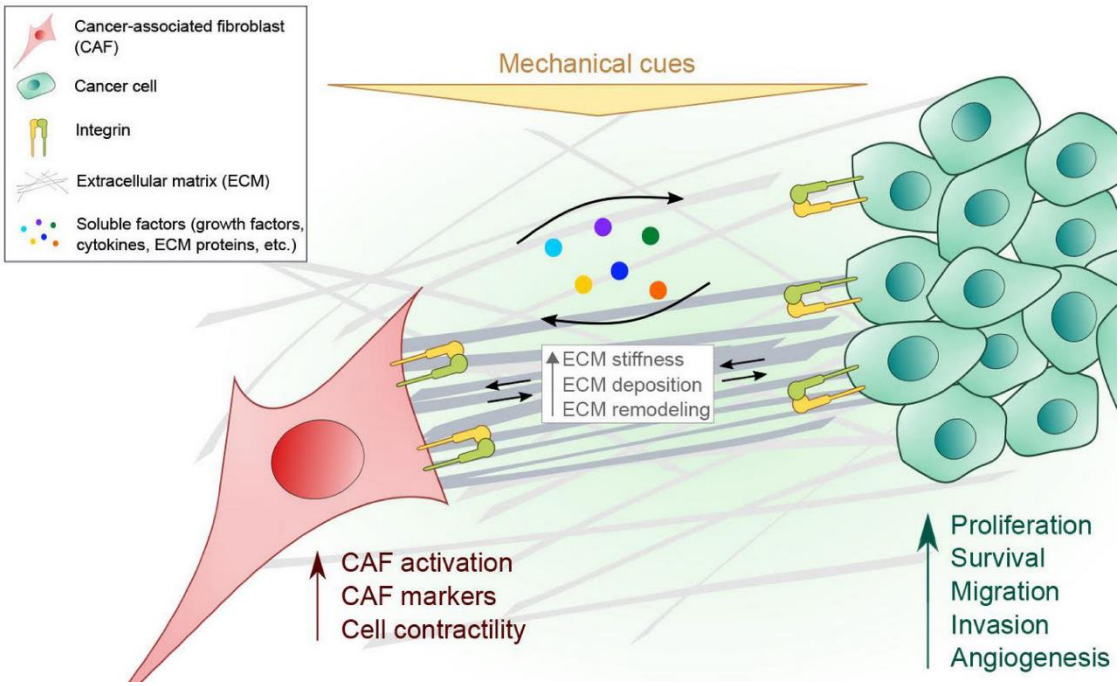

Figure 1: Current model for the tumour microenvironment.

The current tumour model has shifted from a purely biochemical response to a combined mechanical and biochemical environment. Cancer-associated fibroblasts and cancer cells sense mechanical cues such as substrate rigidity, hydrostatic pressure, compressive or shear stress present in the tumour microenvironment. Adapted from the literature (4).

During the development of this thesis, I have tried to understand different aspects of the process of mechanotransduction, by which cells convert a mechanical stimulus into a biochemical signal (5). In order to do this, cells need a mechanical transducer, a transmission element, and a system that effectively affects a biochemical signalling cascade (5). To explain this seemingly complicated mechanism, I will first describe its components, and then pose different cell processes that make use of it.

1.1.1 The cytoskeleton

The cytoskeleton (CSK) is a dynamic meshwork of fibres that stabilizes the cell and binds the nucleus to the plasma membrane (6). It gives mechanical stability and resistance to the cell, and is used both to transmit and to sustain forces (7). Its functions encompass a broad range of actions, including a crucial role in cell division (6, 8, 9), endocytosis (10), and conferring the cell with the ability to move (6, 7). The meshwork is primarily composed of three different kinds of filamentous proteins: intermediate filaments, microtubules, and actin (6, 7). Each of the filaments has a family of adaptor and binding proteins, which modify their properties (7). This makes the structure very complicated in nature. It can contract (11), has components that are under tension (7), and compression (12), and shows a complex viscoelastic response (13).

Microtubules

Microtubules are filamentous cylindrical polymers. These cylinders are rather small, being only around 25-51 nm in diameter (14). However, they can reach impressive lengths such as 175 µm (15). They consist of α-tubulin and β-tubulin (6, 16) also known as subunits. First, the two subunits polymerize in a linear way, which then binds to a previously polymerized subunit side by side, generating the cylinder with a total of 13 fibres (6). Depending on what subunit of tubulin is exposed, the cylinder can have two distinct ends (6). The growth of the microtubule occurs in a polarized manner, since the end containing exposed β-tubulin polymerizes at a higher speed (6, 17), reaching 20 µm/s (18). This

polymerization is highly dynamic, as microtubules can rapidly undergo disassembly and reassembly, in a process known as dynamic instability (6, 19). The rate is modified by several stabilizing or destabilizing proteins that bind to the structure known as Microtubule-associated proteins (MAPs) (6, 20). The rate is also modified by post-translational modifications of the C-terminal region of the α-tubulin (21).

Microtubules are generated from microtubule organizing centres (MTOCs), structures that contain a third type of tubulin, γ-tubulin (22, 23). They nucleate from this point and extend to the edges of the cell. This guidance is used by the cell to transport vesicles by using the microtubule motor proteins kinesin and dynein (24). Microtubules are also crucial for a successful mitosis (25) and form the motile structures that contain flagella (26). In general, microtubules are under compression, and show buckling even when they are one of the most rigid structures of the cell (27). It is therefore understood that microtubules contribute to the mechanical stability of the cell by sustaining tension, but they also push both the nucleus and the plasma membrane at their edges (6, 27).

Intermediate filaments

Intermediate filaments (IFs) are filamentous proteins that crosslink themselves, with microtubules, and also with actin filaments (28). They are a group of apparently different proteins that share a similar diameter of around 10 nm and similar heterogeneous function (6). While there is a seemingly long list of intermediate filament proteins (6, 29, 30), the most important components of this family are, keratin, vimentin, lamins A and C, and desmin (28, 30).

Keratins are expressed mainly in epithelial cells as 28 type I and 26 type II keratins. These units heterodimerize and form filaments that provide structural support. Interestingly, the exact keratins expressed per cell type are different, and this allows classification of epithelial cell subtypes (31, 32). Vimentin, on the contrary, is expressed both in epithelial and mesenchymal cells such as fibroblasts. This IF protein has been found to be implicated in cell adhesion and migration, but its complete function remains still not fully understood (31, 33).

Lamins A and C bind to the SUN complex and to other IFs, and are therefore fundamental in the mechanism described above regarding the anchoring of the nucleus to the CSK (34). The knockdown of lamins affects directly the stiffness of the nucleus, and are the cause of dangerous diseases such as the Emery-Dreifuss muscular dystrophy (35). Desmin is formed by three regions: a central coiled coil, a tail, and a head domain. This IF is fundamental for muscle cytoskeletal structure, and its mutations are implicated in severe muscle-based diseases. However, the exact role of the filaments is not currently known, apart from its known myofibril interlinking function (36). This is quite intriguing, because desmin knockout mice are viable and fertile, but they develop muscle wasting disease (36).

Actin

Actin is one of the most, if not the single most, abundant protein in the majority of eukaryotic cells (37), and has the most number of binding partners of any other protein known to us (37). It exists as a monomer known as G-actin and as a filament, known as F-actin (37, 38). This categorization is a simplification. To start, there are three isoforms, α,β, and γ isoforms (39). On top of this, it can be modified post-transciptionally. In fact, G-actin has been found in at least 80 different structures (37).

G-actin can transition to F-actin, a process that can be mediated (both inhibited and promoted) by a myriad of proteins (6, 37). This process is known as actin fibre nucleation (Figure 2) (40, 41).

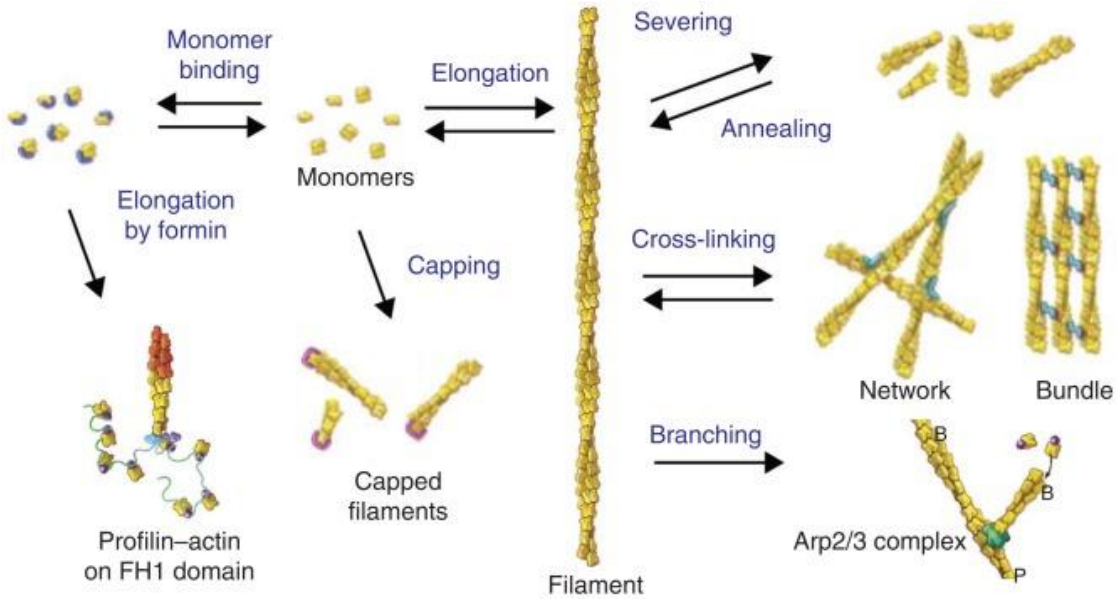

Figure 2 : Illustration of the actin fibre nucleation process.

Actin can be capped and stabilized. It can also be elongated by formin, forming F-actin. These fibers can then branch, cross-link, or break. Adapted from the literature (41).

The reaction for actin nucleation needs to overcome the intrinsic instability of the actin dimer, and the action of the G-actin binding proteins (42) that inhibit it. This is done by other binding proteins known as actin nucleators (43). There are three main groups of these proteins, Arp 2/3, formins, and tandem actin-binding domain nucleators (43, 44).

Once formed, F-actin filaments are made of two polarized polymer chains that turn right-handedly in a helix fashion (Figure 2) (41, 45, 46). Together with the molecular motor protein myosin and other adaptor proteins (47) form the so called stress fibres. Stress fibres bear and transmit forces within the cell and to other structures (6, 47). Myosin continuously pulls on actin fibres from the edge of the cell to the nucleus in a process known as the rearward flow (48), which can generate net force and propel the cell, allowing it to move (49).

One edge of the actin fibres binds to the nucleus through the Linker of Nucleoskeleton and Cytoskeleton (LINC) complex (50–52). Considering that this is again a simplification, the other edge of actin fibres can be bound to other cells

in cell-cell adhesions known as adherens junctions, or to the extracellular matrix (ECM) via cell-ECM adhesions (Figure 3) (53). Both structures involve actin regulatory and linking proteins, as well as transmembrane proteins that subsequently bind to their extracellular ligands (53).

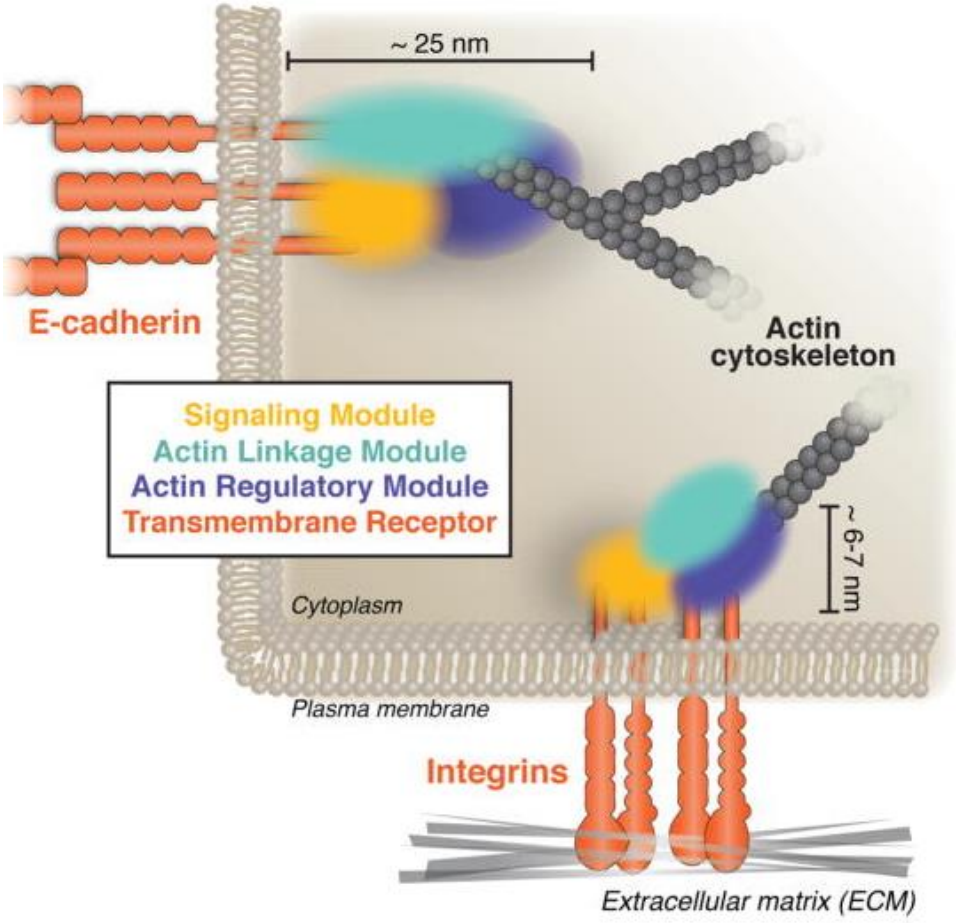

Figure 3: Actin based adhesions to other cells and to the ECM.
Actin is present both in cell-ECM adhesions and in cell-cell adhesions. Adapted from the literature (53).

Finally, it has recently become apparent that both G-actin and F-actin are also present inside of the nucleus, and not only in the cytoplasm as one thought (54). Actin seems to regulate multiple processes spanning from transcription regulation to DNA repair (55).

1.1.2 The plasma membrane

The plasma membrane is the structure that separates the inner part of the cell, the cytoplasm, from the outside. It is formed primarily by phospholipids and proteins. It also contains carbohydrates and other molecules, and can sustain an extracellular sugary structure known as the glycocalyx (56). The lipids have an hydrophobic side and a hydrophytic side, giving rise to a double structure, a lipid bilayer (6). Proteins can anchor at the inside of the membrane, at the outside, or trespass it throughout. The current model that describes this interaction is known as the Fluid Mosaic Model, where proteins and lipids can diffuse along the membrane (Figure 4) (56, 57).

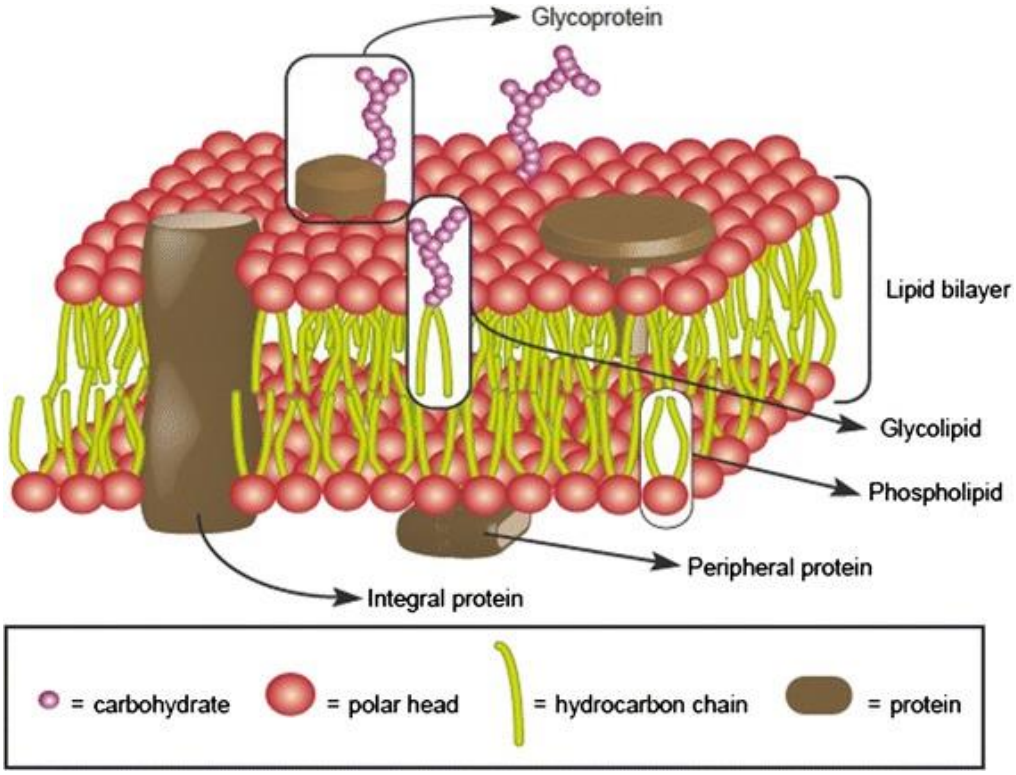

Figure 4: Fluid mosaic model of the plasma membrane.
The plasma membrane is formed by a lipid bilayer. The structure can contain transmembrane proteins, proteins attached to the inner part, or to the outer part. It is also formed by glycoproteins and glycolipids. Adapted from the literature (56).

The membrane also contains ion channels that are sensitive to forces (58), but their study is not part of this thesis.

Of importance, the plasma membrane is where cell-cell and cell-ECM adhesions are located. These adhesions bind the cell to the ECM, and are part of the system that cells use to sense the rigidity of the ECM (59). The plasma membrane also contains mechanosensitive ion channels. These channels mediate calcium ion influx or maintain the electrochemical gradient necessary for it (60). However, I am not going to discuss about them since they were out of the scope of this thesis.

1.1.3 The extracellular matrix (ECM)

The extracellular matrix is a meshwork of proteins and macromolecules that surrounds cells. This structure provides physical support, biochemical, and mechanical guidance to cells (6, 29, 61). Although the extracellular matrix contains up to 300 different types of molecules (62), there are five major components: proteoglycans, elastin, laminin, collagen, and fibronectin (Figure 5) (6, 63).

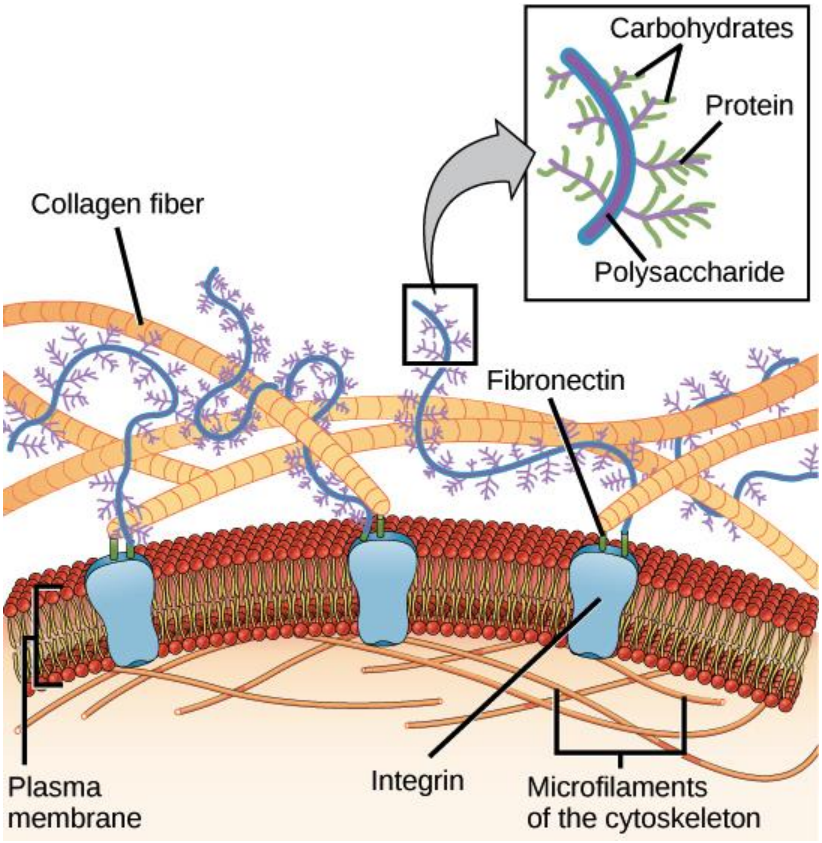

Figure 5: Components of the extracellular matrix.

The extracellular matrix is composed by a meshwork of proteins. This collection

of molecules include proteoglycans, elastin, laminin, collagen, and fibronectin. Adapted from the literature (63).

Proteogylcans

Proteogylcans are a mixture of one protein with glycosaminoglycans attached in a branched fashion. These molecules comprise hyaluronic acid and keratan, dermatan, and heparan sulphates. These are hygroscopic and can accumulate a vast amount of water, providing filling (6, 61). Several of them are implicated in cell signalling, and in multiple functions. These can be grouped in two types. One includes outside of the cell functions such as force resistance and fibre polymerization regulation. The other type includes those that interact with growth factors. These can interact not only at the level of the cell membrane, but also be present at the inner part of the cell, such as serglycin. (64, 65).

Elastin

Elastin is an hydrophobic protein complex made of tropoelastin monomers, fibulins, and microfibrils. These protein complex forms elastic fibres. The main function of this fibres is purely to sustain structure stretch. As such, it is predominant in tissues that are stressed, specially cyclically, such as the heart, the lungs, and arteries. Elastin in hydrophobic and is crosslinked to other molecules in the ECM (64, 66).

Laminin

Laminins are very heavy heterodimers, of around 600 kDa. Different combinations of three subunits, α, β, and γ yield different structures and weights of laminins. They are present in basement membranes, and crosslink to collagen IV. Laminins can also form their own crosslinked network. These are typically found in the separation of different structures in tissues (64, 67).

Collagen

Collagen is made of a triple helix structure formed by three peptide repeats. These chains can have multiple stable combinations, which in the end yield a total of 28 known collagen types (6, 68). Of all of them, the most studied in our

field is collagen IV, since it is part of the basement membrane and generates networks, not only single fibres. This network is polymerized by lysyl oxidase, a type of enzyme that can be segregated onto the ECM. Other enzymes that affect different ECM molecules can also be segregated by the cells to remodel their environment (6, 29, 64, 68).

Fibronectin

Fibronectin (FN) is the main ECM protein involved in the signalling and migration of the cell. It is formed by subunit modules of repeats numbered I, II, and III that create a 250 kDa protein. Fibronectin has multiple binding sites to itself to create multimers. It also has binding sites for collagen, laminin, fibrin, tenascin, among others. Very importantly, in the subunit III, 7-10 repeat, there is an Arg-Gly-Asp binding site that is synergistically affected by another sequence present, Pro-His-Ser-Arg-Asn (69, 70). This is the main binding site for integrins, mechanosensitive transmembrane proteins that are covered in a subsequent section (see section 1.3.2). Of note, fibronectin also contains cryptic binding sites to itself that are exposed upon transmission of tension (71). The importance of fibronectin lies in the fact that it can connect both to integrins at the cell, and to collagen and proteoglycans in the ECM (Figure 6) (72–74). This is why some authors have even called it “the master organizer” (75, 76).

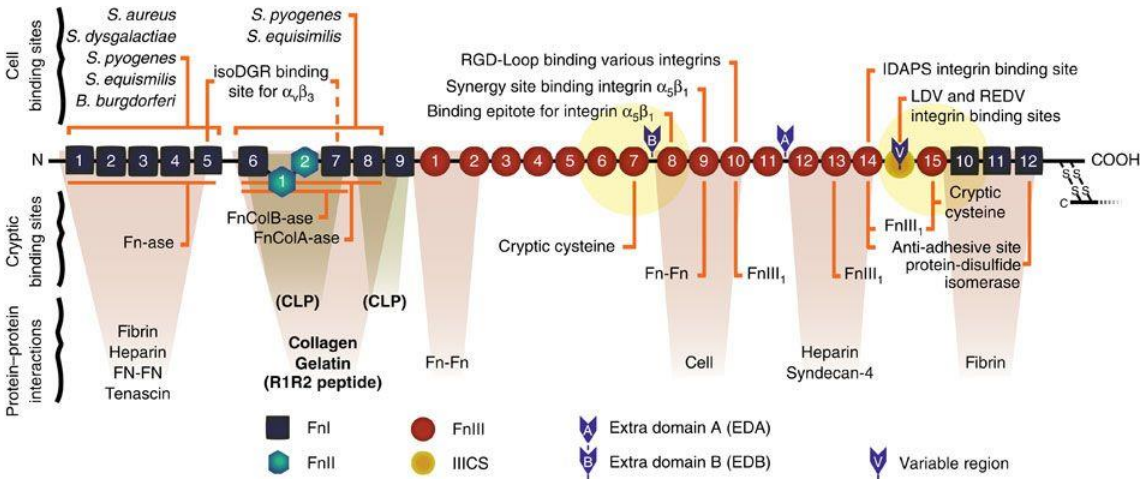

Figure 6:Fibronectin binding sites.

Fibronectin can bind to ECM collagen, other fibronectins, heparin, and fibrin,

among others. It can also bind to the cell through interactions with integrins. Upon application of force, cryptic sites can be unfolded. Adapted from the literature (77).

Functionally, the ECM signals the cells via anchoring, since it provides the homing of the cells. It also signals cells in a tissue dependant manner by allowing the cell to bind to tissue specific receptors. As discussed before, ECM stiffness is integrated as a mechanical signal by the cell. The ECM is also used as a buffer for the presentation of different biochemical growth factors. On top of all these functions, the cell can enzymatically remodel the ECM in response to the stimuli (Figure 7) (64, 78).

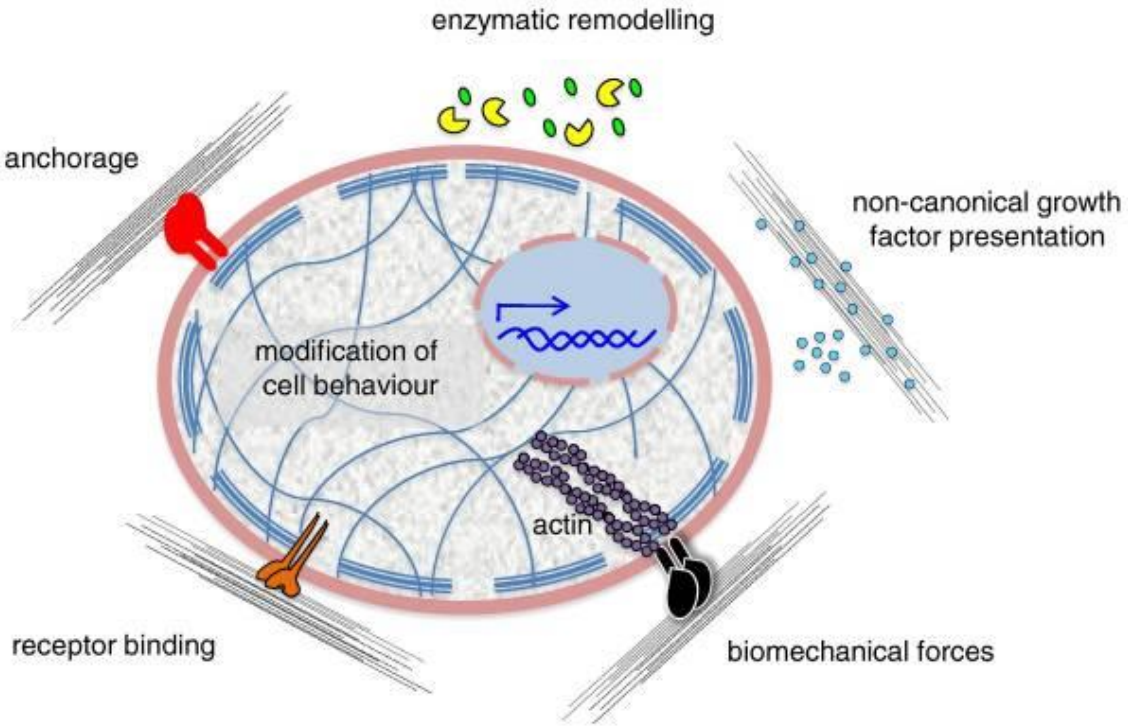

Figure 7. ECM interaction with cells.

The ECM provides anchoring to cells. It also provides tissue-specific receptor binding, and is a buffer of growth factors. The ECM also signals the cells via its rigidity. On top of this, the ECM can be actively remodelled by the cell using enzymes. Adapted from the literature (78)

1.1.4 The nucleus

The nucleus is the cell organelle that contains the genetic information and regulates its expression into proteins (6). It can therefore be thought as the fundamental regulatory centre of the cell. Historically, the regulation of gene expression has been explained purely based on biochemical factors (6). In the recent years, fast paced advances have further characterized the biochemical regulation (79–82). This regulation is fundamentally based on the action of transcription factors (83), proteins that can activate or block (84) the action of RNA polymerase binding onto the deoxyribonucleic acid (DNA). Other proteins that do not bind to DNA but that also regulate gene expression include coactivators, histone deacetylases and methylases, among others (83).

At the same time, mechanical regulation of gene expression is being increasingly more studied (85–89). Three mechanical mechanisms are believed to potentially be affecting gene regulation (90). These are the physical reorganization of chromatin, signalling at the nuclear envelope, and altered cytoskeletal structure due to nuclear remodelling (90). The mechanism that is accumulating more supporting evidence is currently the change in signalling caused by deformations on the nucleus, that then remodel the inner nuclear membrane (90). Of note, the packing of this structure changes the effective availability of transcription factors, and mutations of proteins in this structure cause changes in cell response to force loads (91, 92).

Our current understanding is that increased force application increases the coupling to the CSK in a positive feedback loop that enhances force transmission to the nucleus (90). Via increased deformation of the nuclear pores (93), this nuclear force loading induces import of different transcription factors (93–96) (Figure 8). These transcription factors then alter gene expression (97).

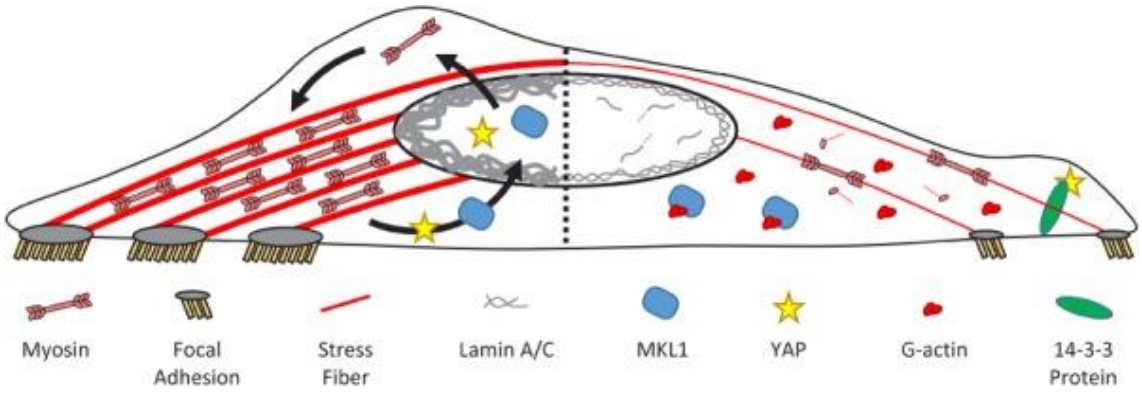

Figure 8: Biophysical stimuli that affect nuclear structure and shape.
Force is transmitted to the nucleus. The nucleus is deformed in response. This is an effective signalling which is then translated into gene regulation. Adapted from the literature (90).

The nuclear membrane is bound externally to the CSK by the LINC protein complex (50–52). This protein complex consists of Sad1 and UNC-88 (SUN), and Klarsicht, ANC-1 and Syne/Nesprin homology (KASH) proteins (98–100). SUN proteins are positioned at the inner part of the nuclear membrane (50), and bind both to lamins (98) and KASH proteins (99). KASH proteins then bind to different CSK proteins (99). The different combinations of SUN-KASH proteins yield the possibility of binding to intermediate filaments, microtubules, and actin (98, 101) (Figure 9). Another protein complex present in the nuclear membrane, the Nuclear Pore Complex (NPC) binds to Dynein (101) (Figure 9).

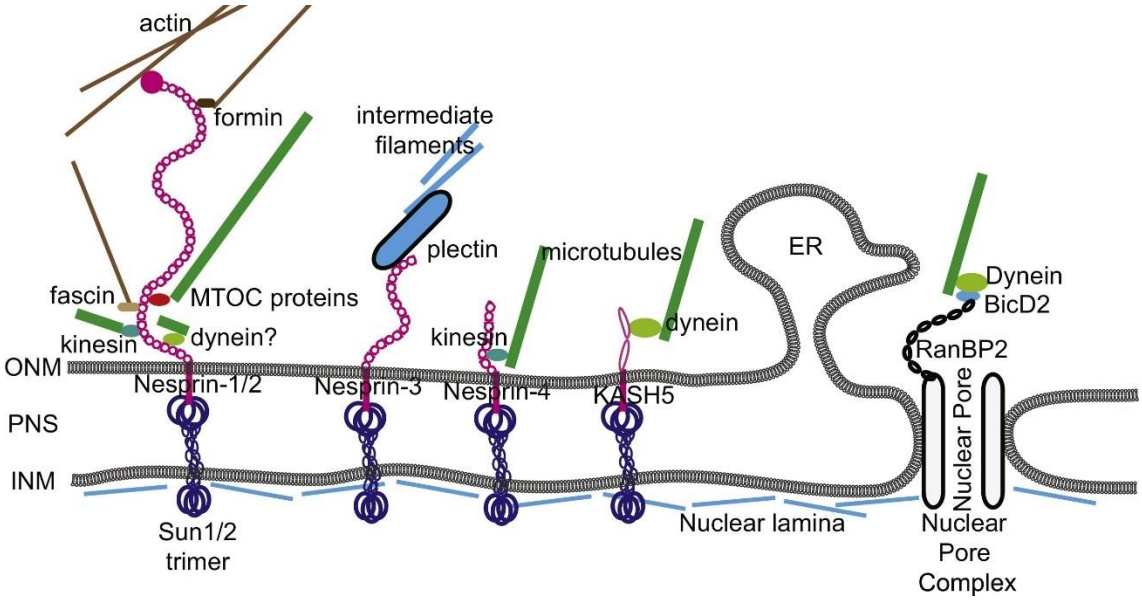

Figure 9: Cytoskeletal proteins that bind to the LINC complex.
Multiple LINC complex proteins bind the nucleous to actin, intermediate filament, and microtubules. The nuclear pore complex can also bind the cytoskeleton via Dynein. Adapted from the literature (101).

Therefore, this structure alone recapitulates two of the three main hypotheses for the mechanical regulation of gene expression that I discussed before. First, the shape of the nucleus and therefore the packing of the nuclear could change because of force application through the LINC complex (98). Second, deformation of the nuclear pores, could forcefully translocate transcription factors inside and outside of the nucleus (93).

While this has been a main area of study recently (93, 102), the mechanism is still not fully understood. It is therefore paramount to find which proteins are part this interaction, and more importantly, which are the protein binding partners that modify this interaction.

1.2 Cell-cell adhesion

Cells are attached to each other by cell-cell adhesions present at the plasma membrane. These structures contain a family of proteins called cell-adhesion molecules (CAMs). CAMs are transmembrane proteins classically categorized in

five functional groups. These protein groups are immunoglobulins, cadherins, selectins and integrins. Immunoglobulins bind to other immunoglobulins as cadherins bind to other cadherins. However, selectins and integrins bind to other ligands. Of importance to this thesis, important types of cell-cell adhesions contain cadherins. Since cadherins are homophilic, they are useful in separating tissues by cell type that express different subtypes of cadherins (6, 29, 41, 103).

Cadherins require calcium ions to generate a union, which needs to be present in the extracellular space. Interestingly, this is where their name comes from (*ca*lcium *d*ependant a*dhe*sion). The cadherin family is characterized by calcium binding domains that are repeated throughout. Historically, cadherins were grouped as classical cadherins and non-classical cadherins depending on their sequence resemblance. This is coincident with the type of functional adhesion where they are present. (6, 104–107)

1.2.1 Desmosomes

Desmosomes link the intermediate filament structure of cells. Desmosomes are prevalent in epithelial sheets and cardiac muscle, among other tissues. The cadherins involved in desmosomes are desmoglein and desmocolin. While these lay on the plasma membrane, they are connected through a layer of adaptor proteins that include desmoplakin, plakoglobin and plakofilin. Plakoglobin and plakofilin also recruit more intermediate filaments to the site of the adhesion forming an aggregate known as the desmosomal plaque (Figure 10) (108, 109).

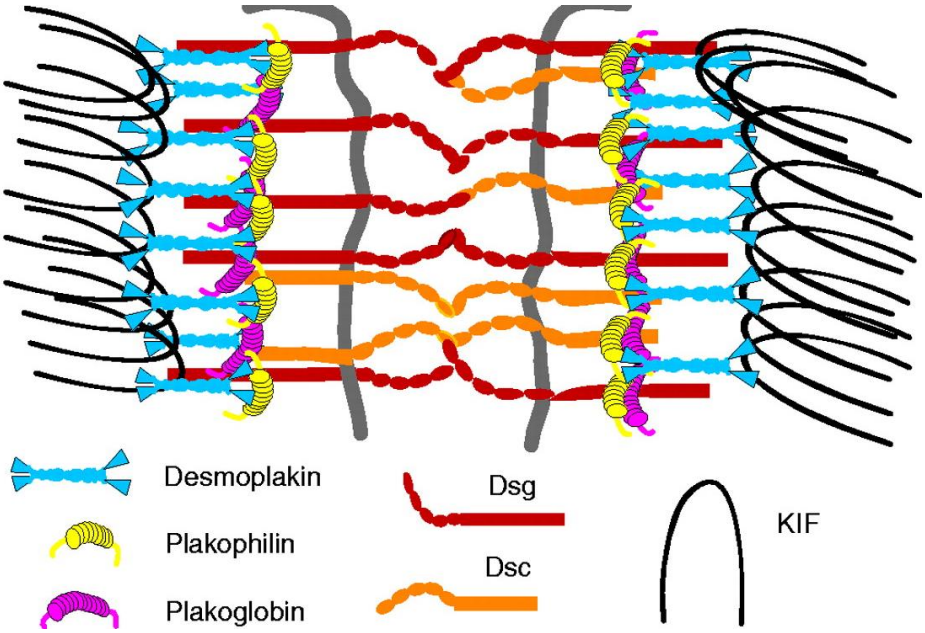

Figure 10: Components of the desmosome.

Desmosomes are formed by desmoglein and desmocolin. Adaptor proteins desmoplakin, plakophilin and plakoglobin bind desmoglein and desmocolin to intermediate filaments. KIF stands for Keratin, component of intermediate filaments. Adapted from the literature (109).

While desmosomes provide mainly anchoring, this is fundamental in health and disease. Autoantibodies against desmogleins are the cause of the Pemphigus, a disease that affects skin causing its destruction by lack of adhesion (110). Desmosomes are also fundamental during development. By differential expression of desmosome cadherins, tissues are organized and segmented. Failure to do so for different reasons can yield to an aberrant development (111, 112). Curiously, these aberrant behaviours can even include hair loss, highlighting the role of desmosomes in the generation of classical biological structures (113).

1.2.2 Adherens junctions

Adherens junctions link the actin cytoskeleton of cells and are formed by the classical cadherins, including e-cadherin and n-cadherin. Cadherins are bound extracellularly to other cadherins and bind intracellularly to catenins. This protein

family includes p120, α-catenin and β-catenin. While p120 and β-catenin bind directly to e-cadherin, it is β-catenin that bind to α-catenin, forming the so-called cadherin-catenin complex (Figure 11) (114–118). This complex contains vinculin, which also accumulates in another type of structure that will be further discussed in detail in a subsequent section (see section 1.3.3) (119). Vinculin binds to actin through a binding site that is exposed under application of force, making its recruitment force-dependant (120). While inhibition of vinculin allows minor punctate adherens junctions to form, in this condition mature adherens junctions fail to form completely (121). Interestingly, other proteins that do not belong to adherens junctions' mature structure are present in punctate adherens junctions. These strikingly include ZO-1 and ZO-2, proteins that belong to mature tight junctions (122). During tight junction formation, ZO-1 and ZO-2 migrate to tight junctions (122). The regulatory ability tight junction protein ZO-1 will be discussed thoroughly (see chapter 4). However, punctate adherens junctions can be form without ZO-1 or ZO-2, so it is assumed that their role is regulatory (123).

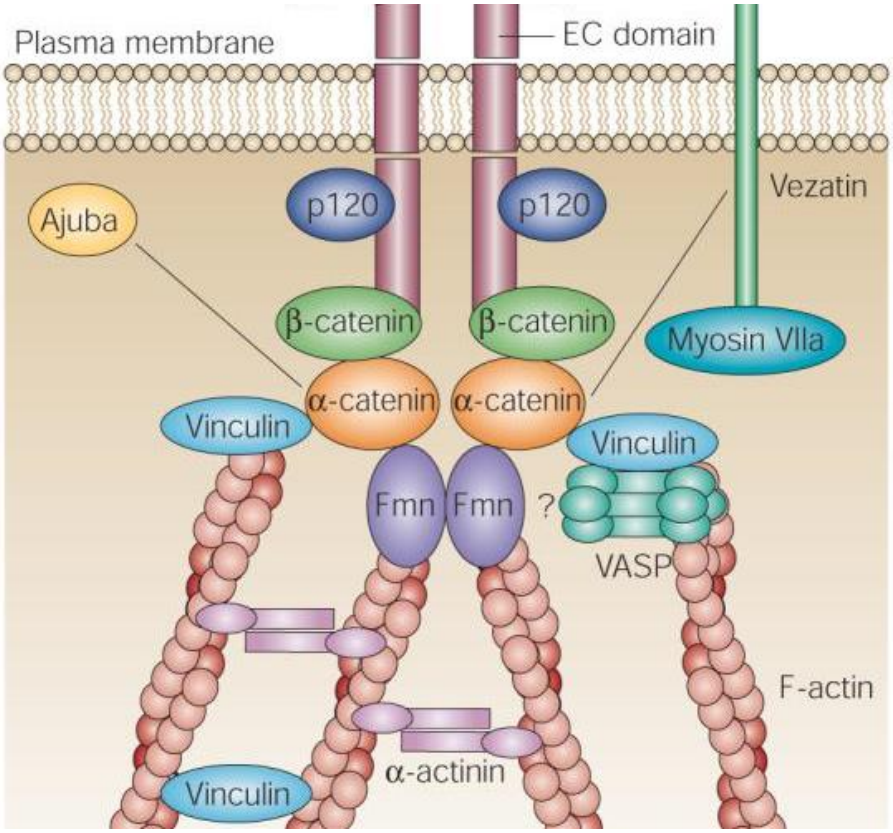

Figure 11: Components of the adherens junctions.

E-cadherin binds to p120 and β-catenin. B-catenin subsequently binds to α-

catenin and vinculin. These proteins then bind to actin filaments. Adapted from the literature (115).

The cadherin-catenin complex cannot form without α-catenin. If the α-catenin binding site for actin is deleted however, the complex can form, but it is much weaker (124). Mice knockout for α-catenin develop cardiomyopathy (125) highlighting its importance in the adherens junction.

Although α-catenin binds to actin, it is clear that this can only occur upon force application (126, 127), as commented above. This fact situates the adherens junction in the centre of the force transmission pathway and makes it mechanosensory, since it responds to forces. The force is applied by myosin pullin on actin, forming the actomyosin bundle. These bundles ultimately form large structures that transmit forces even to other cells, known as stress fibres (6, 115).

1.2.3 Tight junctions

Tight junctions connect the actin cytoskeleton of cells. However, their function is different from the adherens junctions described previously. They are classically found in the most apical part of epithelia forming an extremely tight (hence their name) adhesion. This adhesion forms an impermeable barrier that seals the epithelia (6, 128, 129). Most interestingly, recent research has shown that tight junctions are involved in complex regulatory roles. Tight junctions are formed by transmembrane proteins occludin, tricellulin, claudin and JAM, and cytoplasmic adaptor and regulatory proteins Zona Occludens (ZO) and others such as Apg2, ZONAB, MarvelD3 (Figure 12) (130, 131).

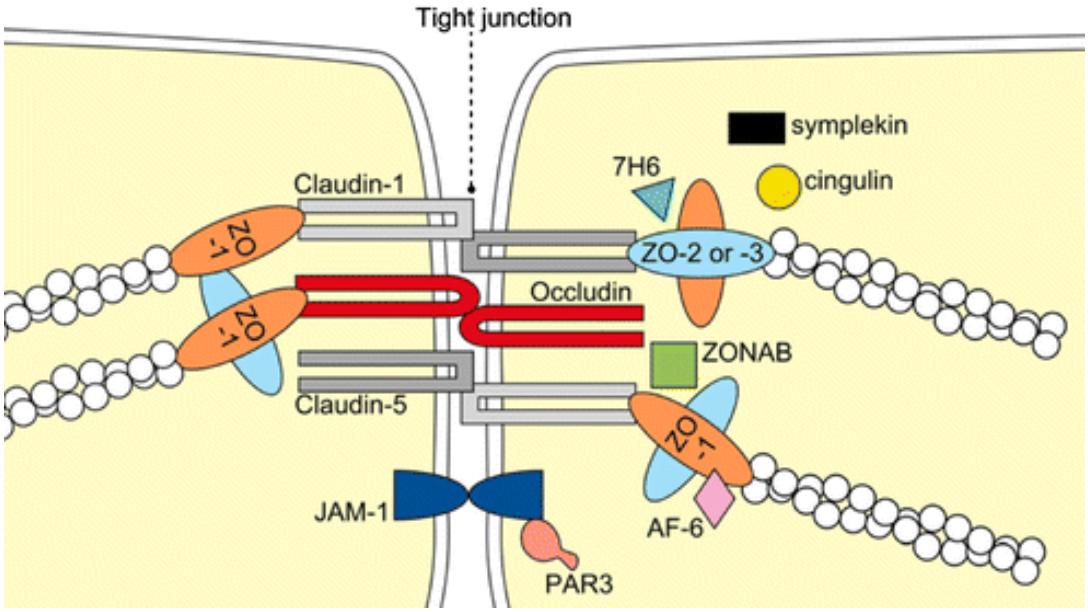

Figure 12: Components of the tight junctions.

Occludins and claudins bind homotypically tightly sealing the intercellular space. Adaptor proteins ZO-1, and other ZO family proteins bind the structure to the actin cytoskeleton. Adapted from the literature (131).

Occludin

Occludin is a transmembrane protein that crosses the membrane four times. As said, it interacts with other occludins, but also with neighbouring claudins. Interestingly, occludin is not structurally needed for the formation of tight junctions. It is however recruited when claudins are present and decreases the permeability of the tight junctions. This highlights the fact that occludin enhances the function of tight junctions, but it is not the most important component of them (131–133).

Claudin

Claudins are the main component of tight junctions. They also cross the membrane four times, but their sequence is very different from occludins. There are more than 56 types of claudins known to date (134). Some claudins can create pores in tight junctions which allow these structures to control the permeability to certain ions (135), so claudins have a double function. On the one hand, tightly seal the adhesion, and on the other, regulate the passage of ions. Most claudins contain a Y-V binding motif in their intracellular tail that allows them

to bind to adaptor proteins, specifically to the PDZ domain of ZO proteins. These adaptor proteins are then the ones which bind to the actin cytoskeleton (131–134, 136).

ZO-1

ZO family proteins are adaptor proteins that bind to claudin and link the tight junctions to actin. There are three known ZO proteins, ZO-1, ZO-2, and ZO-3 (137–140). While the three of them are interesting, I will only discuss ZO-1 because of the impact of this protein on this thesis. As stated before, ZO-1 is present at the initial formation of adherens junctions, and migrates to tight junctions upon maturation. ZO-1 has increasingly accumulated evidence showing its actions as a regulatory protein. It also binds to connexins in gap junctions, so to start with it interacts with multiple types of unions (129, 141, 142).

ZO-1 contains PDZ domains, a SH3 domain, and a GUK domain (Figure 13). It also has independent domains that bind to F-actin, and a C-terminal domain that can bind to α-catenin. ZO-1 also binds to α_5 integrin through a PDZ domain (143–145). The protein also contains active nuclear export and nuclear localization sequences, and it translocates to the nucleus during epithelial to mesenchymal transition (146). There are other cytoskeletal proteins that bind to ZO-1, and these include cortactin, cingulin, and shroom (147–149).

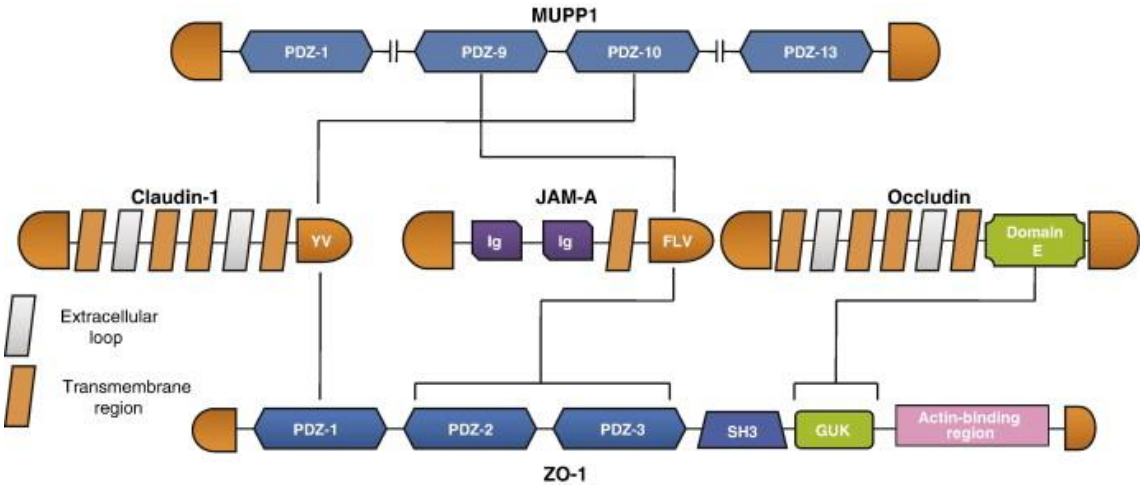

Figure 13: Binding domains of ZO-1.

ZO-1 contains three PDZ domains, one SH3 domain, one GUK domain, and an

actin binding region. Adapted from the literature (145)

The protein can be phosphorilated, which has been described to be done by MAP kinases, and protein kinase C (PKC) (150). Of importance to this thesis, PKCε directly phosphorylates ZO-1, which subsequently undergoes translocation to the edge of the cell and affects cell migration (144). This only occurs when the cell has a free edge, that is, an edge without cell-cell contact. Further, then ZO-1 binds to α5 integrin through a PDZ domain. This modifies the migratory behaviour of cells (144, 151). Extensive research was conducted about this interaction, and it was the focus of the first research paper published during this thesis (see chapter 4).

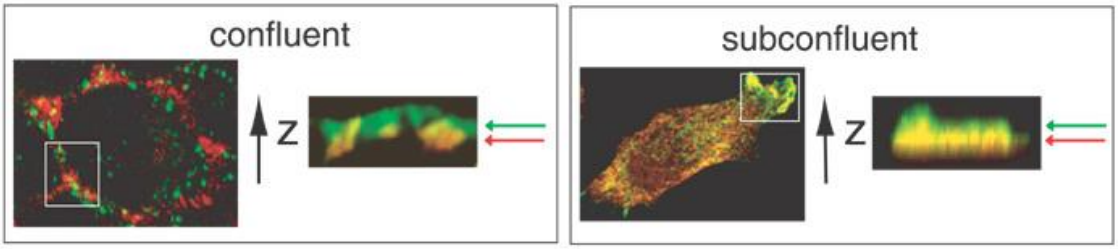

Figure 14: ZO-1 translocation.
ZO-1(green) translocates from tight junctions to the lamellipodia of free edge cells and binds to a5 integrin (red). Adapted from the literature (144)

1.2.4 Other types of cell-cell adhesions

Immunoglobulin adhesions

Immunglobulins are various cell surface proteins characterized for containing one or more (not surprisingly) immunoglobulin domains. The most studied immunoglobulins belong to the major histocompatibility complex, the T-cell receptor, and viral receptors (152, 153). Unlike cadherins, they are calcium independent and they use the immunoglobulin domains to bind each other. Interestingly, they can also bind to integrins, and their cytoplasmatic tail can bind to the actin cytoskeleton and other adaptor proteins (153, 154).

Gap junctions

Gap junctions are punctate adhesions formed by connexins. Connexins form two identical hemichannels that then bind onto a channel and allow transference of ions directly from one cell to another. They are very important in cardiac and neuronal tissue because they effectively couple the cells electrically through the flow of ions (155–157).

Selectin adhesions

Selectins are transmembrane proteins that need calcium to bind, much like cadherins, and contain lectin domains. They bind to different glycoproteins and glycolipids present at other cell membranes and are crucial for the rolling adhesion of leukocytes. Selectin adhesions trigger signals that modulate leukocyte-specific integrin attachment, which then trigger leukocyte migration (158).

Septate Junctions

Septate junctions are very tight adhesions similar to tight junctions. They localize closer to the basal side of epithelia just underneath tight junctions. These junctions share some proteins, but septate junctions have exclusive proteins such as claudin like proteins, neurofascin and contactin. They also contain adaptor proteins that bind them to the actin cytoskeleton. However, there is no described regulatory role for these adhesions (159).

Tunneling nanotubes

Tunneling nanotubes are a recently found type of cell-cell adhesion structure (160). They are long membrane tubes that contain F-actin and sometimes microtubules. Not very much more is known about them, I just included them in this thesis because they seem curious structures. Their functions include transfer of cellular components between cells, electrical coupling of cells, among others (161).

1.3 Cell-Extracellular Matrix adhesion

Cells are attached to the ECM by different types of adhesion structures. These famously include integrin-ECM mediated adhesions, also known as adhesion plaques. The study of the mechanical response through these adhesions has been the focus of large part of this thesis, which is why I will mainly discuss here their formation and components.

1.3.1 Integrin-mediated adhesions

Integrin-mediated adhesions are protein complexes that comprise transmembrane proteins, integrins, bound to adaptor proteins that connect the adhesion to the actin cytoskeleton (6, 162). These adhesions are used to sense the ECM, specifically all its mechanical parameters, rigidity (163, 164), ligand density (165, 166), and viscosity (167). Nascent adhesions are dynamic, and assemble at the leading edge of cells. They allow the cell to attach and propel further, ultimately driving cell migration (162).

Integrin-mediated adhesions form at the edge of the cell while the cell spreads, as small punctate, nascent adhesions that contain integrins (168). This region is called the lamellipodium (169), and is active in nucleation on actin bundles. Adhesions here have a high turnover rate as they assemble and disassemble with a half-time of one minute (170). At this point, adhesions are not still connected to the cytoskeleton, since inhibition of myosin II does not prevent their formation (171). However, they do contain adaptor proteins such as vinculin, paxillin and talin, which are the ones who connect to actin (171). As the cell protrudes, two behaviours can occur. Nascent adhesions can disassemble, and the proteins get recycled, or they can reinforce and mature into longer, more stable, mature focal adhesions (Figure 15).

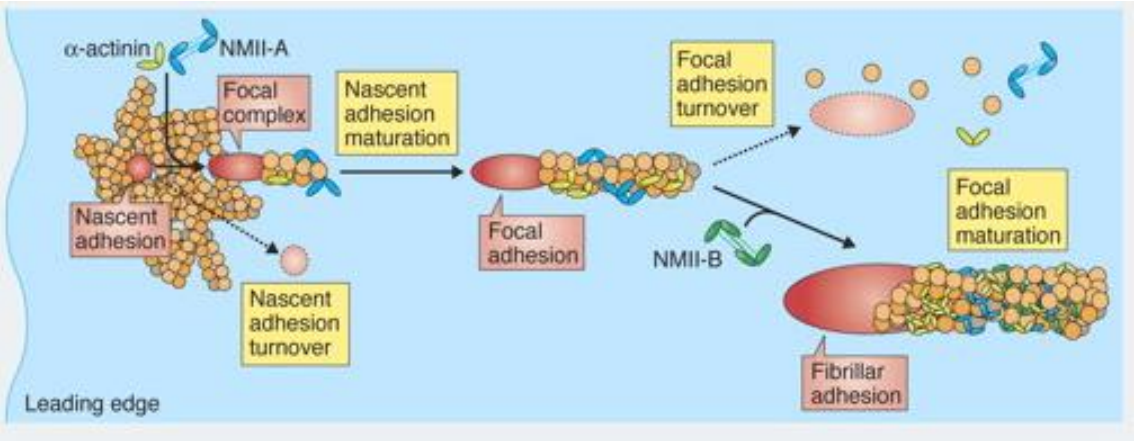

Figure 15. Adhesion assembly and disassembly.
Nascent adhesions mature into focal adhesions, which in time become fibrillar adhesions. Adapted from the literature (162).

As focal adhesions mature, they slow down the retrograde flow of actin as they connect to it through a protein complex including α-actinin (172, 173). Their turnover rate is slowed down (174), and more proteins join the focal adhesion and elongate it in a process that is contractility dependant (174). At this point, the force applied on the focal adhesion modulates a feedback loop. The activation of the proteins in the adhesion through phosphorylation increases further recruits more protein, and more actin, and this triggers increased force transmission (175).

Focal adhesions do not live forever. As the cell progresses, the focal adhesion localizes closer to the centre of the cell, and different proteins join the adhesion, such as tensin and zyxin, and this structure is now called fibrillar adhesion (176). These adhesions now undergo disassembly. This is thought to be driven by the following factors (162): either by contractility (177), interaction with microtubules (178), proteolysis (179), or pH changes (180).

To understand the process of focal adhesion formation, it is very important to understand the components that form them, which I am going to describe in the upcoming points.

1.3.2 Integrins

Integrins are transmembrane heterodimers composed of alpha and beta subunits (181). These subunits bind non-covalently, and multiple combinations exist that will bind to different ligands (Figure 16). Integrins can bind RGD motifs in fibronectin and vitronectin and GFOGER motifs in collagen. They can also bind laminin, and leukocyte-specific ligands (181).

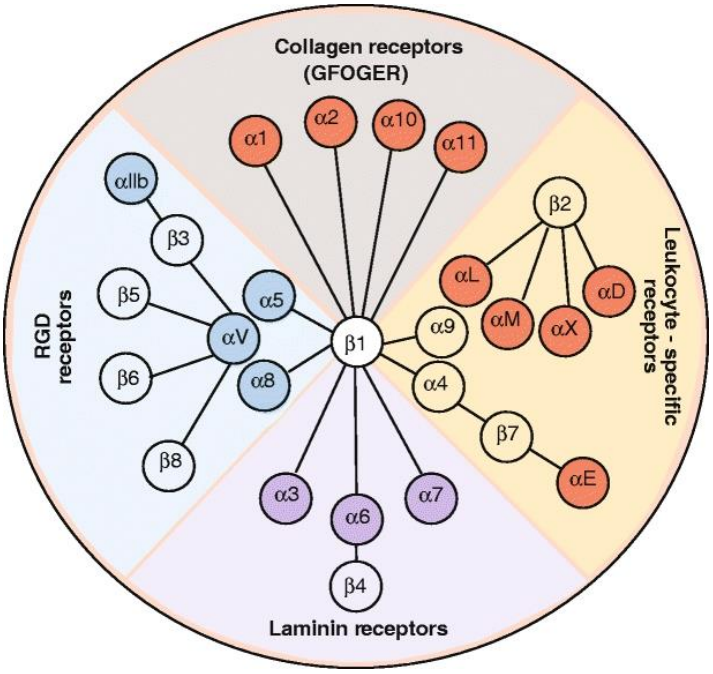

Figure 16: Integrin protein family.
Different combination of α and β integrins can bind to different ligands, including RGD-containing proteins (fibronectin, vitronectin), GFOGER- containing proteins (collagen), laminin, and multiple leukocyte receptors. Taken from the literature (181).

With the exception of $\alpha_6\beta_4$ integrin which binds to intermediate filaments, all other combinations bind the ECM ligand to actin (182). This is done through their extracellular domain, which is most of the protein by size (183). The intracellular domain, however, is much smaller in size (183). This intracellular domain is the target of the adaptor proteins that affect the properties of integrins (184).

Integrins can be in a closed, low affinity state (185). In a process known as inside-

out signalling, an intracellular binding partner can bind the integrin and change its conformation. From this point on, the extracellular domain has much more affinity for its ligand (Figure 17 A-C).

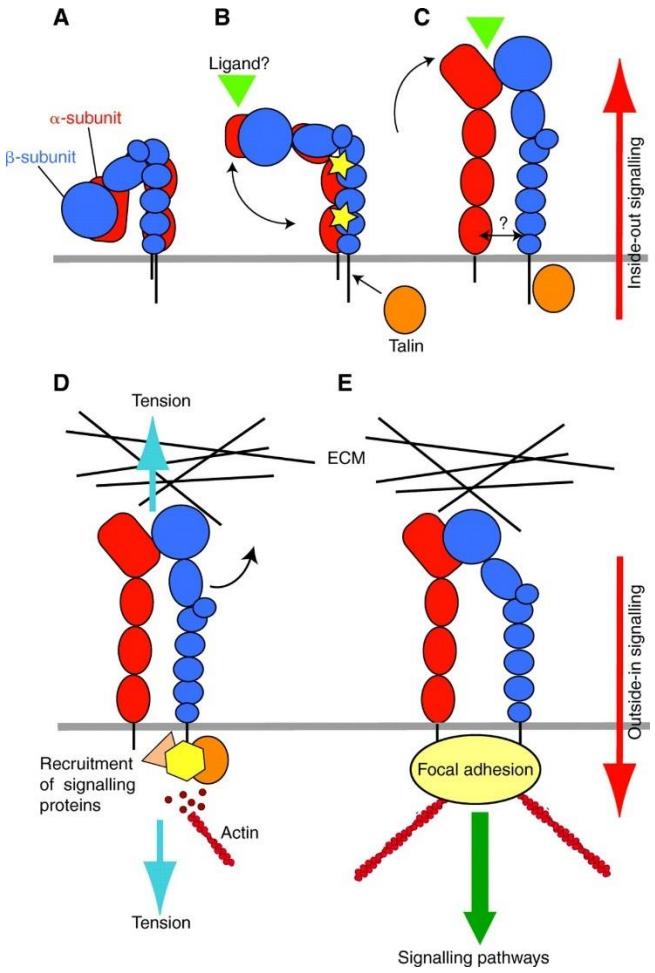

Figure 17: Integrin activation.
Integrins can have different affinity states. They can also be activated from the inside of from the outside of the cell. Taken from the literature (185).

The converse process is also possible, this is where the name of “bidirectional allosteric machines” comes from (182). Application of force through the integrin can trigger more integrins and other proteins to join, increase the effective affinity, and mature into an adhesion (Figure 17 D,E) (185). An intermediate affinity state also exists, where the integrin is not fully extended, but also not fully bent (186), having an intermediate affinity.

Integrins themselves are force sensitive. Their lifetime depends on force application (187), as they behave like a catch bond: With increased force, the lifetime of the bond increases, showing an optimum, to decrease afterwards (187). This, coupled with the fact that multiple integrins can have different affinities for the same receptor (164), make integrins a very good force sensor for a high dynamic range.

The affinity of the integrins for their ligands can also be modified by binding of other proteins to their cytoplasmatic tail (188, 189). These proteins are classically focal adhesion proteins, or integrin binding proteins.

1.3.3 Integrin binding proteins

Talin

Talin is a large protein the structure of which is formed by a large head, a linker, and a rod domain, forming a tail (190). The head can bind focal adhesion kinase, β integrins, and actin among other proteins (191, 192), while the tail contains multiple binding sites (193). First, it also has actin binding sites (194), and a region that allows talin to dimerize (195). Second, it contains another β integrin binding site (196). Third, it contains multiple vinculin binding sites with different affinities (197). Finally, it contains another domain that allows binding of paxillin and even other focal adhesion proteins (193, 198). The list of talin binding proteins has grown in the last years, and as stated in the literature, it will probably keep growing in the future (193). While talin is normally in a closed, inactive state, and the binding sites are not available. However, upon application of force mediated by actin polimerization and myosin contraction, talin unfolds and the sites become available (199, 200). Upon this unfolding, vinculin can bind and this stabilizes talin in the open conformation, triggering adhesion growth and maturation (201). The binding of these other proteins, including vinculin and kindlin help cluster talin with other integrins, but there are negative regulators of this phenomena. Integrin cytoplasmic-associated protein 1 (ICAP1), for example, has been described to bind to β_1 integrin and to supress its activation by

competing with kindlin and talin (202, 203). This makes talin one of the central mechanotransduction proteins, and this is why some authors call it “the master of integrin regulators” (193). In fact, cells can produce two different talins, Talin1 and Talin2 (204). While not completely functionally redundant, cells lacking Talin1 can still attach and form focal adhesions, but if both are missing, this is no longer possible (204).

Vinculin

In a similar fashion to talin, vinculin contains a head and a tail domain joined by a linker (205). The head can bind to talin, β-catenin and α-actinin, among other proteins (206). The tail contains binding sites for its own head, paxillin, and actin (207). Vinculin is coiled in itself via binding of the head and tail domains and distributed in the cytoplasm (208). However, the unfolded, active vinculin is present at focal adhesions (206). How this transition is achieved is not currently clear. The current understanding is that hydrophobic interactions between talin and vinculin allow for the transition (209, 210), but it could also be caused by the interaction with α-actinin (211), or by tension of the actin cortex mediated by Arp2/3 (212). It is however clear that the function of vinculin is to maintain large, mature focal adhesions (213), and activation of integrins via interaction with talin (198), to finally link focal adhesions to the actin cytoskeleton (214).

α-actinin

This protein contains a rod domain that forms an anti-parallel homodimer used to bind to and crosslink actin (215). It also contains other regions that bind β integrins, and vinculin (215). It is needed to form mature adhesions (171), and to connect the adhesions to actin (173). Moreover, α-actinin is fundamental in allowing force transmission through the focal adhesions, and it competes with talin for binding to some β integrins (173). Thus, α-actinin’s function is multiple, interacts with both integrins and actin, and mediates force transmission (215).

Paxillin

Paxillin contains four LIM domains at its C-terminus end that are involved in its anchoring to the plasma membrane and targeting it to focal adhesions (216). At

the N-terminus it contains SH3 binding sites and LD domains. These domains allow docking of focal adhesion proteins including vinculin and talin (216). Interestingly, focal adhesion kinase is located to focal adhesions by paxillin, but paxillin locates to focal adhesions independently (217). Paxillin is phosphorylated by focal adhesion kinase and Src, but also by a myriad of other proteins such as PKC and even Akt (216). This phosphorylation allows scaffolding for other focal adhesion proteins. I have discussed already that this phosphorylation is not needed for the localization of paxillin in focal adhesions. How is it then, that it is needed for subsequent adhesion maturation? The current understanding is that paxillin, regardless of maturation, recruits to focal adhesions at early stage. The literature reports that, in presence of paxillin, focal adhesions grow and reorient quickly (10 minutes) after cyclic stretch. However, upon paxillin knockdown, it takes up to 60 minutes for focal adhesions to grow and reorient (218). This shows that paxillin aids in the early phase of focal adhesion formation, but that other proteins are concomitant to this and can overcome its function in a redundant, although not exactly, manner.

Other focal adhesion proteins

Kindlin can bind to β integrins, and mediates integrin activation in a talin-like fashion (219). However, its study has been much more elusive. It is not clear if kindlin binds solely to integrins, if it binds to talin, or if it binds to both in a regulated manner, nor is known if they bind simultaneously or sequentially (220). What is known however, is that kindlin localizes to focal adhesions much like talin, and helps build the adhesion (221).

Tensin interacts with β integrin, actin, and focal adhesion kinase (222, 223) and localizes preferentially to fibrillar adhesions (223). Tensin is also involved in myofibroblast differentiation in a role that also needs TGF-β. Beyond its importance in focal adhesions, it seems that tensin has deeper regulatory roles (223).

Zyxin is also found in focal adhesions, but also shuttles into the nucleus in

characteristic conditions via a mechanism that is still unknown (224). It contains LIM domains and therefore can be bound by multiple proteins. It can be phosphorylated, and has been related to tumour progession and strikingly at the same time tumour suppression, in different kinds of tumours (224).

ICAP1 (Integrin cytoplasmic domain-associated protein-1) interacts with β integrin (225). Its function is modulated by phosphorylation. Whereas phosphomimetic ICAP1 mutant does not allow cell spreading, a non-phosphorilable mutant increases cell spreading (226). ICAP1 is not found in focal adhesions with clustered integrins, and its function seems to be to disrupt focal adhesions by blocking talin and kindlin binding to integrin (202). Interestingly, ICAP1 ubiquitylanization renders cells irresponsive in velocity to changes in rigidity of the ECM, but still ICAP1 binding to β integrin is not needed for rigidity sensing (227).

1.4 Mechanoresponse

Cells are constantly subjected to forces in the body, which are transmitted through them, and by them. How cells sense, and react to this forces is therefore paramount for the homeostasis of tissues (228). We call the way cells repond to forces the mecahnoresponse (229). The first step for this is to sense these forces, or mechanosensing (230). Then, cells transform the signals by a process known as mechanotransduction (231), integrate it into signalling cascades, and this then causes changes in gene expression therefore completing the cycle of mechanical sensing (85). During this thesis, I have tried to understand how is the mechanical response of integrin-mediated cell adhesions because this specific point has numerous implications in health and disease (232, 233). It is still not completely elucidated how cells respond to different parameters such as rigidity, viscosity, porosity, force loading rates, or compliance.

1.4.1 The issue of mechanosensing

As discussed before, mechanosensing is the first step in the cascade to transduce a physical signal into a biochemical signal (230). A fundamental example of this is rigidity sensing, the process by which cells sense the rigidity of the ECM. In this regard, the body has tissues at different rigidities. From very soft tissues in the brain (234), to very stiff tissues in the skeleton (235). ECM rigidity is also crucial for development (236), differentiation (237), and cancer (233). As discussed previously, cells then transform this signal in the process of mechanotransduction (231).

One of the readouts for the mechanotransduction pathway in rigidity sensing is the localization of the YES-associated protein (YAP) (238). This protein is normally localized at the cytoplasm of cells in soft environments. However, YAP can be phosphorylated, in a process well studied in the Hippo pathway (239), and subsequently translocated to the nucleus. In the nucleus it acts as a transcriptional coactivator interacting mainly with TEAD (240). Its overexpression is associated with metastasis and different kinds of malignancies in cancers such as pancreatic (241) or lung cancer (242).

Another readout for mechanotransduction are the focal adhesions themselves. Adhesions are mostly small and punctate in soft environments, and elongate and generate big patches in stiff environments. Generation of focal adhesions requires force transmission (173), myosin contractility (238), and talin unfolding (243) for maturation.

Ultimately, transmission of force to the nucleus has been shown to translocate YAP, in a process that structurally needs the LINC complex, through active nuclear transport (93) (Figure 18).

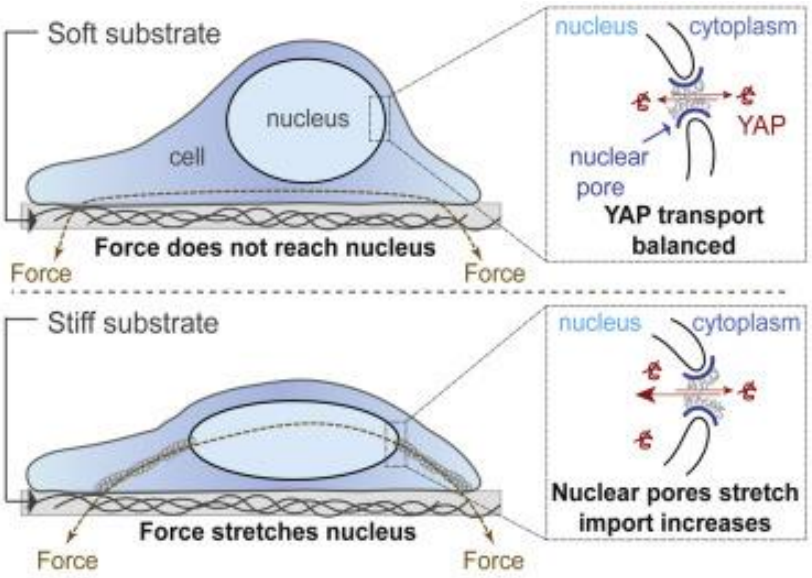

Figure 18. Regulation of mechanotransduction by force application to the nucleus.

Force application to the nucleus through the cytoskeleton changes nuclear transport across nuclear pores, translocating YAP and ultimately changing a mechanical input into a biochemical signal. Adapted from the literature (93).

It is therefore the generation of forces and their transmission to the nucleus what drives the mechanotransduction pathway. It is clear then, that knowing how the cell generates adhesions onto the substrate is fundamental to understand the whole process of mechanosensing.

1.4.2 The molecular clutch

To study the process of mechanosensing we need to understand how cells generate forces, and how they respond to forces. To this end, we use the molecular clutch model as a framework (243, 244). Historically, it was interesting to see that rearward flow speed is inverse to cell migration speed (245). Since the rearward flow of actin was maximal in non-migrating cells, this suggested that the force transmitted to the cytoskeleton was in fact slowing down the flow of actin, and therefore propelling the cell. This observation led to the first publication about the “molecular clutch of force transmission” (246), in an analogy to a clutch in a mechanical motor.

In recent years, it has become clear that this model is valid to explain nucleation and growth of focal adhesions and force transmission (93, 102, 166, 243), and it was the main model used in the laboratory during my thesis.

The molecular clutch model is based on the first proposal by Chan and Odde (244). Myosin contracts on actin filaments at a maximum speed if not opposed by any other force (244). If there is a force opposing myosin, then the speed of the rearward flow will decrease proportionally (247). This will continue until the force opposing myosin matches the maximum force applicable by myosin (248). As discussed before, the molecular components of the adhesions change their lifetime as a function of the force, like catch bonds (187). Therefore, force transmission will increase until destabilized again if the force is too high (244).
On top of this, cells can actively recruit more molecules and adaptor proteins to the adhesion, as I have discussed previously, upon for example, unfolding of talin due to a force trigger (243). This can explain how in some cell types there is an increase and decrease in force transmission as a function of ECM rigidity (244) but in others there is a subsequent phase or force reengagement (102, 164).

Therefore, the model explains the cell behaviour in the following way. Integrins bind and unbind the ligand in the substrate depending on their binding rate. Myosin pulls on actin freely. If engaged, myosin pulls on the substrate through the adaptor protein and integrin complexes, the clutches. Adaptor proteins such as talin unfold like slip bonds (249), since the time taken to unfold the protein decreases with applied force. However, integrins bind and unbind the ligand like catch bonds (187), since the time taken to unbind increases with force applied. This determines a crossover point between the two curves (Figure 19). Prior to this point, the integrins unbind before talin can unfold, there is no reinforcement, and the adhesion fails to form. However, past a given force threshold, talin unfolds before integrins unbind, and this event triggers reinforcement. This reinforcement involves vinculin locking talin in the unfolded conformation and recruiting more integrins and adaptor proteins to the adhesion (201). This event triggers the mechanotransduction pathway transmitting force to the nucleus as described before. By tuning the binding rates of the components of the clutch the

cell can therefore tune its mechanoresponse (Figure 19) (93, 102, 166, 243).

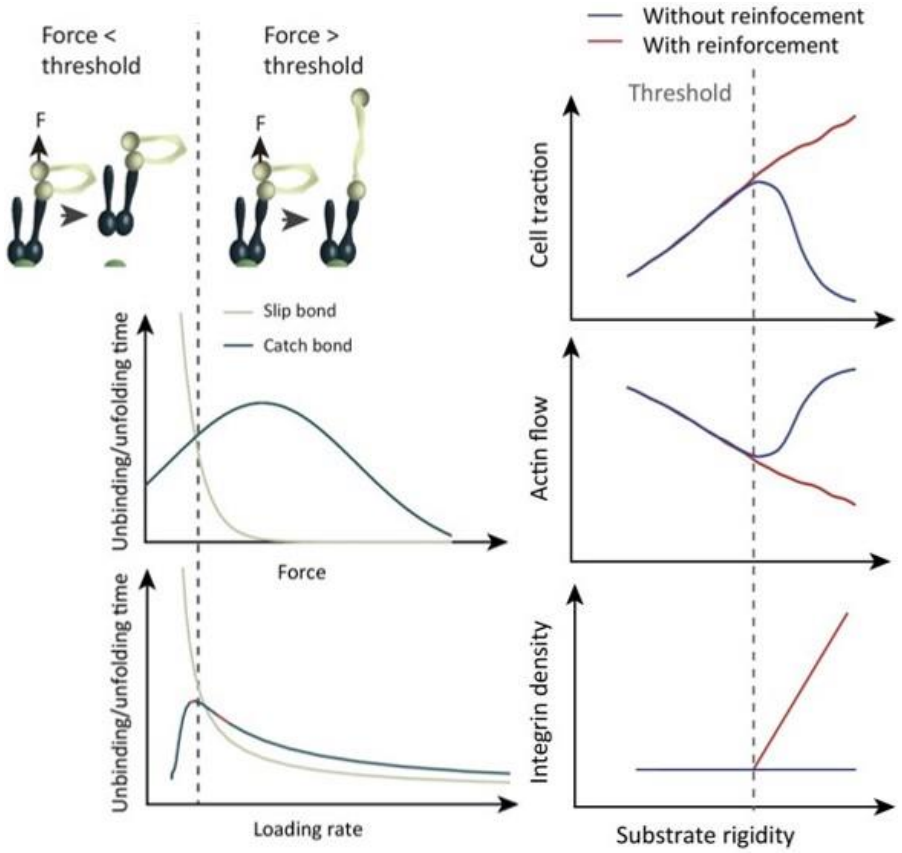

Figure 19. The molecular clutch model of adhesion explains adhesion nucleation.

Talin unfolds like a slip bond. As force application increases, talin unfolding time decreases. Integrins unbind like catch bonds. As force application increases, talin unbinding time increases, until force breaks the bond. Both curves determine a crossover point at a force threshold. Before the force threshold, integrins unbind before talin can unfold. Past the threshold, talin unfolds before integrins can unbind, triggering vinculin binding and subsequent adhesion reinforcement. Adapted from the literature (102).

The molecular clutch model explains adhesion nucleation and reinforcement based on a force threshold (102, 243, 244). However, forces exerted on and by cells are typically dynamic (247). For instance, if one considers the role of rigidity, the clutch model prediction is that increasing rigidities will not directly regulate a specific value of force, but the rate of force loading, i.e., the loading rate. This is

because a given rate of actomyosin contraction will generate force faster if it is pulling on a stiff substrate, than if it is pulling on a soft substrate. This does not invalidate the model. The unbinding of integrins and the unfolding of talin as a function of the force can be assessed experimentally (187, 249) (Figure 19). If this lifetime as a function of the force applied is known, the same curves as a function of the force loading rate can be computed (Figure 19) (102, 250). This curve as a function of the loading rate also exhibits a crossover point between the unbinding of integrins and the unfolding of talin (102). Therefore, the model applies both for an absolute force value and for a force loading rate value (102). Interestingly, the shape of this dependency does not matter as long as there is a crossover point between both curves. Moreover, the dependency on force loading rates is proven at the molecular level. Indeed, fundamental molecular mechanisms like bond rupture depend on the force loading rate (251, 252). Other single molecule events like protein unfolding also depend on the force loading rate (253).

1.4.3 The fundamental physical magnitude sensed by cells

While the prediction of the molecular clutch model of adhesion is that the fundamental magnitude sensed by cells is the force loading rate (102), it is still not clearly proven. To date, there are different hypothesis regarding which is this fundamental magnitude.

Displacement

The first hypothesis on how cells sensed rigidity was that cells applied constant displacements on the substrate. This came from the observation that cells seeded on micropillars of different rigidity applied different forces (254). This force was proportional to the spring constant of the pillars (Figure 20) (254).

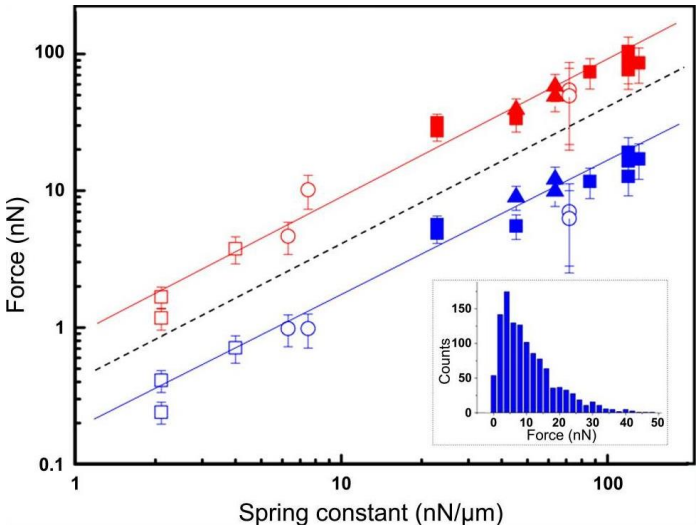

Figure 20. Force applied by cells on micropillars of different rigidities.
Cells apply constant displacement, different force, on micropillars of different rigidities. Taken from the literature (254).

Concomitant with this, increased recruitment of vinculin was observed for the high force regime compared to the low force regime. While this was a very important contribution, further information was needed to explain differential force responses in other uniform substrates of different rigidities.

Force

Another hypothesis for rigidity sensing was based on force thresholds. This hypothesis came from the fact that talin domains unfolded at different forces and subsequently determined vinculin binding (201). The authors commented on a biphasic behaviour or vinculin binding in vivo. In this model, below a small force threshold of 5 pN (force exerted by 1 myosin), talin would not unfold and there would be no subsequent binding of vinculin nor adhesion growth (Figure 21) (201).

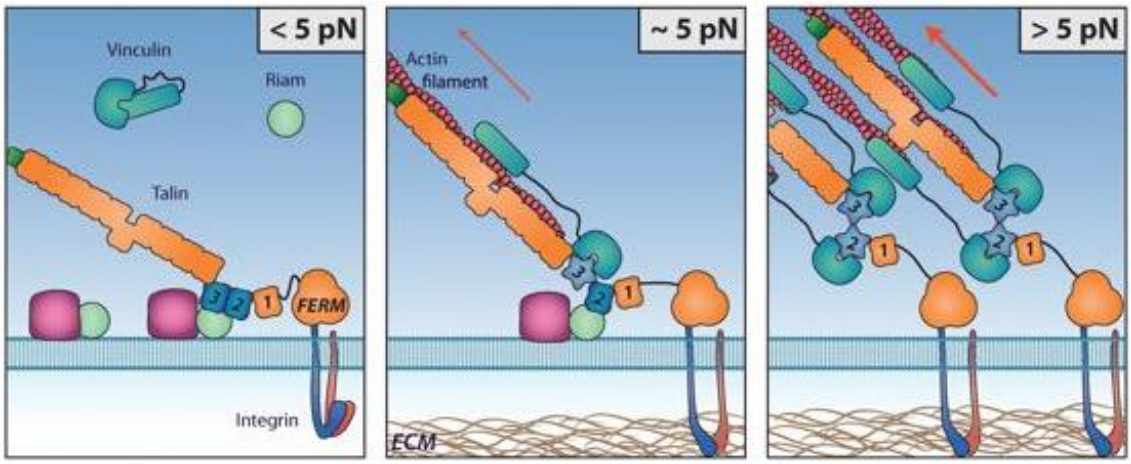

Figure 21. Talin unfolding at a force threshold.

Below a threshold of 5 pN talin would not unfold and vinculing would not bind. Breaching the force threshold would cause talin unfolding and vinculin binding, increasing force transmission and triggering adhesion reinforcement. Adapted from the literature (201).

Above this force threshold, the first domain of talin would unfold, and vinculin would bind, triggering adhesion growth. While this is a very important contribution, but more information was needed to explain how cells responded to a continuous regime of rigidities.

Both displacement and Force

The third proposed hypothesis for rigidity sensing has been that cells may have two different mechanisms. This came from the following observation. Upon seeding cells on micropillars of 0.5 µm in diameter, cells exerted constant displacement (255). This was in agreement with the data presented before (254). However, upon seeding cells in larger micropillars of 2 µm in diameter, cells exerted constant force (255). This agreed with the other hypothesis. Thus, the authors commented that the mechanism on sub-micrometre scale would be locally balanced whereas on micrometre and above scale forces would be balanced at a larger scale. Other authors report cells exerting constant displacements when seeded on soft gels and constant force when seeded on stiff gels (256). This result can be compared to the results observed in pillars, generalized to different gel stiffnesses. In conclusion, this hypothesis explains

initial rigidity sensing by very small contractions, while it explains later adhesion growth by other larger mechanisms (255). While this was an excellent advancement, it only partially explains the mechanism. In fact, deformations and forces exerted by cells are quite dynamic (236, 247, 257). It is then clear that this hypothesis is not sufficient to explain cell behaviour in a broader context.

Force loading rate

The hypothesis during my thesis was that rigidity sensing was determined by the force loading rate. This idea comes from the fact that cells could be sensitive precisely to the dynamics of force. As discussed previously, molecular bond rupture and protein unfolding depend on the force loading rate (251–253). Changes in mechanical parameters of the ECM could regulate the force loading rate of integrin-ECM binding and talin unfolding (243), thereby regulating the mechanical response of cells. This was first hypothesised based on the clutch model by Chan and Odde (244). The strength of this model is that it can recapitulate all previous hypothesis.

First, if an adhesion clutch is engaged, increased stiffness increases force transmission, recapitulating the first hypothesis (254).

Second, subsequent reinforcement of an adhesion requires talin unfolding. As discussed previously, in this model this occurs at a crossover point between the binding/unbinding times of integrins and folding/unfolding times of talin as a function of the force loading rate applied (243). This crossover point can be found both for absolute force values and also for force loading rate values (102). This effectively explains and expands the second hypothesis (201) through a rate mechanism.

Third, slipping at soft regimes where integrins unbind before talin can unfold explain the sub-micrometre displacements. Further clutch engagement and reinforcement through binding of other proteins explains micrometre displacements and adhesion growth, reconciling the third hypothesis (255).

Chapter 2. Aims of the thesis

2.1 General aim

The general aim of this thesis was to study the mechanical response of integrin-mediated cell adhesions, in response to both integrin binding partners and force loading rates.

2.2 Specific aims

1. To study the mechanical implications in cell-matrix adhesions of the interaction between integrin α5β1 and tight junction protein ZO-1.

2. To determine the fundamental mechanical variable detected by the cells during mechanosensing.

Chapter 3. Methods

3.1 Methods for the first study

MCF10A cell culture and transfection

MCF10A cells were grown as described previously (151), and tested negative for mycoplasma contamination. Cells were transfected using the Lipofectamine 3000 transfection kit (Invitrogen) following manufacturer's instructions using either a pool of 3 siRNAs (151), or 5 ng of the plasmid (ZO-1-168S→A-FLAG) (S168A), a kind gift from the laboratory of Johanna Ivaska (144). Five days after transfection cells were trypsinized and used for experiments. S168A plasmid has a point mutation in Serine 168 which impairs its binding to α5, and is tagged with the FLAG peptide for identification.

Magnetic tweezers and bead-recruitment experiments

Magnetic tweezers experiments were carried out as previously described (151, 164, 278). Briefly, carboxylated 3 μm magnetic beads (Invitrogen) were coated with a mixture of biotinylated pentameric FN7-10 (a four-domain segment of fibronectin responsible for cell binding and containing the RGD and PHSRN motifs (69) and biotinylated BSA at 1:200. For measurements, cells were first plated on silanized coverslips coated with 40 μg ml^{-1} of laminin (Sigma) to ensure that the α5β1 blocking antibody used to disrupt adhesion to fn affected only cell-bead and not cell-substrate interactions. Fn-coated beads were then deposited on the coverslips for 35 minutes, and attached to cells. The magnetic tweezers were then used to apply a square force of 0.5 nN on beads attached to cells. Cells were imaged using a Nikon-rate Eclipse Ti microscope with a 40x air objective (NA 0.60). The time taken for the beads to detach was assessed.

Immunostaining

Immunostainings on glass and gels were performed as described previously (151, 164). Fluorescence images were then acquired with a x60 objective. Adhesion intensity was determined by assessing the mean paxillin intensity on a whole cell normalized the mean intensity of the cell cytoplasm background. Adhesion density was determined manually by assessing the number of adhesions in a 11 μm^2 circle divided by the area. Adhesion length was measured manually by tracing a line on top of it. To quantify integrin recruitment to beads, FN7-10 coated 3 μm carboxylated silica beads (Kisker Biotech) were attached to cells, and protein recruitment (with respect to cytoplasmic levels) was calculated assessing the fluorescence intensity of beads (I_{bead}) the cytoplasm ($I_{cytoplasm}$) and image background ($I_{background}$) as:

$$a.u. = \frac{I_{Bead} - I_{Background}}{I_{Cytoplasm} - I_{Background}} \quad (1).$$

Correlation between ZO-1 and β1 intensity images was measured by calculating Pearson's correlation coefficient by using ImageJ plugin JACoP (283).

Preparation of polyacrylamide gels and traction measurements.

Polyacrylamide gels of 12 kPa were prepared as described in the literature (284), and incubated with 10 μg ml^{-1} FN (Sigma) overnight at 4ºC. Gels were then sterilized with UV light and washed once with PBS 1X for immediate use. Traction forces were computed using Fourier-transform traction microscopy with finite gel thickness (285) as previously described (286). To calculate cell tractions in cell monolayers, we used a previously described system of PDMS stencils (151) to pattern cell monolayers on rectangle-shaped monolayers. We then allowed cells to spread for 4h and calculated tractions as previously described (151).

Protein quantification

Protein expression levels were measured using western blot as previously described (151, 164). For the quantification of phosphomyosin light chain 2 (pMLC) and myosin light chain 2 (MLC), the membrane was first probed for

pMLC, then stripped using Restore Western Blot Stripping Buffer (Thermo Fisher Scientific), and then reblocked and reprobed for MLC. Protein concentrations are reported relative to the control.

Antibodies

Primary antibodies used were anti-ZO-1 rabbit polyclonal (Invitrogen, 61-7300), anti-GAPDH mouse monoclonal (6C5, Santa Cruz Biotechnology, sc-32233), anti-Myosin Light Chain rabbit polyclonal (Cell Signaling, #3672), anti-phospho-Myosin Light Chain rabbit polyclonal (Cell Signaling, #3671), anti-FLAG rabbit polyclonal (Sigma Aldrich, F7425), anti-activated-β1 mouse monoclonal (12G10, Abcam, ab30394), anti-β1 mouse monoclonal (K20, Beckam Coulter, IOTest CD29-FITC), anti-paxillin rabbit monoclonal (Y113, Abcam, ab32084), 1:200 for immunostainings, and 1:500 for western blot. For western blot, the secondary antibodies used were peroxidase-conjugated anti-mouse IgG (Jackson Immuno Research, 715-035-151), and peroxidase-conjugated anti-rabbit IgG (Merck Millipore, AP132P), diluted 1:5000. For immunofluorescence, the secondary antibodies used were Alexa Fluor 488 anti-rabbit (Invitrogen, A-21206) and Alexa Fluor 555 anti-mouse (Invitrogen, A-21422), diluted 1:200. To block α5β1 integrin function, the antibody used was anti-α5β1 mouse monoclonal (JCS5, Millipore, MAB1969, 10 μg ml^{-1})

Statistical analysis

All independent datasets were first checked for normality using the d'Agostino-Pearson K2 normality test. One-way or two-way (for time-lapse experiments) ANOVA was performed for more than 2 comparisons. For one-to-one comparisons we used a t-test. For multiple comparisons we used a Dunnet modified t-test. If datasets were not normal, we used a Kruskal-Wallis test. All error bars shown are standard error of the mean.

3.2 Methods of the second study

Cell culture and reagents

Mouse embryonic fibroblasts (MEFs) were cultured as previously described (173), using Dulbecco's modified eagle medium (DMEM, Thermofischer Scientific, 41965-039) supplemented with 10% FBS (Thermofischer Scientific, 10270-106) and 1% penicillin-streptomycin (Thermofischer Scientific, 10378-016), and 1.5% HEPES 1M (Sigma Aldrich, H0887). Talin 1-/- MEFs were cultured as previously described(302), using DMEM supplemented with 15% FBS, 1% penicillin-streptomycin, and 1.5% HEPES 1M. Cell cultures were routinely checked for mycoplasma. CO_2-independent media was prepared by using CO_2-independent DMEM (Thermofischer Scientific, 18045 -054) supplemented with 10% FBS, 1% penicillin-streptomycin, 1.5% HEPES 1M, and 2% L-Glutamine (Thermofischer Scientific, 25030-024). Media for optical tweezers experiments was supplemented with Rutin (ThermoFischer Scientific, 132391000) 10 mg/L right before the experiment.

Transfection

Talin 2 was knocked down as previously described (302), by transfecting Talin 1-/- MEFs using the Neon Transfection System (Thermofischer Scientific) with a plasmid encoding a short hairpin RNA (shRNA) targeting the nucleotide sequence 5'-GATCCGAAGTCAGTATTACGTTGTTCTCAAGAGAAACAACGTAATACTGAC TTCTTTTTTTCTAGAG-3'. For optical tweezers experiments, cells were transfected with pEGFP-Paxillin previously described(303), using the Nucleofactor 2b Device (Lonza).

Antibodies and compounds

Primary antibodies used were anti-Paxillin rabbit clonal (Y113, abcam, ab32084), and anti-YAP mouse monoclonal (63.7, Santa Cruz Biotechnology, sc-101199), 1:200. Secondary antibodies used were Alexa Fluor 488 anti-mouse (A-11029, Thermo Fischer Scientific), Alexa Fluor 488 anti-rabbit (A-21206; Thermo Fischer

Scientific), and Alexa Fluor 555 anti-rabbit (A-21429, Thermo Fischer Scientific) 1:500. Compounds used were Blebbistatin (Sigma Aldrich) 50 µM, Jasplakinolide (J4580, Sigma Aldrich) 25 nM, phalloidin (Alexa Fluor 555 phalloidin, Thermo Fischer Scientific) 1:1000, and Hoechst (33342, Thermo Fischer Scientific) 1:2000.

For immunofluorescence, the secondary antibodies used were Alexa Fluor 488 anti-rabbit (A-21206; Thermo Fischer Scientific) and Alexa Fluor 555 anti-mouse (A-21422; Thermo Fischer Scientific) diluted 1:200.

Preparation of stretchable membranes

Stretchable polydimethylsiloxane (Sylgard 184 Silicone Elastomer Kit, Dow Corning) membranes were prepared as previously described (93). A mix of 10:1 base to crosslinker ratio was spun for 1 minute at 500 rpm and cured at 65º C overnight on plastic supports. Once polymerized, membranes were peeled off and assembled onto the stretching device. After assembly, membranes were plasma cleaned for 1 minute, treated with 3-aminopropyl triethoxysilane (APTES, Sigma Aldrich) 10% in ethanol for 1 h at 65 °C, and with glutaraldehyde (Sigma Aldrich) 1.5% in phosphate-buffered saline 1X (PBS, Sigma Aldrich) for 25 min at room temperature.

Then, polyacrylamide gels were prepared and attached to membranes. To this end, polyacrylamide gels were first prepared by adapting previous protocols (166, 265). Polyacrylamide gels were polymerized between two glass coverslips treated with 2% dimethyldichlorosilane (Plus One Repel Silane, GE Healthcare). For 0.6 kPa gels, the mix contained 4% acrylamide (BioRad), 0.03% BisAcrylamide (BioRad), 2% 200-nm-diameter dark red fluorescence carboxylate-modified beads (Fluospheres, ThermoFischer Scientific), 0.5% ammonium persulphate (APS, Sigma Aldrich), and 0.05% tetramethylethylenediamine (TEMED, Sigma Aldrich), in PBS 1X. After polymerization, one coverslip was detached, and the gel was then attached to the PDMS membrane. To this end, it was pressed against the prepared stretchable PDMS membrane and left overnight at 37 °C in an incubator with humidity control. The remaining coverslip was removed the next day.

Polyacrylamide gels were coated using a protocol adapted from the literature (304). Briefly, gels were covered with a mix containing 10% HEPES 0.5M Ph 6, 0.002% BisAcrylamide (BioRad), 0.3% 10 mg/ml N-hydroxysuccinimide (NHS, Sigma Aldrich) in dimethyl sulfoxide (DMSO, Sigma Aldrich), 1% Igracure (Sigma Aldrich), 0,0012% tetraacrylate (Sigma Aldrich), in milliQ water. Gels were then covered with a glass coverslip and illuminated with UV light for 10 minutes. After exposure, the glass coverslip was removed, and gels were washed twice with HEPES 25mM Ph 6 and twice again with PBS. Gels were then incubated with 10 µg/ml of fibronectin in PBS overnight at 8ºC, washed the next day thrice with PBS and immediately used. The rigidity of the gels was measured using Atomic Force Microscopy as previously described(93).

Cell stretch

Cells were seeded on 0.6 kPa gels attached to previously mounted stretchable PDMS membranes. After attachment, cell media was changed to CO2-independent media. Cells were then stretched at 37ºC continuously for 1 hour with one signal type (square or triangle), at one amplitude (20%, 10%, 5%, or 2.5%), and at one frequency (2Hz, 1Hz, 0.5Hz, 0.25Hz, 0.125Hz) to produce different force loading rates. After stimulation, cells were immediately fixed and prepared for immunostaining.

Immunostainings

Immunostainings were performed as previously described (166). Cells were fixed with 4% paraformaldehyde for 10 minutes, permeabilized with 0.1% Triton X-100 for 4 minutes, blocked with 2% Fish-Gelatin in PBS 1X for 1 hour, incubated with primary antibody for 1 hour, washed with Fish-Gelatin-PBS for 30 minutes, incubated with secondary antibody for 1 hour, washed with Fish-Gelatin-PBS for 30 minutes, and mounted using ProLong Gold Antifade Mountant (ThermoFischer Scientific).

For immunostainings of animal tissue, at the end-point of experiments animals were sacrificed by exsanguination and during residual heart beating lungs were

perfused through the vasculature with ice-cold PBS 1X. Lungs were immediately excised *en bloc* with the heart and intrabronchial cannulas and perfused with cold OCT:PBS (3:1) (Optimal Cutting compound, Company). Lungs were then placed in cassettes with OCT on a dry ice platform and frozen at -80 º C. Lung blocks 70-µm thick were cut with a cryostat (Thermo Scientific, Massachusetts, MO) and attached to slides. Lung slices were then washed with PBS and fixed with paraformaldehyde 4%. and After three more washes, tissue was permeabilised with 0.2 % Triton X-100, blocked with 10% FBS and incubated for 30 seconds with TrueBlack (Biotium) to reduce ECM autofluorescence. The primary antibody was incubated overnight at 4ºC, and after three washes the secondary antibody was incubated during 90 minutes at room temperature. Finally, lung slices were counterstained with NucBlue (Thermo Scientific, Massachusetts, MO) to stain the nuclei and mounted with Fluoromount (Dako). Two lung slices from each lung were imaged in three different fields to a total of six images per condition.

Once the samples were prepared, images of stretched cells were acquired with 60x objective (NIR Apo 60X/WD 2.8, Nikon) with an upright microscope, images of cells on glass were acquired with 60x objective (Plan Apo VC 60X/WD 0.31-0.28, Nikon) with a confocal inverted microscope, and images of animal tissue were acquired with 60x objective (Plan Apo VC Oil 60X/WD 0.13, Nikon) with a confocal inverted microscope.

Image analysis

Focal adhesion length was quantified manually by assessing the length of three representative adhesions in paxillin stainings at the cell edge, for n cells. Nuclear to cytoplasmic ratio of YAP was quantified manually by segmenting the nucleus using Hoechst (single cells) or NucBlue (rat lung slices) and using the following formula:

$$a.u. = \frac{I_{nucleus} - I_{background}}{I_{cytoplasm} - I_{background}} \qquad \text{eq. 1}$$

Similarly, protein recruitment to beads was quantified manually by segmenting

the bead area using the brightfield image and using the following formula:

$$a.u. = \frac{I_{bead} - I_{background}}{I_{cytoplasm} - I_{background}} \quad \text{eq. 2}$$

In both cases, $I_{cytoplasm}$ and $I_{background}$ refer to the average fluorescence intensity of the cytoplasm and background (i.e., areas with no cells). I_{bead} and $I_{nucleus}$ refer to the average fluorescence intensity of the nucleus and bead. In the case of rat lung immunostainings, lung cuts were randomized before quantification. Six (6) areas coming from two (2) different cuts were analysed, where twenty (20) cells per area were quantified taking the closest from the geometric centre of the image.

Optical Tweezers

The optical tweezers system was adapted from a previous setup (259). Briefly, the optical tweezer uses a near-infrared fibre laser (λ = 1064 nm, YLR-5-LP; IPG Photonics) that passes through two acoustooptical modulators (DTSX-400-1064; AA Opto-Electronic) which are modulated by a variable frequency driver (Voltage Controlled Oscillator, DRFA10Y2X-D41k-34-50.110; AA Opto-Electronic). After modulation, the beam size is expanded and coupled into an inverted microscope (Eclipse Ti-e; Nikon Corporation) from the rear port. The beam is coupled in the optical path of the microscope by a dichroic mirror and focused in the object plane through a water immersion objective (Plan Apo VC WI, 60x, NA=1.2; Nikon Corporation). To measure the force, the condenser was replaced by a force sensor module (Lunam T-40i; Impetux Optics, S.L.), which was positioned according to the manufacturer procedure. The module is precalibrated and gives direct access to the force applied by the tweezer on any trapped object. To correct for focal drifts during the measurements, the Perfect Focus System (PFS, Nikon Corporation) was used. The sample is heated by a self-built heating chamber, keeping it at 37° C. Image acquisition was done using a spinning disk system (CSU-W1 (Yokogawa); Intelligent Imaging Innovations Inc.) and a CMOS camera (Orca-flash4.0v2; Hamamatsu Photonics K.K.). All hardware was controlled using the custom written LabVIEW programs (National Instruments Corporation).

Beads were coated as described previously (278). Briefly, carboxylated 1 µm polystyrene beads (Micromod) were coated with a mixture of biotinylated pentameric FN7-10 (a four-domain segment of fibronectin responsible for cell binding and containing the RGD and PHSRN motifs (69)) and biotinylated bovine serum albumin at a ratio of 1:10.

Glass slides were coated with fibronectin 10 ug/ml in PBS overnight and rinsed thrice with PBS. Cells were then seeded on the glass. Once attached, beads were added. One bead was subsequently trapped and placed on the surface of a cell, and the stimulation was then started by using 120 mW of laser power to displace the bead 0.1 µm in x and y from the centre of the trap for 160 seconds by using a triangle or square signal of one frequency (4Hz, 2Hz, 1Hz, 0.5Hz, 0.25Hz, 0.125Hz) to produce different force loading rates. To compensate for the cell dragging the bead towards the nucleus, the optical trap was repositioned at intervals of 32 seconds.
Bead speeds and force loading rates were measured using respectively the displacement and force signals of the optical trap. Using a custom-made MATLAB program, each signal was detrended and then divided into linear segments of individual cycles and fitted to straight lines to obtain the slopes. The stiffness was calculated as described previously (278) by estimating the transfer function between the force and the displacement data at intervals of 32 seconds, and at the frequency of stimulation.

Atomic Force Microscopy

AFM experiments were carried out in a Nanowizard 4 AFM (JPK) mounted on top of a Nikon Ti Eclipse microscope. For experiments pulling on beads, Fibronectin or biotin-BSA coated beads were functionalized as described previously (278). Briefly, carboxylated 3 µm silica beads (Polysciences) were coated with a mixture of biotinylated pentameric FN7-10 (a four-domain segment of fibronectin responsible for cell binding and containing the RGD and PHSRN motifs (69)) and biotinylated bovine serum albumin (Sigma Aldrich) at a ratio of 1:10. The beads where then attached to the cantilevers using a non-fluorescent adhesive (NOA63,

Norland Products) to the end of tipless MLCT cantilevers (Veeco). Cells were seeded on fibronectin coated coverslips and a force curve at each retraction velocity was acquired for each of the cells. Cells were kept at 37°C using a BioCell (JPK). The spring constant of the cantilevers was calibrated by thermal tuning using the simple harmonic oscillator model.

For experiments pulling on cells, we followed the protocol described in the literature (267). Briefly, cantilevers were submerged in sulfuric acid 1M for 1h. They were then washed with milliQ water and plasma cleaned for three minutes. After this, cantilevers were incubated with 0.5 mg/ml biotin-BSA and left overnight in a humid chamber at 37ºC. Next day they were washed thrice with PBS and incubated with 0.5 mg/ml Streptavidin and left in a humid chamber at room temperature for 30 minutes. Again, they were washed thrice with PBS and reincubated with 0.4 mg/ml biotin-ConcanavalinA for 30 minutes in a humid chamber at room temperature, after which they were washed thrice with PBS and stored under PBS for use. We used a Nanowizard 4 AFM (JPK) on top of a Nikon Ti Eclipse microscope. ConcanavalinA-coated MLCT-O cantilevers were calibrated by thermal tuning. Then, cells were trypsinized, resuspended in CO_2 independent media and allowed to recover for 5 minutes. Rounded cells were attached to MLCT cantilevers by exerting 3 nN forces on top of a region of a coverslip with no coating and incubated for 5 minutes. The measurement of the adhesion forces was done by approaching the cell at the same velocity of the corresponding withdraw velocity, keeping for 10 seconds and withdrawing until the cell was fully detached.

The maximum detachment force was determined by analysing the retraction F-D curve. A MATLAB program was used to extract and analyse F-D curves from JPK data files. The maximum detachment force was calculated as described in the literature (305) by subtracting the baseline offset from the minimum force value in the curve. We calculated the stiffness by fitting a line on part of the retraction curve between the beginning of AFM retraction and the point that indicates maximum retraction force.

Differential rat lung ventilation

Six pathogen-free male Sprague Dawley rats (350-450 g) were randomly

distributed in the different experimental groups (3 for 2.1Hz-0.1Hz and 3 for 1.1Hz-1.1Hz). Animals were housed in controlled animal quarters under standard light, temperature and humidity exposure. All experimental procedures were approved by the Ethical Committee for Animal Research of the University of Barcelona (Approval number 147/18).

Animals were anesthetized intraperitoneally using 20% urethane (10 mL/kg). After confirmation of deep anaesthesia by tail and paw clamp, animals were tracheostomised and each lung of the rat was independently cannulated (16G; BD Bioscience, San Jose, USA). After muscular relaxation with 0.4 mg/kg pancuronium bromide (Sigma Aldrich, St. Louis, MO) intravenously injected through the penile vein, each lung was connected to a customized small rodent ventilator, with a pressure sensor connected at the entrance of each cannula to monitor animal ventilation according to the conditions explained below. Correct cannulation of each lung was confirmed by opening the chest wall and observing proper independent inflation and deflation of each lung. Animals were ventilated with a tidal volume of 7 ml per kg of animal weight (kg-bw) and with a positive end expiratory pressure of 3 cmH_2O. Control ventilation was set to a typical frequency of 1.1 Hz with the same tidal volume (3.5 ml/kg-bw) in each of the two lungs of the rat (minute volume of 462 ml/min/kg-bw). To test the effect of varying the loading rate on YAP, a different ventilation frequency was applied to each lung while maintaining the control tidal volume. One lung was ventilated at 0.1 Hz and the other one at 2.1 Hz. In this way, each lung was ventilated with a different loading rate (21 ml/min/kg-bw and 441 ml/min/kg-bw) whereas the animal received the same total minute ventilation, hence keeping O_2 and CO_2 blood gas levels thereby discarding any systemic effect induced by differential ventilation.

Statistical analysis

No statistical methods were used to determine sample size before execution of the experiments. All independent datasets were first checked for normality using the d'Agostino-Pearson K2 normality test. One-way ANOVA was performed for more than 2 comparisons. Normal one-to-one comparisons were carried out by using a t-test. In case of time-paired data, we used a paired t-test. Multiple comparisons were made using Dunnet's modified t-test. Non-normal multiple

datasets were compared using Kruskal-Wallis' test, while non-normal two-dataset comparison was done using Man-Whitney's test. For two factor comparisons the test used was two-way ANOVA, after which Sidak's multiple comparisons test was performed. All statistic tests were two-sided. All central tendency values are mean and error bars shown are standard error of the mean. Significance is considered for $p<0.05$.

3.3 Implemented setups

During the development of this work I used different experimental setups. Regarding the magnetic tweezers, the instrument was already implemented in the laboratory and used previously (151, 164). The stretch system was already implemented and I contributed in developing a software to increase its capabilities (258). The optical tweezers was developed by the laboratory of Timo Betz in Münster (259) and I wrote a very small modification to perform my experiments. In appendix C I leave a copy of the script to extract the displacement and force measured from the raw data. The atomic force microscope was also implemented in the lab (243) and I contributed by adapting the functionalizing of microspheres and by implementing the single cell AFM protocol, which can be found in appendix C.

3.3.1 Magnetic Tweezers

Magnetic tweezers can be divided in low force and high force magnetic tweezers. The kind implemented in our laboratory was of high force, as described previously (173). The instrument consists of a magnetic core surrounded by a copper coil. An intensity runs through this coil, magnetizing the core. The core then generates a constant but nonhomogeneous magnetic field. Higher magnetic field closer to the tip then pulls magnetic particles towards the tip (260).

Software implementation

The software controlling the magnetic tweezers was written in LabVIEW. If

superparamagnetic particles are used in the experiment, the particles exhibit no pull when there is no magnetic field (260). Upon application of a magnetic field, the particles get pulled immediately. Therefore, the software controlled the intensity running through the coil producing different kinds of waves. This strategy allowed for pulling particles with constant, square or potentially any waveform wanted. The software was in fact connected to a voltage to intensity controller, and the application was thus voltage controlled analogically. Extensive details of the software can be found in my undergraduate final degree project.

Execution

Superparamagnetic beads were coated with a ligand of interest using a previously described protocol (173) and let to attach to cells. The tip of the magnetic tweezers was then approached at a controlled distance by using a micromanipulator and the experiment could then start. The setup could be used to measure relative stiffening “reinforcement” of the beads (173, 261) or to measure the detachment time of beads (262).

Specific care needed to be taken when performing these experiments. We always tried to use a low intensity (1 A), and not to use the same sample of cells for long. First, the tip dissipates power quadratically with increasing intensity (263). Second, the magnetic field is controlled in a 120º degree angle in front of the tip (264). Farther than this, the body of the tip dominates, and the beads are no longer pulled towards the tip and therefore the force is not controlled. Third, we had no control for humidity nor CO_2 in this setup, and thus the media dried, and special care needed to be taken regarding changing the media for cell viability.

Calibration

The setup was calibrated by using viscosity standards by adapting a previously described protocol (173). Non-magnetic beads were suspended in a highly viscous dimethylsiloxane fluid. Next, superparamagnetic beads were suspended at a low density. The tweezer was then submerged in the fluid and let to stabilize. Force was subsequently applied, and the beads were pulled towards the tip. By tracking their position and subtracting the drift of the fluid, the drag force could be

computed and therefore the force curve of the tweezer computed.

3.3.2 Stretch

Several stretch systems are described in the literature (95, 258, 265). Our system consisted of a flexible polydimethylsiloxane (PDMS) membrane clamped between two rings joined by O-rings in the interface. The rings were placed on top of a loading post that had vacuum access. By controlling the pressure of the vacuum, the extension of the PDMS and therefore the amount of stretch could be controlled.

Software implementation

I wrote the software of the stretch system in LabVIEW. The structure is divided in two sections.

A first piece of the program reads continuously on the pressure sensor and the actively sent pressure. This piece of the software was a requirement for users that only wanted to read more precisely the value of the pressure but that would manually actuate the mechanism.

A second piece of the program can actuate the mechanism by a voltage controlled vacuum pressure actuator.

The vacuum actuator is fed by the vacuum line in the laboratory that is much higher than the pressure required to stretch the membrane (-550 mmHg break the actuator). The actuator can be set to manual, thereby requiring a push-button to allow vacuum in, in a pre-established amount by a potentiometer. In this position, the release of the pressure is derived through an electro valve that connects automatically to ambient pressure upon pressing of the button again. If the controller is set to software control, the amount of vacuum can be controlled with the software using different waveforms, amplitudes, frequencies, for a wanted duration, and using a composed wave. This composed wave allows for a controlled loading ramp, a constant phase, and a controlled unloading ramp, and was a requirement for a publication (258).

Execution

Upon mounting of the PDMS membranes on the rings, they could be coated, and cells subsequently attached. Attaching polyacrylamide gels was also possible by using a previously described protocol (265). The setup was used to measure the response of cells to static stretch, stretch release, and cyclic stretch.

Special care needed to be taken to lower the friction of the PDMS membrane to the post. We used preheated Vaseline at 37ºC at the interface of the post and the membrane. On top of this we created a small Vaseline reservoir at the edges of the post by cutting at the centre of the circular post. Inevitably, the friction limited the amount of loading rate applicable, as the system did not respond instantaneously. Since the unloading of the pressure had to pass through the electro valve of the actuator, this limited the rate of unloading. To get this contribution below the rate of our operations, we made a small inlet at the entry very close to the ring. The actuator could in normal operation compensate for it and the rate was then the input of the software, with the sole exception of the square waves, were as discussed, immediate response was impossible (see chapter 5).

Calibration

We calibrated the amount of stretch by measuring the displacement of fluorescent beads on top of polyacrylamide gels upon application of stretch as described in the literature (258, 265). A limitation of this is that the image can only be taken in static application and not during cyclic stimulation. From experiments carried out by other colleages, it seems that the first two or three pulses apply much more stretch than the rest. Because of this, I applied 10 minutes of stretch cycles before starting the calibration. If there is an effect, I assumed it would be negligible since in the experiments I performed the system was cycling for 1 hour, much more than two or three cycles.

3.3.3 Optical Tweezers

The optical tweezers setup was developed by the laboratory of Timo Betz in

Münster (259), where I was a visiting student. They consisted on a near-infrared laser in a controlled position by an acousto-optic deflector. When focused on particles with higher refractive index than the media, the system could trap them as described in the literature (259). The force was measured by a force sensor that gave direct access to the value given a pre-calibrated constants.

Software implementation

The software was written by the laboratory of Timo Betz. My contribution was a small state by which we applied the signals in periods of 32 seconds. The reason why we chose this number is multiple. First, the signal cannot be used continuously since the bead is pulled towards the centre of the cell by the rearward flow with a force that exceeds the applicable force of the tweezers (266). Therefore, we needed to stop the signal to reposition the laser at the centre of the bead. The amount of time had to be proportional to the period of all the applicable frequencies, and we needed to minimize the time allocated to take the image and reposition to make it negligible to the total time of the application of the signal. Given these circumstances, the possibilities were 2^n seconds starting at 8s. This first value was too short and made the amount of time allocated to taking the image and repositioning too large in comparison; 16s seemed a good compromise, but I found that I could push to 32s without losing too many beads from the trap. However, 64s was too much and too many beads escaped the trap. Thus, the software first repositioned the laser, then stimulated the bead, then took an image, and repeated, in a state fashion.

Execution

Transfected paxillin-GFP cells were plated on glass slides prepared in an aluminium chamber of 400 µm thickness as limited by the force sensor given by the manufacturer. Another glass coverslip was placed on top sealing the chamber. The previously coated beads were flushed in by an inlet. Since beads with diameters lower than 3 µm do not attach to cells in the absence of force, I trapped floating beads. I then approached to the membrane of cells and started the experiment. This setup was used to measure the reinforcement of the bead-cell system in a similar fashion to magnetic tweezers, while at the same time

monitoring the build-up of the transfected paxillin-GFP to the bead.

Special care needed to be taken with laser power. I used 120 mW of laser power, and consequently used an OD30 filter in the force sensor. Application of too much power could kill the cells.

Calibration

The system was pre-calibrated by the manufacturer.

3.3.4 Single-cell atomic force spectroscopy

The atomic force microscope setup had been used previously in the laboratory (164). Briefly, a cantilever with a specially shaped tip is built in a support. The position of the tip is tightly controlled by means of a piezo actuator and measured with a laser that reflects on the top of the cantilever. This then impacts on a sensor that gives access to the position. By approaching the tip to a substrate and measuring the force-distance curves, the stiffness of substrates can be measured.

Software implementation

The software used was the one provided by JPK.

Execution

As described in chapter 5, we implemented two different kinds of protocols.
First, we adapted the functionalization of beads to the AFM. To do so, we coated silica beads with FN7/10 as described in the literature (164, 173). We then used the protocol to attach microspheres by using UV glue to flat cantilevers.
Second, we adapted the protocol of single cell force spectroscopy from the literature (267). We first coated the flat cantilever tips with concanavalin A. We then trypsinized the cells and resuspended them for them to round up. We subsequently pushed them to an uncoated region in a glass slide and pressed with 3 nN. As the cell attached after 5s, we retracted the tip and waited 5 minutes for the cell to perfectly adapt. We then carried out the experiment.

Special care was taken to seal the controlled temperature chamber in which the experiment was conducted. I resealed the interfaces with nail polish and pushed a thin PDMS membrane in the middle of the plastic-glass interface for the system to close better. If not done, the cantilever had massive drifts that did not allow for consistent measuring, mainly caused by media flows. Not all cells attached, but when successful, the setup was used to measure stiffness and peak force at different cantilever retraction rates.

Calibration

The spring constant of cantilevers was calibrated by thermal noise as described previously (164).

Chapter 4. Results

4.1 Binding of ZO-1 to α5β1 integrins regulates the mechanical properties of α5β1–fibronectin links

Fundamental processes in cell adhesion, motility, and rigidity adaptation are regulated by integrin-mediated adhesion to the extracellular matrix (ECM). The link between the ECM component fibronectin (fn) and integrin α5β1 forms a complex with ZO-1 in cells at the edge of migrating monolayers, regulating cell migration. However, how this complex affects the α5β1-fn link is unknown. Here we show that the α5β1/ZO-1 complex decreases the resistance to force of α5β1-fn adhesive complexes in cells at the edge of migrating monolayers, while also increasing α5β1 recruitment. Those changes can be explained by a ZO-1 mediated increase in both the binding and unbinding rates of α5β1-fn links. Consistently with a molecular clutch model of adhesion, this effect of ZO-1 leads to a decrease in the density and intensity of adhesions in cells at the edge of migrating monolayers. Taken together, our results unveil a new mode of integrin regulation through modification of integrin-ECM binding dynamics, which may be harnessed by cells to control adhesion and migration.

General processes in development, wound healing, or cancer are driven by cell adhesion and migration, which are determined by the interaction between cells and the extracellular matrix (ECM) (268). This interaction is largely mediated by integrins, and specific ECM-integrin links such as those formed by the ECM protein fibronectin (fn) and integrin α5β1 are involved in crucial cellular processes in signalling and mechanotransduction (5, 164). Integrin-mediated functions are regulated by a myriad of integrin-binding adaptor proteins (269, 270), which can affect both their activation and biochemical signalling (230, 271) and their mechanical properties (186, 272, 273). In turn, the affinity and mechanical properties of integrin-ECM links (and specifically of α5β1-fn links, not to be

confused with the multiple chemical bonds binding the two proteins) regulate mechanotransduction, and the ability of cells to both transmit forces to the substrate and transduce them into downstream biochemical signals (164, 243). Thus, regulation of integrin mechanics by adaptor protein interactions emerges as a potential way to tune mechanotransduction.

An adaptor protein described to bind to α5β1 is tight junction protein ZO-1, which is generally localized to cell-cell adhesions (274, 275) but binds to the α5 subunit of α5β1 (143, 144). The formation of this complex affects cell motility (144), and is crucial for cytokinesis (9). The formation of the α5β1/ZO-1 complex is mediated by PKCε-dependent phosphorylation of ZO-1. Once phosphorylated, ZO-1 then translocates to cell lamellipodia, but only in subconfluent cells. This interaction is believed to stabilize and polarize cells since if disrupted, directional persistence and migration velocity are modified in different cell types (144, 151). Interestingly, both alterations in α5β1 and ZO-1 are related to malignant phenotypes (276, 277). Thus, ZO-1 acts as a regulator of α5β1 integrins, and we hypothesized that its effect could be mediated by changes in mechanical properties of the α5β1-fn link.

Disruption of the α5β1/ZO-1 complex affects cell motility

In this study we used the human mammary epithelial cell line (MCF10A) that is a well-established model for cell migration. To check that ZO-1 was translocating to the lamellipodia of cells at the edge of monolayers, we seeded a monolayer of cells on 12 kPa gels coated with 10 μg ml^{-1} of fn and stained them for activated β1 and ZO-1. As previously described (144), ZO-1 localized to cell-cell contacts in confluent cells, and to the lamellipodia in cells at monolayer edges (Figure 22A). Co-localization with α5β1 only occurred at the level of lamellipodia (Figure 22A, B, C).

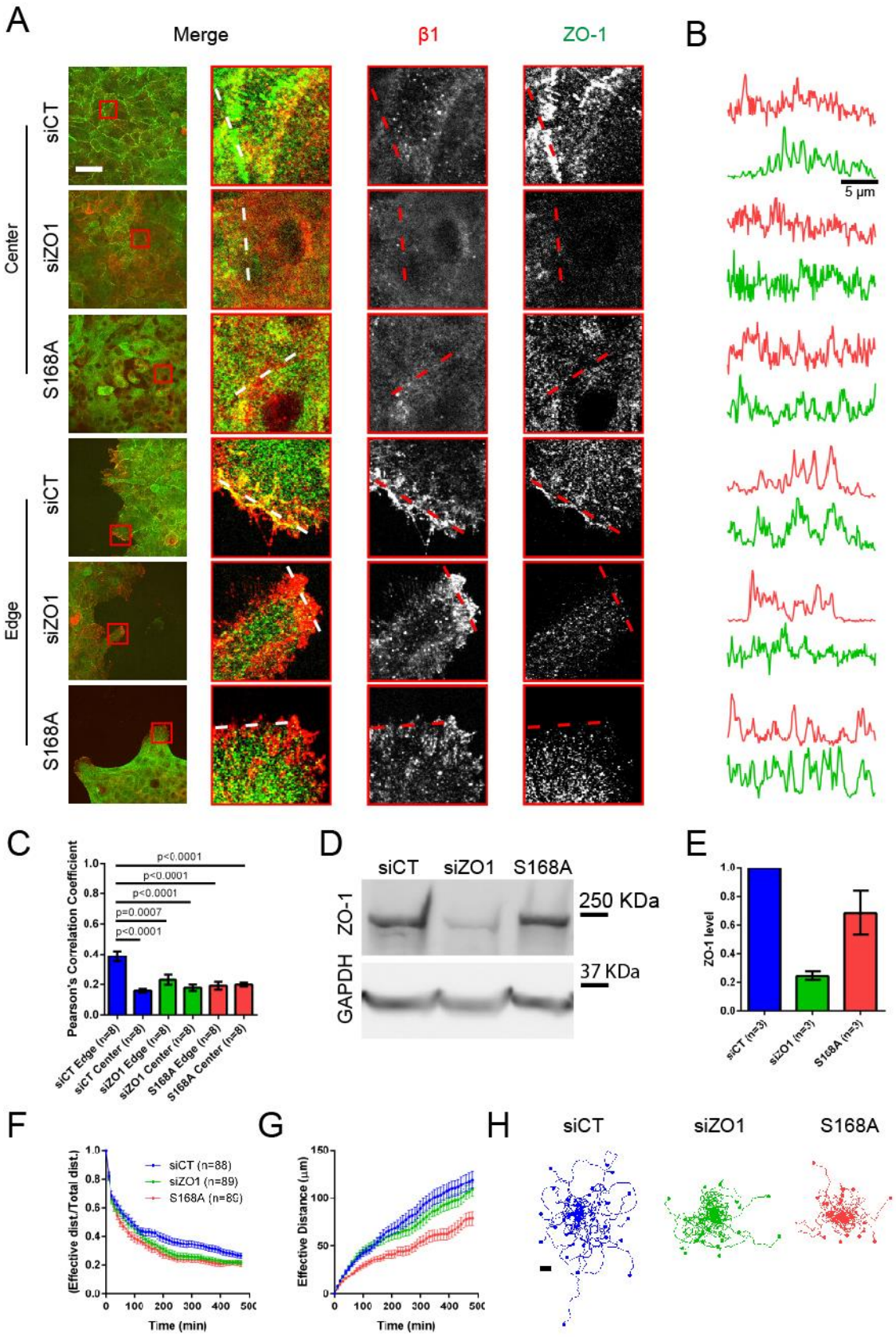

Figure 22: ZO-1 forms a complex with α5β1 at the edge of monolayers that affects cell motility.

(A) ZO-1 and α5β1 staining of cells at the edge and center of monolayers seeded on 12 kPa gels coated with fn. FLAG antibody was used to stain for ZO-1 S168A. Insets show the area marked with a red square. Scale bar is 50 μm. (B) Normalized profile plots of the ZO-1 and α5β1 intensity profiles shown in the red lines in A. Scale bar is 5 μm. (C) Pearson's correlation coefficient of ZO-1 and α5β1 stainings at the edge and at the center of monolayers. (D) ZO-1 western blot of cells transfected with non-targeting siRNA (siCT), ZO-1 siRNA (siZO-1) and the ZO-1 plasmid (S168A). (E) Quantification of the western blot of cells transfected with non-targeting siRNA (siCT), ZO-1 siRNA (siZO-1) and the ZO-1 plasmid (S168A). (F) Directional persistence of migrating single cells (effective distance/total distance) on 12 kPa gels coated with fn. Significant differences were found between siCT and other conditions ($p = 0.0003$). (G) Effective distance of migrating single cells on 12 kPa gels coated with fn. Significant differences were found between S168A and other conditions ($p < 0.0001$). (H) Migrating single cell tracks (480 minutes) for each condition (n=30). Error bars represent the s.e.m. of n number of data points. Images representative from 3 experiments.

To study the effects of the α5β1/ZO-1 complex we impaired its formation by using a combination of siRNA targeting ZO-1 (siZO1) and independently by transfecting a dominant negative ZO-1 plasmid (S168A) that impairs binding of endogenous ZO-1 to α5 (9, 144). As a control, we used cells transfected with a non-targeting siRNA (siCT). ZO-1 concentrations were lowered to around 25% in siZO1, and only slightly affected in S168A-transfected cells (Figure 22D, E). ZO-1 had reduced expression in siZO1 cells both at the center and at the edge of monolayers (Figure 22A). Consistently with its reported inability to bind α5, S168A did not localize to lamellipodia, nor co-localize with α5β1 in any case (Figure 22A, B, C). Confirming the dominant negative effect of S168A, total ZO-1 in S168A cells was also unable to localize to lamellipodia (Suplement, Figure 26).

Previous studies have demonstrated a role of the α5β1/ZO-1 complex in cell migration in different cancer cell lines, but its role in normal mammary epithelial cell is poorly understood (144). To assess this, we seeded cells on the same 12 kPa gels. We then tracked the cells for 8 hours and assessed their directional persistence as the ratio between their effective travelled distance (radial distance from the starting point) and their total travelled distance (sum of the total path). As previously shown, siZO1 and S168A cells were significantly less directional than siCT (Figure 22F, G, H).

Thus and in agreement of previous work (144), our data confirmed that ZO-1 localizes to the lamellipodia of monolayer edge cells, and depleting ZO-1 or preventing its association with α5 affects cell migration.

ZO-1 binding to α5 decreases integrin-fn adhesion resistance to force

To investigate if ZO-1 binding to α5β1 affected the α5β1-fn link, we used a setup based on magnetic tweezers. We first coated superparamagnetic beads with FN7-10, a fn fragment (Coussen et al., 2002; Elosegui-Artola et al., 2014), which binds mechanically to cells primarily through α5β1 (278). We allowed beads to attach to cell monolayers for 35 minutes, and then pulled on them using the magnetic tweezers with a force of 0.5 nN until beads detached, both at the subconfluent edge and at the center of monolayers (Figure 23A, B).

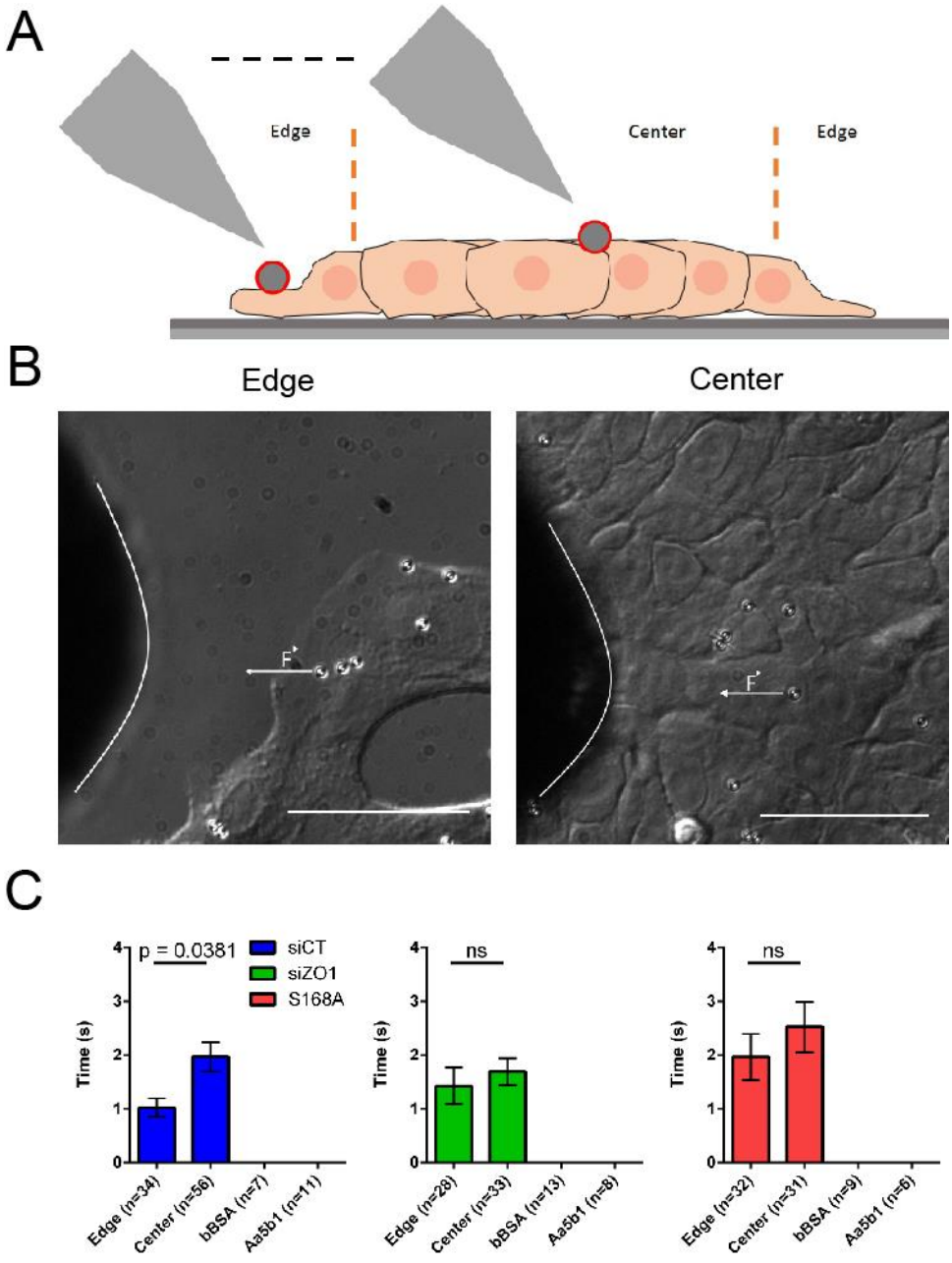

Figure 23: Disruption of the α5β1/ZO-1 complex increases α5β1-fn link resistance to forces only at the edge of monolayers.

(A) Cartoon depicting the experimental setup with magnetic tip pulling on beads attached to cells both at the edge and center of cell monolayers. (B) Magnetic tip applying a magnetic field producing 0.5 nN of force to beads, both at the edge (left) and at the center (right) of monolayers. (C) Time taken to detach beads for each condition either at the center or at the edge of monolayers. Beads were coated with FN7-10 (with or without incubating with an α5β1 blocking antibody, (Aα5β1) or bBSA. Scale bar is 50 μm. Images f. 4 exp.

In siCT cells, bead detachment times significantly decreased at monolayer edges with respect to the monolayer center (Figure 23C). This difference was lost both in siZO1 cells and in cells transfected with S168A, showing that this differential regulation is mediated by ZO-1, and by its ability to bind α5. As negative controls, beads detached immediately when coated with either biotinylated bovine serum albumin (bBSA), or with FN7-10 in cells preincubated with an α5β1 blocking antibody (Aα5β1) (Figure 23C). This indicates that the measured adhesion strength was specific to fn, and mediated by α5β1 integrins.

Formation of the α5β1/ZO-1 complex increases α5β1-fn recruitment

The measured effects in adhesive strength could be mediated by changes in the resistance to force of integrin-fn links, or by changes in integrin recruitment. To assess potential changes in integrin recruitment, we incubated non-fluorescent FN7-10 coated silica beads with cells (164), fixed the cells, and stained them for ZO-1 and activated β1 (Figure 24A) and total β1 (Suplement, Figure 27). All conditions showed recruitment of activated and total β1 to beads (Figure 24B and Suplement, Figure 27) both at the edge and at the center of monolayers. Further, beads at the edge of siCT cells increased recruitment of ZO-1 and active (but not total) β1 with respect to the center (Figure 24B and Suplement, Figure 27). Thus, whereas the interaction between ZO-1 and α5β1 occurring specifically at monolayer edges does not affect total integrin population, it increases the recruitment of the active fn-bound α5β1 integrins.

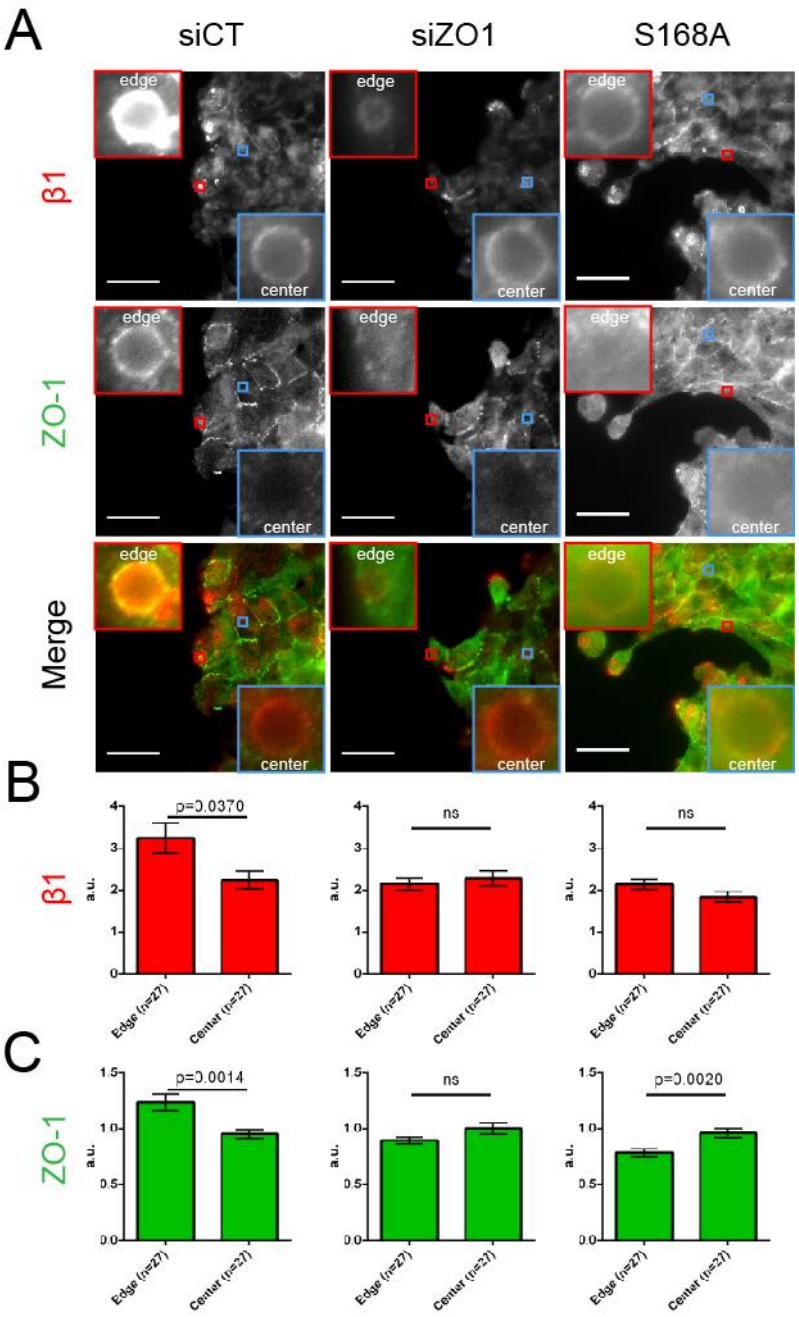

Figure 24: Disruption of the α5β1/ZO-1 complex decreases α5β1-fn recruitment at the edge of monolayers.

(A) β1 and ZO-1 staining of silica beads coated with FN7-10 attached to monolayers. (B) β1 recruitment to silica beads coated with FN7-10 attached at the edge and at the center of monolayers. (C) ZO-1 recruitment to silica beads coated with FN7-10 attached at the edge and at the center of monolayers. FLAG antibody was used to stain for ZO-1 S168A. Scale bar is 50 µm. Insets show the area marked with red/blue squares. Images representative from 3 experiments.

In summary, the interaction between ZO-1 and α5β1 specific to monolayer edges affected α5β1-fn links by increasing their recruitment, but reducing their resistance to force. This shows that cell-bead detachment under force is regulated by the off-rate of the link, and not by the recruitment (or affinity) which would lead to the opposite result. Further confirming this direct link to the properties of integrin-fn links, neither bead detachment times nor integrin recruitment were affected by impairing cell contractility with blebbistatin (Supplement, Figure 28). Thus, our results are consistent with ZO-1 affecting α5β1-fn links specifically at monolayer edges, both by increasing their off-rates (thereby reducing resistance to force) but also their on-rates (thereby increasing recruitment).

Adhesion formation is affected by the α5β1/ZO-1 complex

According to our previously described molecular clutch model of adhesion formation (164), a concomitant increase in both on- and off- rates (as induced by ZO-1) should decrease force loading in integrins, impairing mechanotransduction, subsequent force transmission, and formation of adhesions. We did not observe changes in force transmission in the different conditions (Supplement, Figure 29), possibly because the potential decrease mediated by ZO-1 was compensated by increased myosin phosphorylation in siCT cells compared to other conditions (Supplement, Figure 28). However and consistent with model predictions, the number and intensity of paxillin-rich adhesions at monolayer edges decreased in siCT cells when compared with siZO-1 cells and cells transfected with S168A (Figure 25A, B). As expected, we did not observe differences in adhesion formation at the centre of monolayers (Figure 25A). Interestingly, even though their intensity and density was lower (Figure 25B, C), adhesions in siCT cells were significantly longer than in other conditions (Figure 25D). This suggests that mechanical regulation of the α5β1-fn link by ZO-1 may readily explain adhesion formation but not later maturation processes, which may depend on other factors (171).

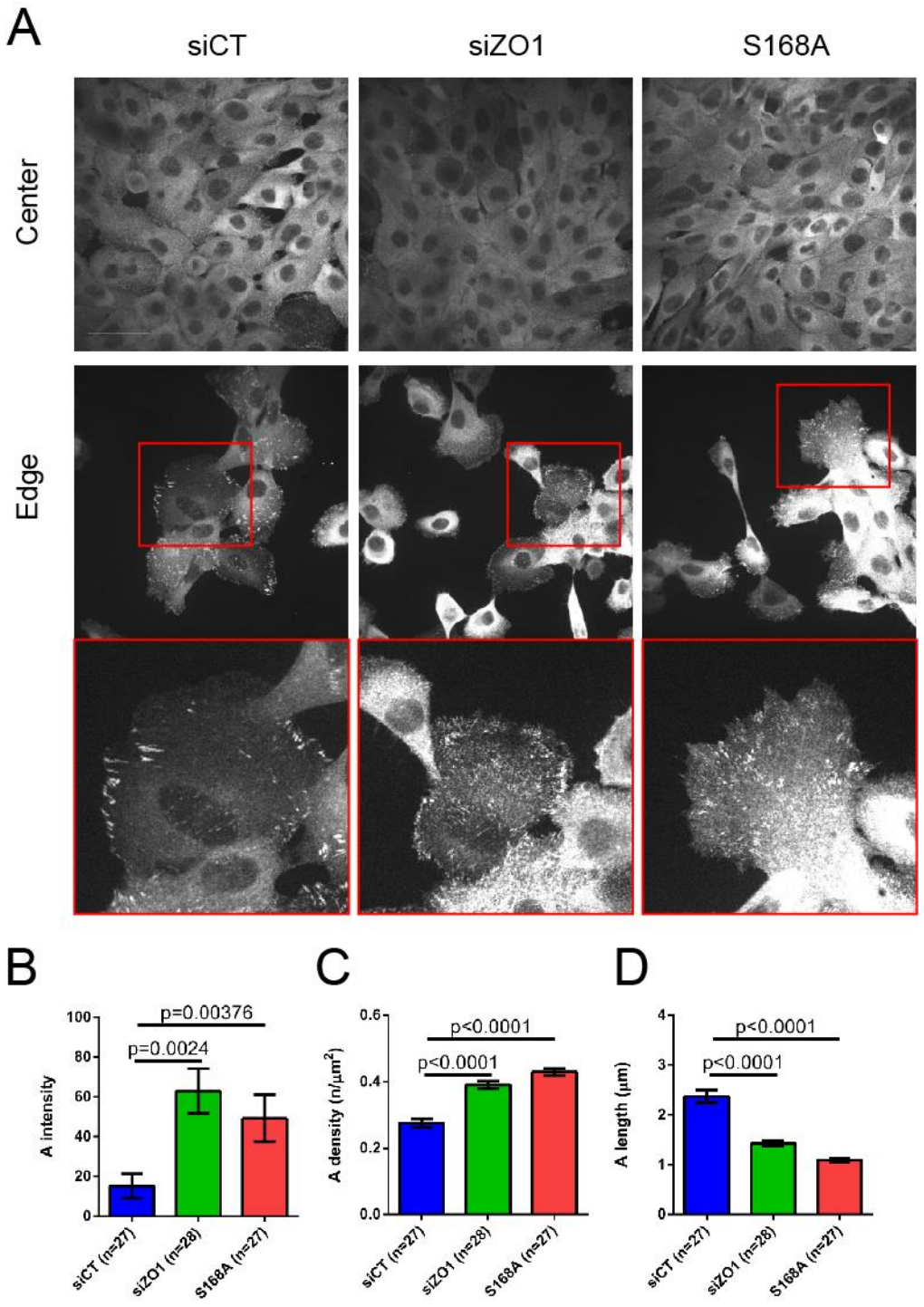

Figure 25: Disruption of the α5β1/ZO-1 complex leads to a higher number of smaller nascent adhesions.

(A) Paxillin staining at the subconfluent edge and at the center of monolayers. (B) Quantification of adhesion intensity. (C) Quantification of adhesion density. (D) Quantification of adhesion length. Scale bar is 50 µm. Insets show the area marked with a red square. Images representative from 3 experiments.

Supporting information

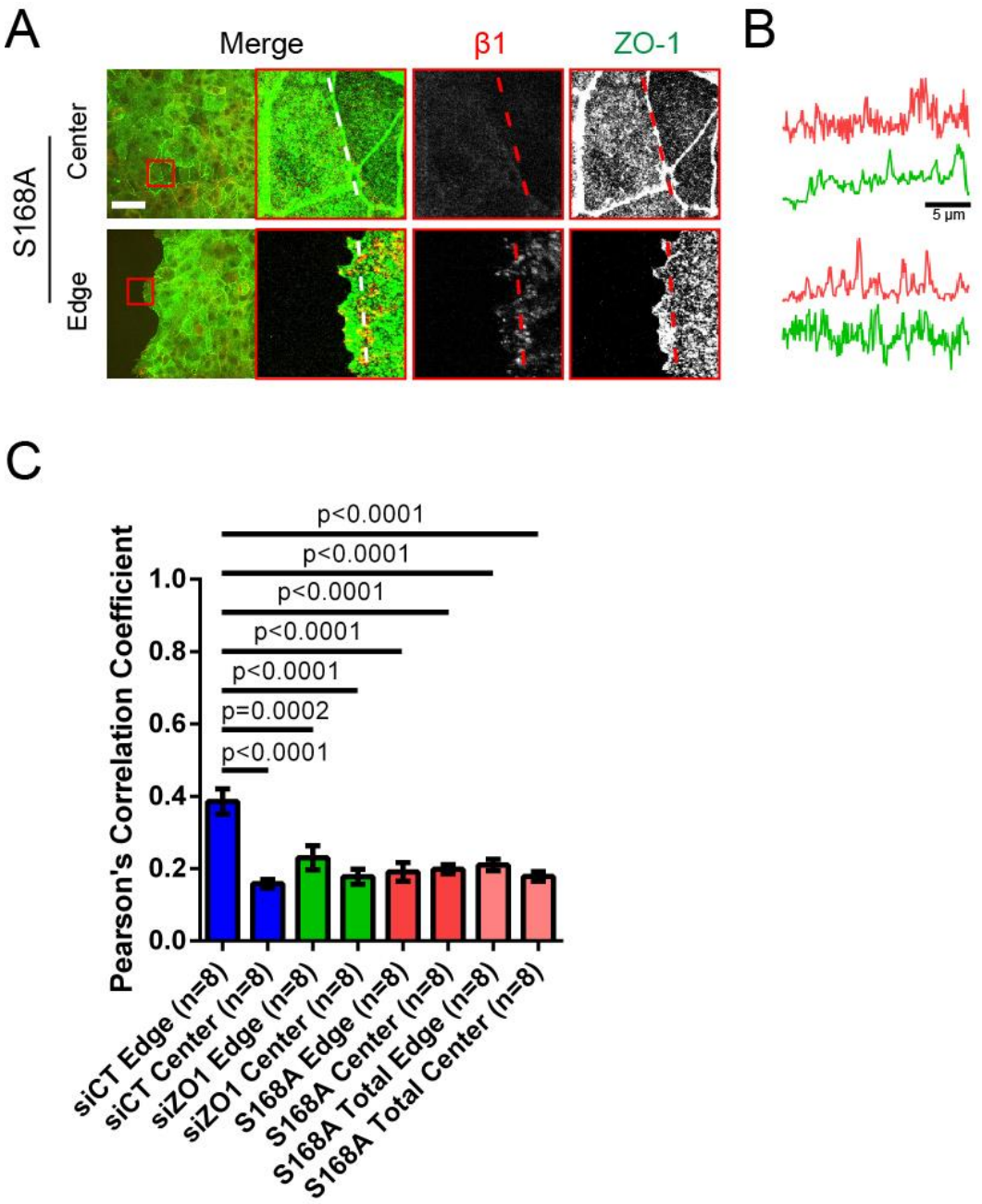

Figure 26: For S168A, total ZO-1 does not co-localize with α5β1 and localizes to cell-cell adhesions.

(A) Total ZO-1 and α5β1 staining of cells at the edge and center of monolayers seeded on 12 kPa gels coated with fn. Insets show the area marked with a red square. Scale bar is 50 µm. (B) Normalized profile plots of the ZO-1 and α5β1 staining. Scale bar is 5 µm. (C) Pearson's correlation coefficient of ZO-1 and α5β1 stainings at the edge and at the center of monolayers (including data in Figure 22). Images representative from 3 experiments.

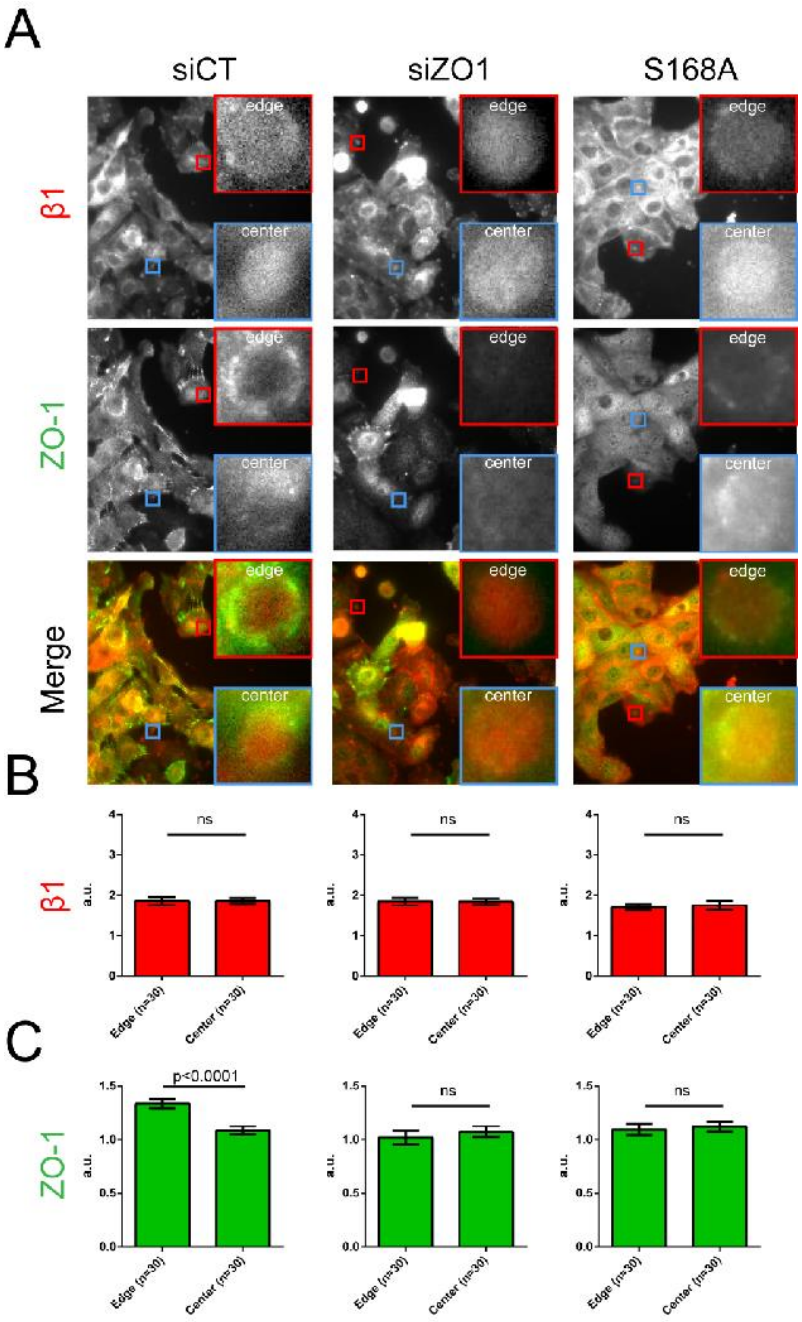

Figure 27: Disruption of the α5β1/ZO-1 complex does not decrease the recruitment of the total fraction of α5β1-fn at the edge of monolayers.

(A) Total α5β1 and ZO-1 staining of silica beads coated with FN7-10 attached to monolayers. (B) Total α5β1 recruitment to silica beads coated with FN7-10 attached at the edge and at the center of monolayers. (C) ZO-1 recruitment to silica beads coated with FN7-10 attached at the edge and at the center of monolayers. Scale bar is 50 µm. Insets show the area marked with red/blue squares. Images representative from 3 experiments.

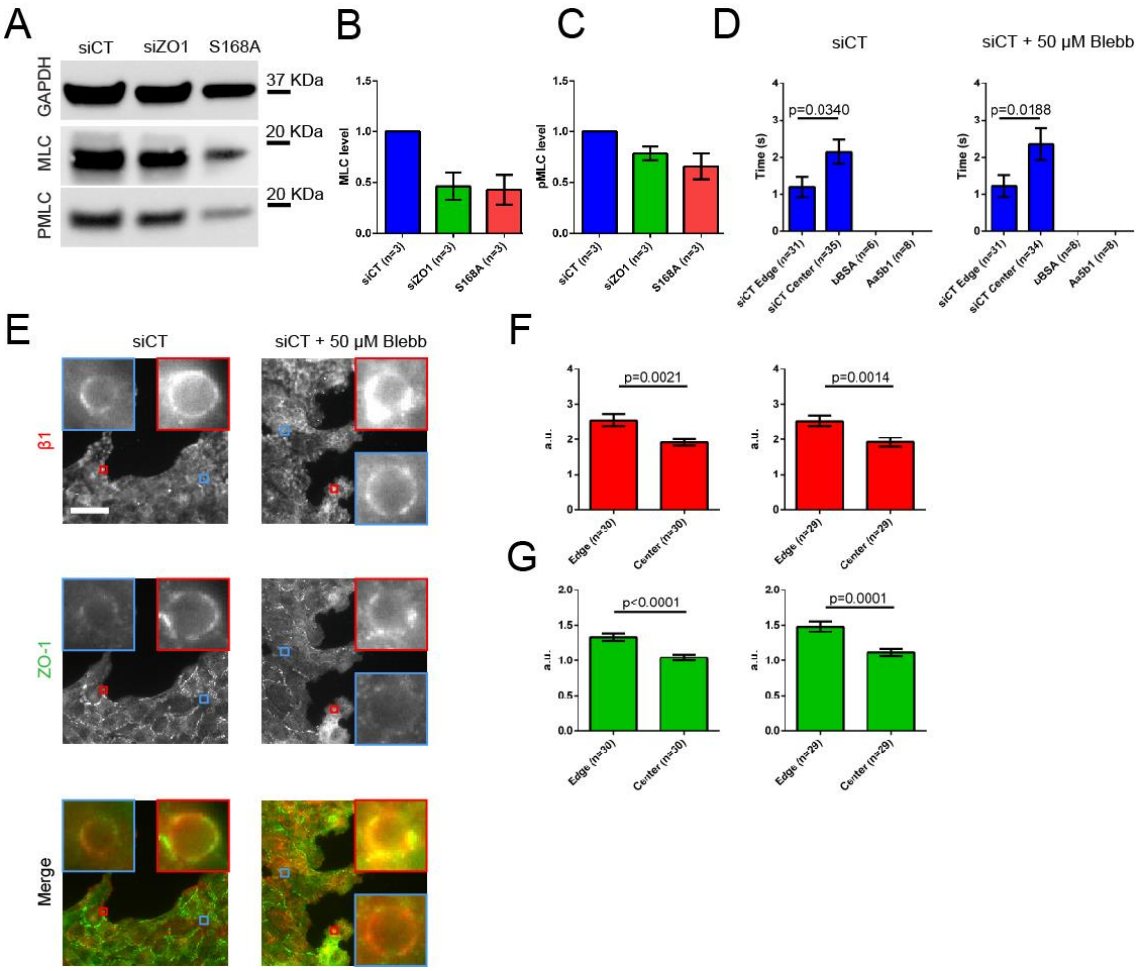

Figure 28: Disruption of the α5β1/ZO-1 complex decreases cell contractility, but contractility alone does not affect recruitment of α5β1 or bead detachment time.

(A) Western blot bands of pMLC for siCT, siZO1 and S168A. (B) Quantification of the western blot of MLC for siCT, siZO1 and S168A. (C) Quantification of the western Blot of pMLC for siCT, siZO1 and S168A. (D) Time taken to detach beads for siCT and siCT + 50 µM of blebbistatin either at the center or at the edge of monolayers. Beads were coated with FN7-10 (with or without incubating with an α5β1 blocking antibody, Aα5β1) or bBSA. (E). α5β1 and ZO-1 staining of silica beads coated with FN7-10 attached to monolayers. (F) α5β1 recruitment to silica beads coated with FN7-10 attached at the edge and at the center of monolayers. (G) ZO-1 recruitment to silica beads coated with FN7-10 attached at the edge and at the center of monolayers. Scale bar is 50 µm. Insets show the area marked with red/blue squares. Images f. 3 transfections.

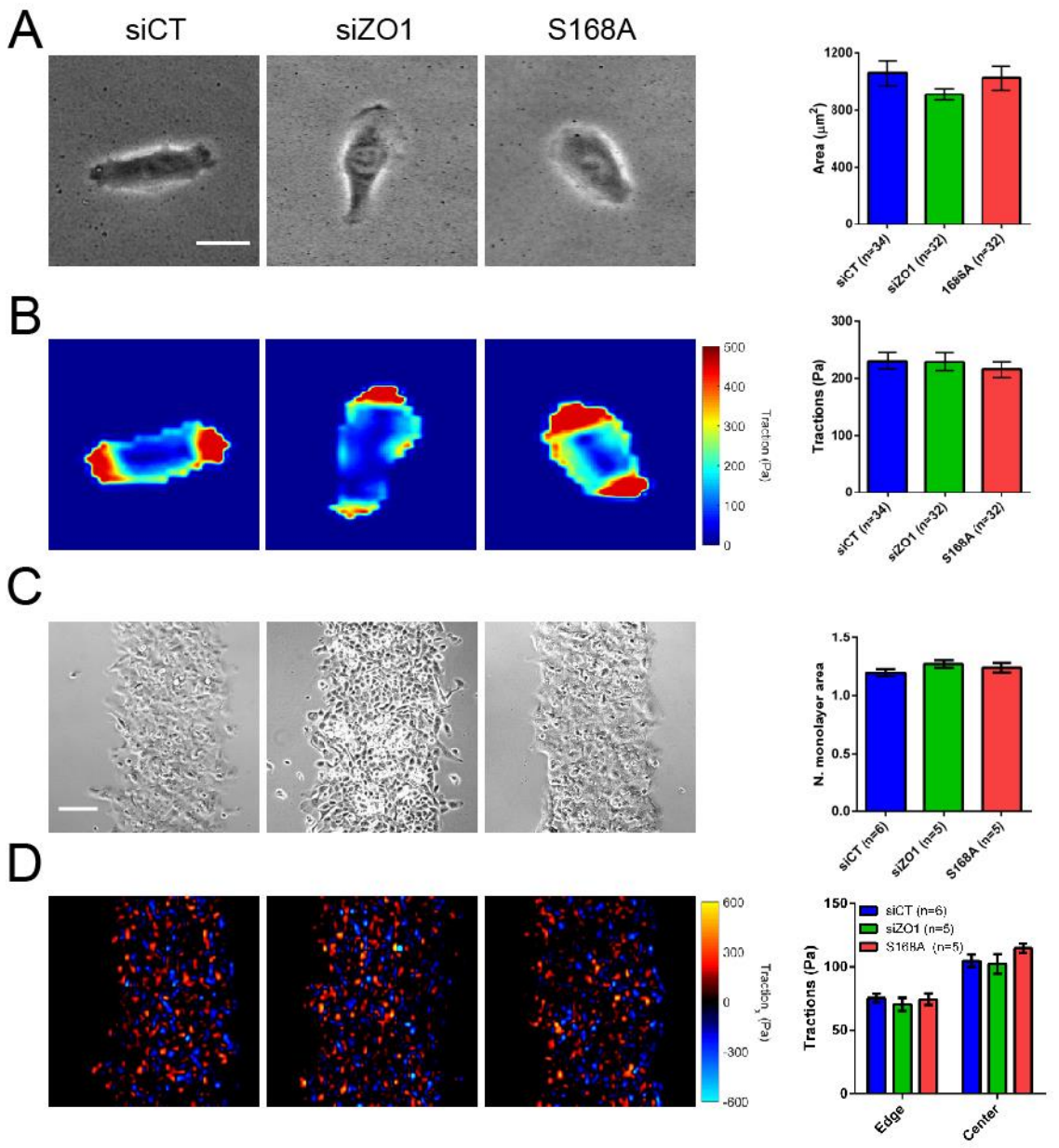

Figure 29: Disruption of the α5β1/ZO-1 complex does not impair generation of cell tractions.

(A) Phase contrast images of cells plated on 12 kPa gels coated with fn, and quantification of cell area. (B) Cell traction maps and quantification of mean cell traction. (C) Phase contrast images of migrating cell monolayers at 4h of expansion plated on 12 kPa gels coated with fn, and quantification of monolayer area. (D) Migrating cell monolayer at 4h traction maps and quantification of mean monolayer traction at the edge (30 µm edge) and at the center. Scale bar is 10 µm for single cells and 100 µm for cell monolayers. Images representative from 3 experiments.

4.2 Force loading rate drives mechanosensing

Cell response to force regulates essential processes in health and disease. However, the fundamental mechanical variable that cells sense and respond to remains unclear. It has been proposed that this variable could be the force transmitted between cells and their surrounding extracellular matrix (ECM), the ECM deformation resulting from those forces, or a combination of both. Instead, here we show that the rate of force application (known as the loading rate) is the fundamental driver of mechanosensing. By applying different dynamic force regimes to cells through substrate stretching, optical tweezers, and atomic force microscopy, we find that increasing loading rates trigger talin-dependent mechanosensing, leading to adhesion growth and reinforcement, and YAP nuclear localization. However, if the associated cell deformation rates are higher than a given threshold, the cytoskeleton softens (fluidizes), decreasing force loading rates and preventing reinforcement. By stretching rat lungs *in vivo* at different rates, we show that this mechanism is also translated to the organ level. Taken together, our results show that the force loading rate drives mechanotransduction both *in vitro* and *in vivo*, in a process driven by the coupling between cytoskeletal reinforcement and fluidization.

Cells are constantly subjected to forces transmitted through tissues (231, 287), which regulate major processes in health and disease (232, 233). Despite this importance, the fundamental mechanical variable that cells sense and respond to is unknown, and has been a matter of intense debate (254, 256, 288). Mechanosensing molecules such as the integrin-actin adaptor protein talin respond to specific values of applied force (201), but it has been suggested that cells respond not directly to force but to the associated deformations exerted on the extracellular matrix (ECM) (254, 289) or even to a combination of force and deformation (255, 256). However, in most physiological scenarios, forces and deformations are highly dynamic (102, 236, 247, 257), and a sensing system based on a given fixed magnitude of force or deformation may not be effective.

Alternatively, cells could be sensitive to force dynamics per se. Specifically, force

sensitive molecular events such as bond rupture (251, 252) or protein unfolding (253) have long been predicted and measured to depend on the rate of force application, known as the loading rate. This dependency is in fact an implicit underlying assumption of the molecular clutch theory, which has been employed to model how cells generate and transmit forces to sense passive mechanical factors such as ECM rigidity (243, 244), viscosity (167), or ligand density (166). In this framework, changes in such passive mechanical factors regulate the loading rate, affecting molecular events such as integrin-ECM binding or talin unfolding (201, 243). This hypothesis is attractive in that it relates cell sensing of passive ECM mechanical factors to the sensing of directly applied forces, in a unified mechanism. However, whether the loading rate is indeed the driving parameter of mechanosensing is unknown.

To address this issue, we seeded mouse embryonic fibroblasts on very soft (0.6 kPa in rigidity) fibronectin-coated polyacrylamide gels. We then used a previously described device (258) (Figure 30 a) to stretch the gels, thereby applying a mechanical stimulus well known to trigger mechanosensing (95, 290).

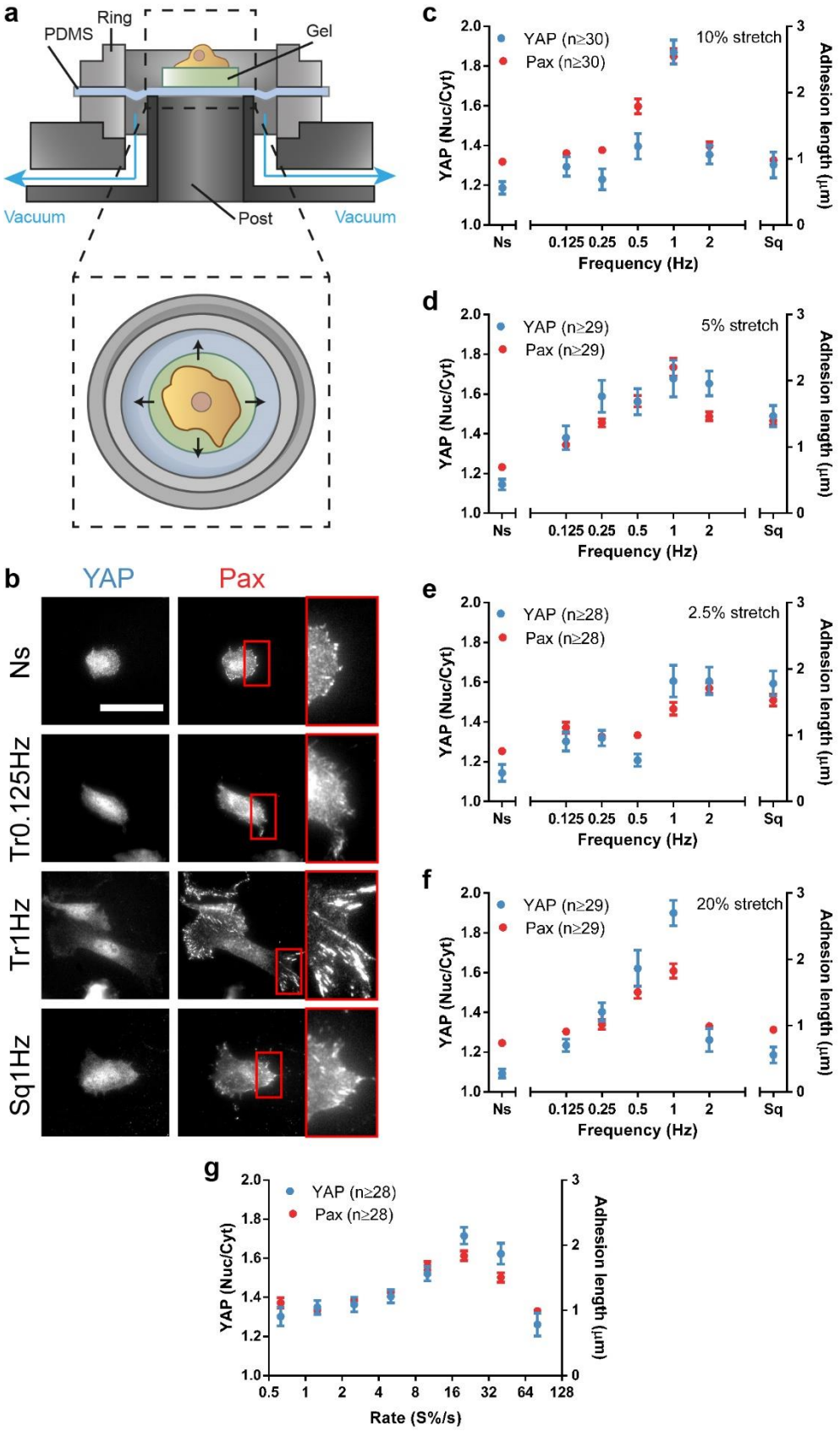

Figure 30: The rate of cell stretch drives mechanosensing in a biphasic manner.

a, Illustration of the stretch setup. **b**, YAP and paxillin stainings of cells stretched by 10% using the setup using triangular (Tr) and square (Sq) signals at different frequencies. Ns, non-stretched cells. In the paxillin image, areas circled in red are shown magnified at the right. **c-f**, Quantifications of YAP nuclear to cytoplasmic ratios and focal adhesion lengths for cells stretched at 10% (c), 5% (d) 2.5% (e), and 20% (f). Results are shown for non-stretched cells (Ns), cells stretched with triangular signals at different frequencies, and cells stretched with a square signal at 1 Hz. **g**, Data from triangular signals in c-f grouped as a function of the applied stretch rate (stretch amplitude times frequency). Scale bar is 50 µm.

Using this device, we controlled the rate of stretch independently of the stretch magnitude by applying cyclic triangular loading/unloading signals with the same amplitude, but with increasing frequencies from 0.125 to 2 Hz (Supplement, Figure 34 a-h). After stretching cells for one hour and then fixating them, we carried out stainings to monitor the growth of paxillin-containing cell-matrix adhesions, and the nuclear translocation of the transcriptional regulator YAP, two well-known mechanosensitive events (238, 291). Cells either non-stimulated or stimulated at 10% stretch with low frequencies showed largely cytosolic YAP and only small punctate paxillin-containing adhesions, indicating that mechanosensing was not triggered (Figure 30 b,c, and Suplement, Figure 35 c-e). Increasing the frequency progressively stimulated cells to translocate YAP to the nucleus and to form long adhesions. This mechanosensing response was mediated by the mechanosensitive protein talin (243), since its knock-down eliminated both responses (Suplement, Figure 35 c-f). However, increasing the frequency only increased response up to a point: above 1 Hz, fast stretching failed to trigger adhesion growth or YAP nuclear translocation (Figure 30 b,c). To decouple the effect of the stretch rate from that of the number of stretch cycles applied (which increased with frequency), we stretched cells at a frequency of 1 Hz, but instead of applying a progressive triangular signal, we applied stretch as fast as possible. This led to a quasi-square signal where the stretch rate more than doubled with respect to the corresponding triangular signal, and was thereby slightly above that of the triangular 2 Hz signal (Suplement, Figure 34 b,h).

Accordingly, applying a square rather than triangular 1 Hz signal abrogated the paxillin and YAP response, shifting the results to values even below the 2 Hz triangular signal (Figure 30 b,c).

To further control the stretch rate, we repeated the frequency sweep by applying different amounts of stretch, from 2.5% to 20% (Figure 30 d-f). Progressively decreasing/increasing the stretch amplitude led to lower or higher responses at low frequencies, respectively. Interestingly, decreasing the stretch amplitude also progressively eliminated the decrease in mechanosensing responses triggered at high frequencies, completely eliminating the 1 Hz peak in the case of 2.5% stretch. After grouping the data, a clear biphasic Pax/YAP response was observed as a function of the stretch rate (i.e., stretch magnitude times frequency, Figure 30 g) but no clear response was observed as a function of the cumulated magnitude of stretch (i.e., stretch magnitude times number of applied cycles, Suplement, Figure 35 a).

Whereas these results clearly show a role of stretch rate independent of its magnitude, they do not discriminate between possible effects of the force loading rate and the cell deformation rate, both of which increase with stretch frequency. Further, they do not discriminate either between cell-scale effects and local mechanosensing effects, which can be triggered at the single adhesion level (291, 292). To address these fundamental questions, we used a previously described optical tweezers setup (259) (Figure 31 a).

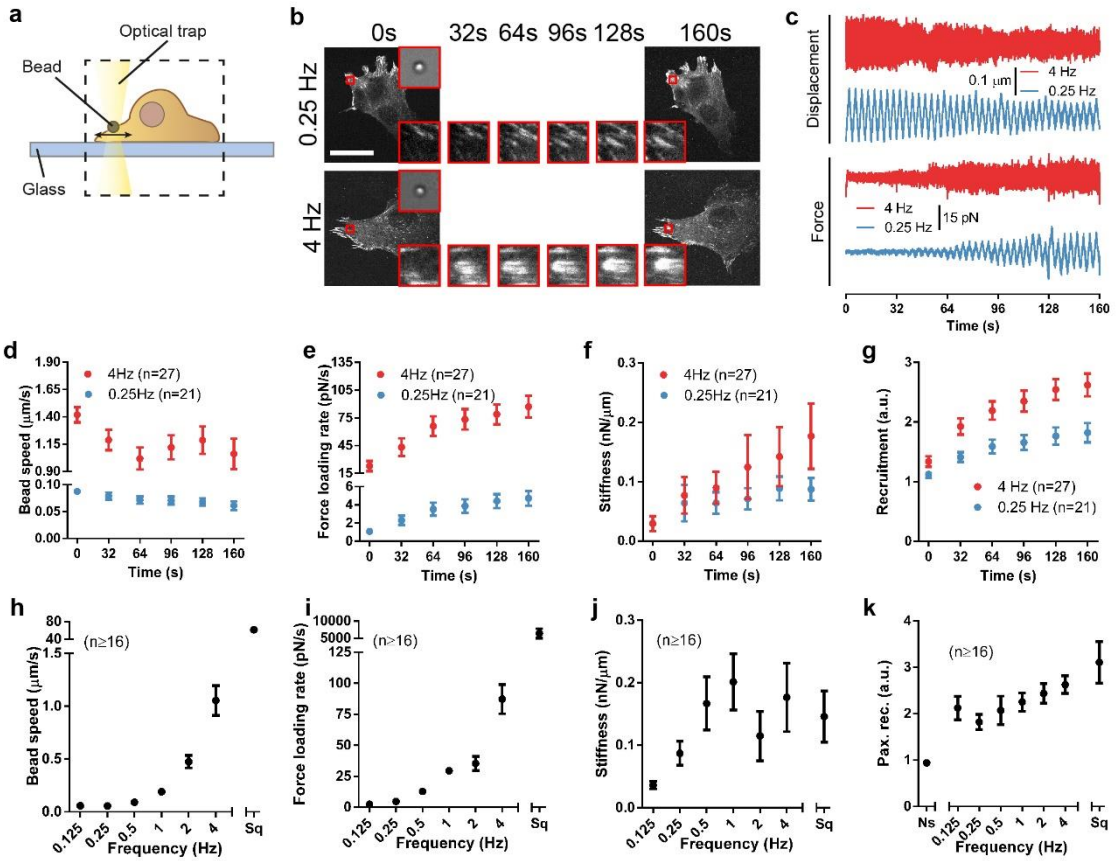

Figure 31: The loading rate of force application to single adhesions drives their maturation.

a, Illustration of the optical tweezer setup. **b**, Images of cells transfected with GFP-paxillin during force application with triangular signals at 0.25 Hz and 4 Hz, shown as a function of time. The area circled in red indicates the position of the stimulated bead, which is shown magnified at the top-right corner (brightfield image) and bottom-right corner (GFP-paxillin image). Magnified GFP-paxillin images are shown at different timepoints. **c,** Example traces of displacement and forces for beads stimulated at 4 Hz and 0.25 Hz. **d-g**, Bead speed (d), force loading rate (e), stiffness (f), and recruitment of GFP-paxillin at beads (g) as a function of time for beads stimulated at 4 Hz and 0.25 Hz. **h-k,** Bead speed (h), force loading rate (i), stiffness (j), and recruitment of GFP-paxillin at beads (k) for beads at the end of the experiment (160s) for all conditions. Scale bar is 50 µm.

We seeded cells transfected with GFP-paxillin on glass, trapped fibronectin-coated 1 µm diameter beads, attached them to the cell surface, and applied

forces to cells by displacing the optical trap horizontally with triangular signals of the same amplitude, but different frequencies (Figure 31 b,c, and Suplement, Figure 36 a). Initially, this stimulation led to bead displacements of ~0.2 μm and applied forces of 10-15 pN, which did not show any significant trend with frequency (Suplement, Figure 36 b-d). With time, force application led to the mechanosensing process known as adhesion reinforcement (Figure 31 b). This was characterized by a progressive reduction in bead displacements (Figure 31 c) and speeds (Figure 31 d), a measure of applied deformation rates. Concomitantly, there was an increase in applied forces (Figure 31 c), loading rates (Figure 31 e), the effective stiffness of beads (the ratio between forces and displacements, Figure 31 f), and recruitment of paxillin to beads (Figure 31 b,g). As previously described (292), unstimulated beads did not recruit paxillin (Figure 31 b,k). High frequencies led to higher deformation rates (speed), loading rates, bead stiffness, and paxillin recruitment than low frequencies (Figure 31 h-k). However, and unlike in the case of stretch, the response was monotonic, and no decrease in reinforcement or paxillin recruitment was observed even at very high frequencies (Figure 31 k). Applying a square rather than triangular 1 Hz signal dramatically increased force loading rates by almost two orders of magnitude (Figure 31 i). Accordingly, it increased, rather than decreased, paxillin recruitment (Figure 31 k).

These results are consistent with a role of the loading rate, which unlike the deformation rate, increased concomitantly with paxillin recruitment both with time (within each experiment) and with frequency. Overall, our data thus suggest that loading rates drive mechanosensing/reinforcement at the local adhesion scale, whereas an additional mechanism abrogates cell-scale response to very high stretch rates. We hypothesized that this additional mechanism could be related to fluidization, the process by which deformations applied to the cytoskeleton partially disrupt it, making it softer (293, 294). Fluidization has been described to depend both on the rate (295) and magnitude (294) of applied deformation, thereby potentially explaining why the decrease in stretch-induced mechanosensing was only observed above a threshold stretch frequency, but also depended on the degree of applied stretch (Figure 30 c-f). Thus, at high

levels of stretch or stretch rates, cytoskeletal softening would reduce the loading rates being applied to adhesions, since loading rates depend not only on the rate of deformation but also on the stiffness of the structure being deformed. In optical tweezers experiments, applied cytoskeletal deformations likely remain too low to induce fluidization.

To test whether increased deformation rates lead to fluidization, we attached cells in suspension to a flat Atomic Force Microscope (AFM) cantilever, placed them in contact with a fibronectin-coated glass, and pulled at different speeds (Figure 32 a,b).

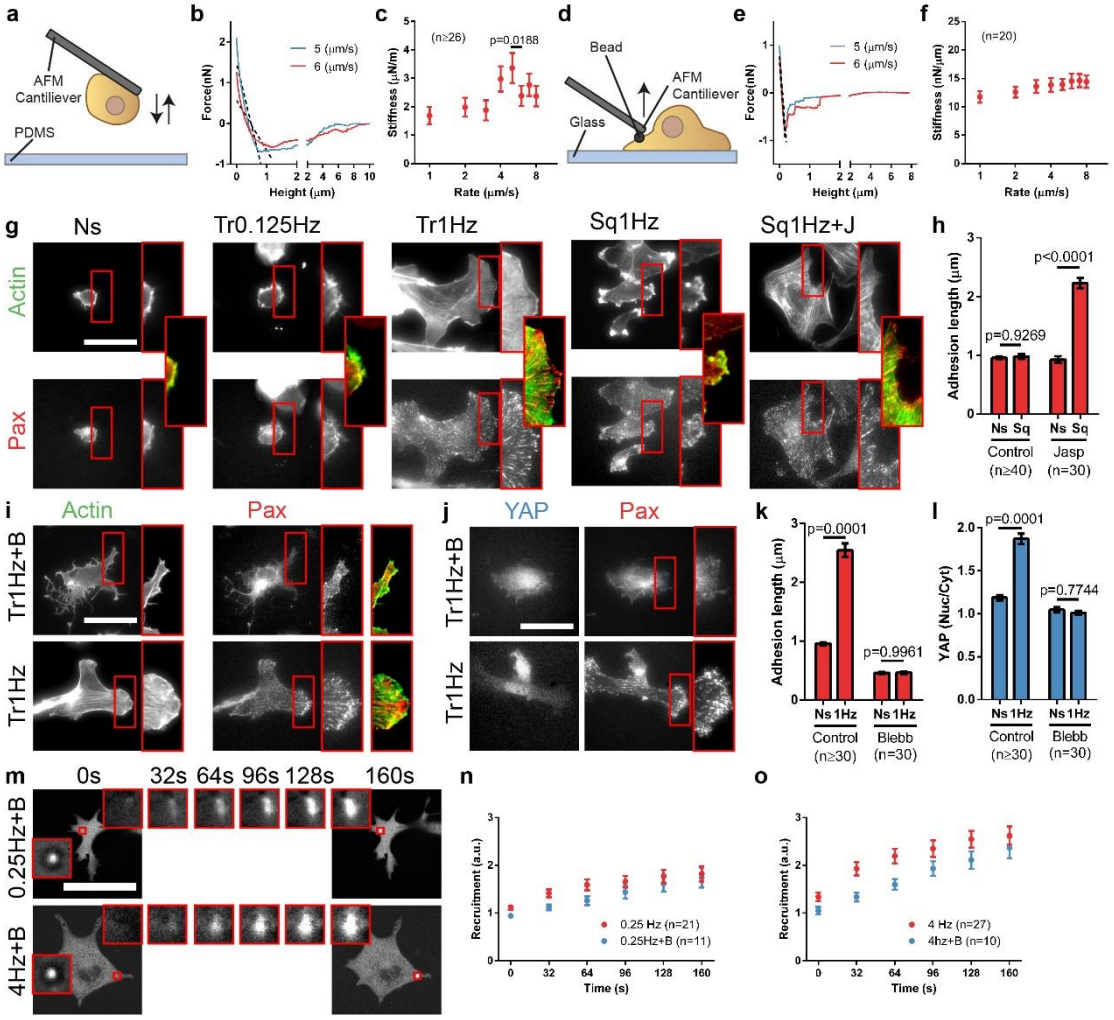

Figure 32: The force loading rate induces mechanosensing, but is limited by cytoskeletal fluidization at high deformation rates.

a, Illustration of the single cell AFM setup. **b**, Example cantilever retraction curves of the single cell AFM experiments. Dashed lines show the slope of the force/deformation curves used to calculate effective stiffness values. **c**, Stiffness

as a function of the retraction speed for cells attaching to a fibronectin-coated substrate. **d,** Illustration of the bead AFM setup. **e,** Example cantilever retraction curves of AFM experiments. **f,** Stiffness as a function of the retraction speed for fibronectin-coated beads attaching to cells. **g**, Actin and paxillin stainings for cells either not stretched or stretched by 10% with triangular signals (0.125 Hz, 1 Hz) or square signals (1 Hz, with or without Jasplakinolide treatment). Areas circled in red are shown magnified at the right of each image, and shown as a merged image (actin, green, paxillin, red). **h**, Quantification of the adhesion length for control cells, and cells treated with Jasplakinolide. **i**,**j** Actin and paxillin (i) and YAP and paxillin (j) stainings for cells stretched by 10% with a triangular 1 Hz signal, with or without blebbistatin treatment. **k,l,** Corresponding quantifications of adhesion length (k) and YAP nuclear to cytosolic ratios (l). **m,** Images of blebbistatin-treated cells transfected with GFP-paxillin during force application with triangular signals at 0.25 Hz and 4 Hz, shown as a function of time. Areas circled in red are shown magnified at different timepoints. **n,o,** Corresponding quantifications of recruitment of GFP-paxillin at beads at 0.25 Hz (n) and 4 Hz (o). Scale bar is 50 µm.

In these conditions, cells remained rounded, thereby mimicking the low-stiffness phenotype that cells exhibited before being stretched. We then measured the effective stiffness of cells as they were being pulled (Figure 32 c). Increasing pulling speeds first increased stiffness, but between pulling speeds of 5 and 6 µm/s there was a sharp decrease, indicating a cytoskeletal fluidization event. Calculating an approximate equivalence, the range of stretch at which cells failed to mechanosense (10% stretch between 1 and 2 Hz, for cells of ~ 20 µm in size) corresponds to 4-8 µm/s in deformation, thereby matching the order of magnitude of AFM results. Interestingly, this decrease in stiffness was also associated with lower cell detachment forces, as previously reported (267) (Suplement, Figure 37 a). To mimic optical tweezers experiments, we carried out a modified experiment in which we attached fibronectin-coated 3 µm beads to AFM cantilevers, placed them in contact with the lamellipodia of previously adhered fibroblasts, and pulled at different speeds (Figure 32 d,e). Consistently with optical tweezers

experiments, no fluidization was observed (Figure 32 f). Of note, measured stiffness values in AFM bead experiments were at least one order of magnitude higher than in whole cell AFM experiments (Figure 32 c,f). This suggests that in local bead experiments, high cytoskeletal resistance led to deformations too low to produce fluidization.

We then validated the respective roles of reinforcement and fluidization through different experimental predictions. First, reinforcement and fluidization should lead respectively to either an increase or decrease in cytoskeletal organization. Indeed, cells stretched by 10% with a 1 Hz triangular signal, where focal adhesions were largest, formed clear actin stress fibres connected to adhesions, whereas those stretched at very low or very high rates showed a largely unstructured cytoskeleton (Figure 32 g). Second, preventing cytoskeletal fluidization should rescue adhesion formation at high stretch rates. Accordingly, cells treated with Jasplakinolide, a drug which stabilizes actin fibres by preventing their depolymerization (296), formed both actin stress fibres and large focal adhesions in response to 10% stretch with a 1 Hz square signal, whereas control cells did not (Figure 32 g,h). Finally, we treated cells with the myosin contractility inhibitor blebbistatin (296). This affected the actin cytoskeleton by eliminating stress fibres (and thereby force transmission through them), but still retaining a dendritic actin network in lamellipodia (enabling local force application with optical tweezers, Suplement, Figure 37 c,d). In such conditions and as expected, mechanosensing was abrogated in response to stretch (Figure 32 i-l), but not to local force application (Figure 32 m-o).

To conclude our study, we assessed whether the role of the force loading rate could also be observed at an organ level *in vivo*. To this end, we used a previously described setup (297) to subject each of the two lungs of a rat to independent mechanical ventilation (Figure 33 a).

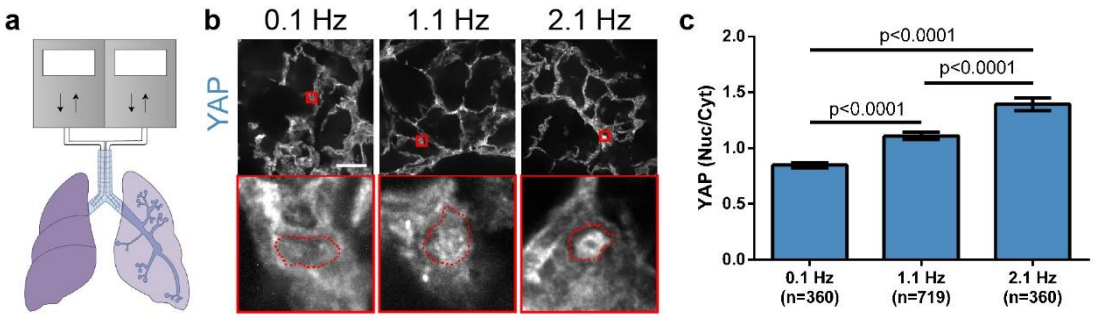

Figure 33: Increasing rates of lung ventilation *in vivo* induce YAP nuclear localization.

a. Illustration of the rat lung ventilation setup illustrating that each lung was independently cannulated and ventilated to induce different loading rates in the right and left lung. **b**, YAP staining of rats ventilated at 0.1 Hz, 1.1 Hz, and 2.1 Hz. Areas circled in red are magnified below each image. In magnified images, nuclear contours (as determined from Hoechst stainings) are shown in red. **c**, Quantification of YAP nuclear to cytoplasmic ratios for rat lungs ventilated with same tidal volume at 0.1 Hz, 1.1 Hz, and 2.1 Hz. Scale bar is 50 µm.

This setting allowed us to compare the effects of locally varying the mechanical loading rate in both lungs without interfering with the systemic animal gas exchange. After 1 hour of stimulation, lungs were excised and immunostained, and lung alveoli were imaged. The 3D, *in vivo* setup led to paxillin immunostainings without sufficient resolution to quantify adhesion shapes, but YAP nuclear to cytosolic ratios could be assessed (Figure 33 b,c). Whereas, as expected, no significant differences were found between right and left lungs when ventilated at the same frequency (Figure 38 a), we found increased levels of nuclear YAP with increased ventilation frequency (Figure 33 b,c). These results could not be explained by regulation of oxygen levels, since overall ventilation in the animal was kept constant when differential ventilation was applied to both lungs. Further, hypoxia increases YAP levels (298–300), as opposed to the effect we see in slowly ventilated (0.1 Hz) lungs. Thus, our results suggest that loading rate controls ventilation-induced mechanotransduction at the organ level in the lungs.

Extended Data figures and tables

Supplementary information

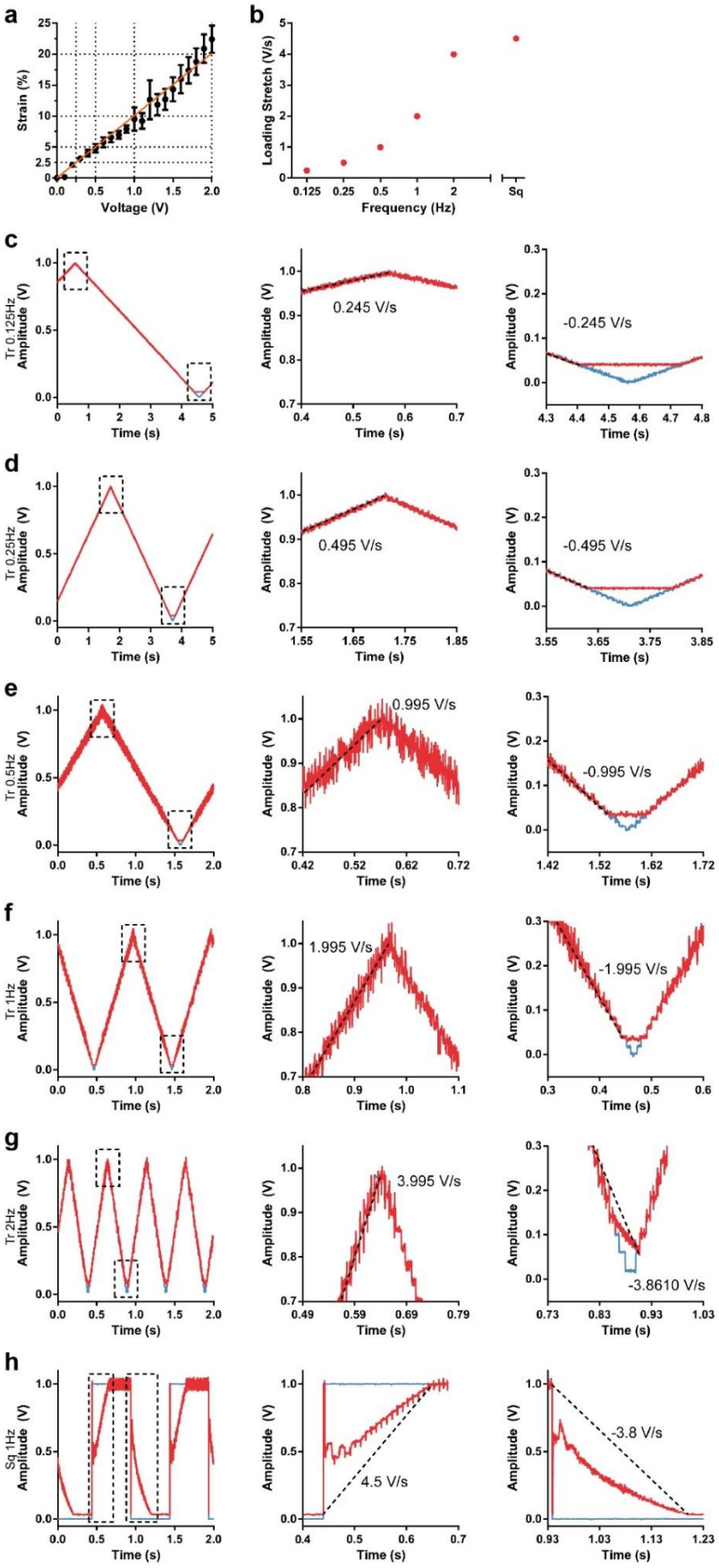

Figure 34: Additional characterization of the cell stretch setup.

a, Calibration of measured gel stretch as a function of the voltage applied on the pressure transducer. **b**, Applied stretch rate as a function of frequency applied. **c-h,** Example traces of applied and measured voltage signals at the pressure transducer for triangular signals at 0.125 Hz (c), 0.25 Hz (d) 0.5 Hz (e), 1 Hz (f), and 2 Hz (g), and square signals at 1Hz (h).

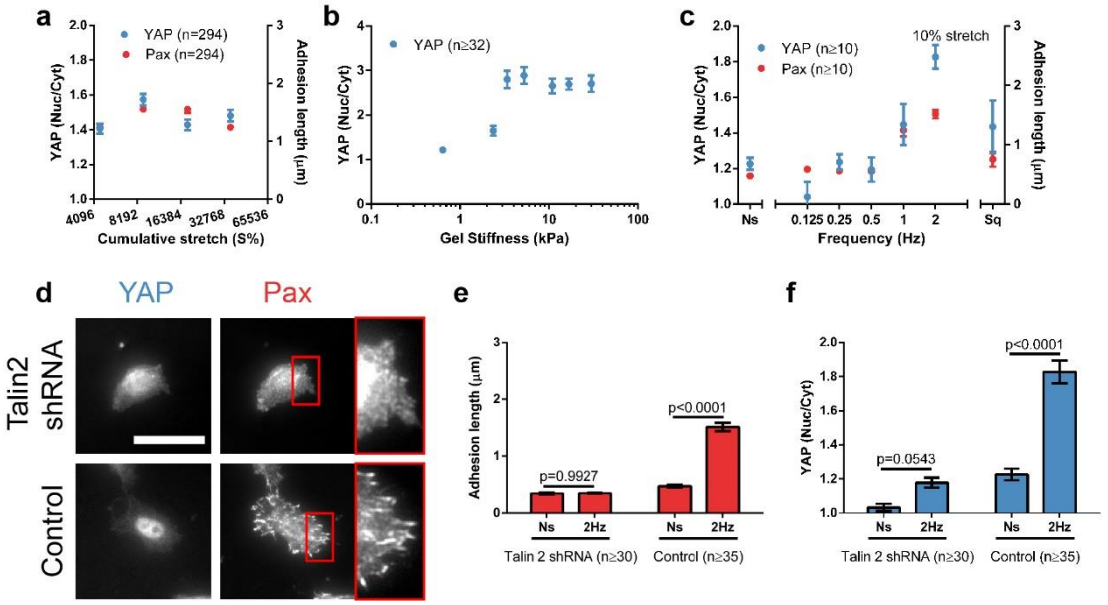

Figure 35: Additional information on stretch experiments.

a, Quantification of YAP nuclear to cytoplasmic ratios and focal adhesion lengths for all conditions as a function of the sum of total stretch received during the entire period of stimulation (stretch amplitude times the number of applied cycles). **b,** Quantification of YAP nuclear to cytoplasmic ratios for control cells plated on gels of increasing rigidity. **c,** Quantification of YAP nuclear to cytoplasmic ratios and focal adhesion lengths for Talin 1 knockdown (control) cells stretched at 10%. These cells overexpress talin 2 and have a wild-type phenotype(243) , and are the control for subsequent talin 2 depletion. **d,** YAP and paxillin stainings of Talin 1 knockdown (control) cells, and Talin 2 shRNA cells stretched at 10%, 2 Hz. In the paxillin image, areas circled in red are shown magnified at the right. These cells showed the peak of response at 2 Hz, and subsequent comparisons were therefore carried out at this frequency. **e,f** Quantifications of focal adhesion lengths (e) and YAP nuclear to cytoplasmic ratios (f) for Talin 1 knockdown (control) cells, and Talin 2 shRNA cells either not stretched (Ns) or stretched at 10% with a frequency of 2 Hz. Scale bar is 30 µm.

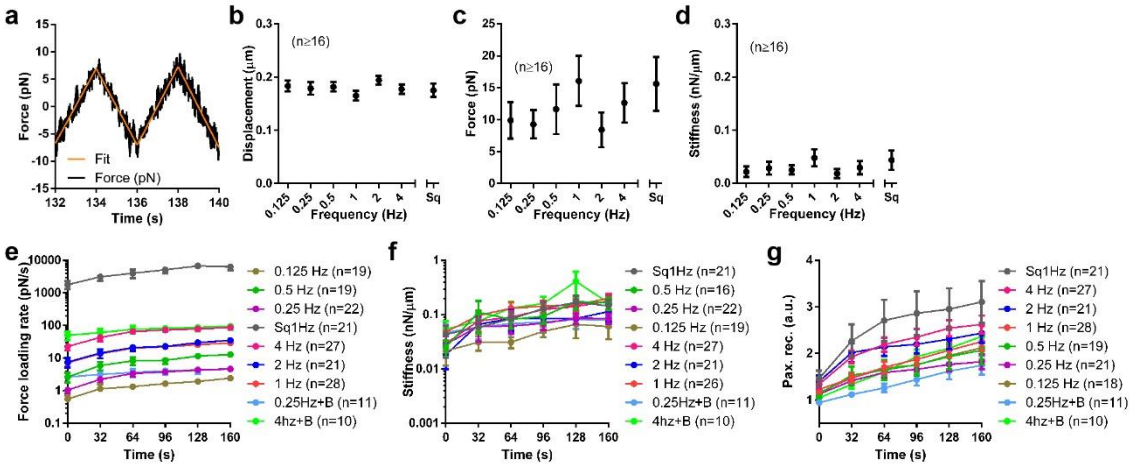

Figure 36: Additional results of the optical tweezers experiments.

a, Example trace and fit of a measured force signal. To calculate force loading rates, the slope of the fitted lines was taken. **b,** Bead displacement amplitude at time 0s for all frequencies. **c,** Bead force amplitude at time 0s for all frequencies. **d,** Bead stiffness at time 0s for all frequencies. **e,** Force loading rate as a function of time for all conditions. **f,** Stiffness as a function of time for all conditions. **g,** Recruitment of GFP-paxillin to beads as a function of time for all conditions.

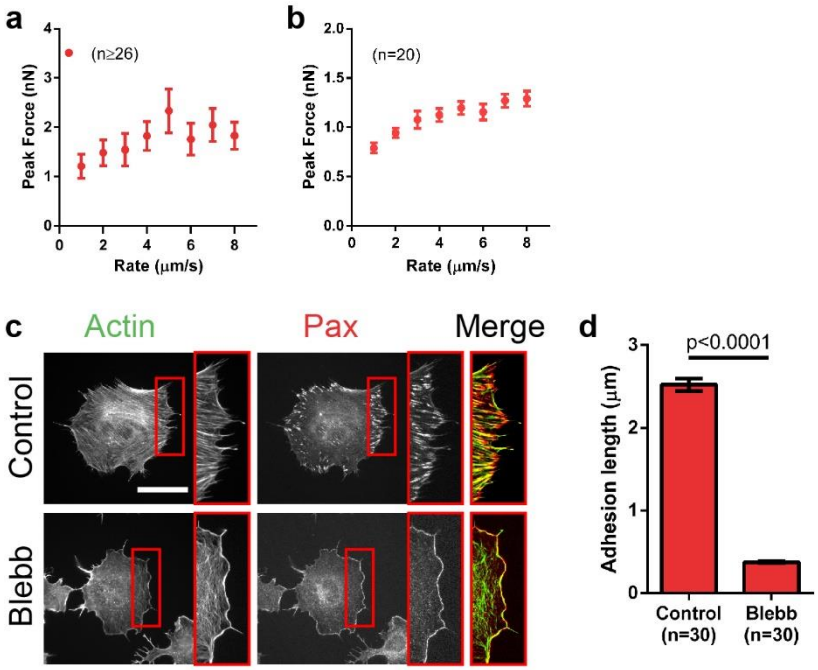

Figure 37: Additional AFM and blebbistatin data.

a, Peak force during cantilever retraction as a function of the retraction speed for cells attaching to a fibronectin-coated substrate. **b,** Peak force during cantilever retraction as a function of the retraction speed for fibronectin-coated beads attaching to cells. **c**, Actin and paxillin stainings in control cells seeded on glass with or without blebbistatin treatment. Areas circled in red are shown magnified at the right of each image, and shown as a merged image (actin, green, paxillin, red). Blebbistatin disrupts actin stress fibres but not lamellipodial actin. **d**, Quantification of the adhesion length for control cells, and cells treated with blebbistatin. Scale bar is 50 µm.

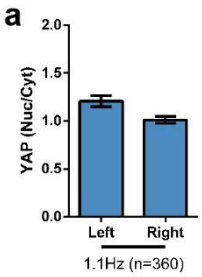

Figure 38: Additional information of the rat lung ventilation system.

a, Quantification of Yap nuclear to cytoplasmic ratios for left and right rat lungs ventilated at 1.1 Hz. No significant differences were observed.

% Acrylamide	% Bis-acrylamide	Young's modulus (kPa) (Mean ± s.e.m., N=3 gels, n=30 points)
4	0.03	0.64 ± 0.02
5.5	0.04	2.37 ± 0.04
6.16	0.04	3.40 ± 0.06
7.46	0.04	5.26 ± 0.11
7.5	0.1	10.94 ± 0.15
7.55	0.16	16.80 ± 0.22
12	0.15	29.92 ± 0.31

Table 1: Polyacrylamide gel rigidities measured with AFM

Figure panel	n value
1c	YAP: n=40, 30, 30, 30, 30, 30, 30 cells Paxillin: n= 66, 30, 30, 30, 30, 30, 40 cells
1d	YAP: n=50, 29, 30, 30, 30, 30, 30 cells Paxillin: n= 50, 29, 30, 30, 30, 30, 30 cells
1e	YAP: n=30, 29, 30, 30, 28, 30, 29 cells Paxillin: n=30, 29, 30, 30, 28, 30, 29 cells
1f	YAP: n=38, 30, 30, 30, 29, 30, 30 cells Paxillin: n=38, 30, 30, 30, 29, 30, 30 cells
1g	YAP: n=29, 59, 90, 118, 120, 90, 59, 30 cells Paxillin: n=29, 59, 90, 118, 120, 90, 59, 30 cells
2h	n=18, 21, 16, 26, 21, 27, 21 beads
2i	n=18, 21, 16, 26, 21, 27, 21 beads
2j	n=18, 21, 16, 26, 21, 27, 21 beads
2k	n=18, 21, 18, 22, 19, 28, 21, 27, 21 beads
3c	n=30, 30, 27, 29, 27, 27, 27, 30 curves
3h	Control ns: n=66 cells; Control sq: n=40 cells
3k	Control ns: n=66 cells; Control 1Hz: n=30 cells
3l	Control ns: n=66 cells; Control 1Hz: n=30 cells
Sup 1a	n=3 membranes
Sup 2b	n=33, 35, 32, 33, 32, 33, 32 cells
Sup 2c	YAP: n=40, 10, 9, 10, 10, 35, 10 cells Paxillin: n=40, 10, 9, 10, 10, 35, 10 cells
Sup 2e	Talin 2 shRNA: n=30, n=30; Control: n=40; n=35
Sup 2f	Talin 2 shRNA: n=30, n=30; Control: n=40; n=35

Sup 3b	n=18, 21, 16, 26, 21, 27, 21 beads
Sup 3c	n=18, 21, 16, 26, 21, 27, 21 beads
Sup 3d	n=18, 21, 16, 26, 21, 27, 21 beads
Sup 4a	n=30, 30, 27, 29, 27, 27, 27, 30 curves

Sup. Table. 2: Exact n values for figures reporting n≥

Chapter 5. Discussion

Regarding our results on the study of the mechanical implications in cell-matrix adhesions of the interaction between integrin α5β1 and tight junction protein ZO-1 (see section section 4.1) our results reveal how tight junction protein ZO-1, an integrin regulator, affects the mechanics and dynamics of α5β1-fn links, increasing their affinity and decreasing their ability to withstand forces. This effect suggests an increase in both binding and unbinding rates between fn and α5β1, which can explain the associated decrease in adhesion density and intensity caused by ZO-1 at monolayer edges. In turn, the faster binding dynamics caused by ZO-1 association may facilitate the migration of control versus ZO-1 depleted cells by facilitating adhesion remodelling. How ZO-1 association leads to the observed mechanical changes in α5β1-fn links, and the combination of mechanical and biochemical factors by which it affects behaviours such as cell migration, remain to be elucidated. Further, those effects may depend on substrate stiffness, coating and cell type: whereas we measured that ZO-1 depletion decreased myosin phosphorylation and did not affect cell-matrix force transmission, studies using other cell types, matrix coatings, and conditions have found even (279) or increased myosin phosphorylation (280) and increased contractility (151, 281). However and in general terms, our results exemplify how adaptor proteins can regulate integrin function not only by affecting their activation or affinity for ECM ligands, but also their mechanical properties under force.

Previous work has shown how adaptor proteins such as talin, α-actinin, or vinculin mediate integrin activation and mechanotransduction, leading to increased adhesion strength and reinforcement (278, 282). Here we demonstrate an alternative and counter-intuitive mechanism, by which another adaptor protein (ZO-1) promotes activation but decreases mechanical resistance. Because such mechanical regulation is bound to impact in downstream mechanosensing

processes, this provides an interesting and novel way to regulate cell adhesion, mechanorresponse, and function in general.

Regarding our results on the study to determine the fundamental mechanical variable detected by the cells during mechanosensing (see section section 4.2) our results show that force loading rates drive mechanosensing by increasing reinforcement and adhesion growth at the local adhesion level, in a talin-dependent way. However, if mechanically induced deformations are too high or too fast, the cytoskeleton fluidizes, thereby decreasing force loading rates and mechanosensing. This provides a unifying mechanism to understand how cells respond not only to directly applied forces, but also to passive mechanical stimuli such as tissue rigidity or ECM ligand distribution, where we have reported similar biphasic dependencies of focal adhesions and YAP localization (166). Further, it also provides a framework to understand how the seemingly opposed concepts of reinforcement and fluidization, previously analysed within the context of cell rheology (229, 294), are coupled to drive mechanosensing. Potentially, this framework could be extended to explain mechanosensing mechanisms beyond focal adhesion formation and YAP, such as the actin-dependent nuclear localization of MRTF-A (96). *In vivo*, the extremely wide range of loading rates in different contexts (from very fast in the respiratory (287) or cardiovascular (231) systems, or in vocal cord vibration (301), to very slow in progressive ECM remodelling in cancer (232)), could thus be central to understand how mechanosensing is regulated. In lung alveoli, we only observed the initial reinforcement phase, suggesting potential large-scale mechanisms to buffer against cytoskeletal fluidization. However, in other contexts both reinforcement and fluidization may be at place, and could even be harnessed to establish the levels of mechanical loading required to trigger specific responses.

The mechanical mechanism of cell system failure in response to force loading rates is shown to be fluidization. However, this response is shown to depend not only on single focal adhesions components but also on actin, and potentially including other cytoskeleton components. In fact, the exact protein component of the chain connection that fluidizes is not identified. While it is clear that the

component is not present in the adhesions themselves, it is proven that it is in the connection that transmits the force to the nucleus. One possibility would be that this protein was present at the level of integrin adaptor proteins. This is however unlikely, since adaptor proteins typically recruit to adhesions and the results show that one of these adaptor proteins, paxillin, does localize. Another possibility is that the protein is present at the cytoskeleton binding layer. While certainly possible, some data points out to the fact that this is not the case. Results show that upon disruption of contractility, the system still exhibits cortical actin that can connect to the integrin-mediated adhesions. The last possibility is that this protein is present in the cytoskeleton itself. Different options would therefore exist, including actin stabilizing proteins or maybe other cytoskeleton components. However, this still remains to be elucidated.

Overall, the results also highlight the importance of two different groups of factors in the regulation of the mechanical response of cells. On the one hand, the biochemical factors regulating the mechanoresponse of integrin-mediated adhesions. On the other hand, the mechanical factors involved in the same response. Not only the results show the physical variable underlying the physical response of the cell system, but they also show how biochemical factors such as protein binding partners contribute and modulate this response. Interestingly, this allows the cell system to increase its specificity. By tuning the biochemical factors simultaneously to responding to different mechanical challenges, cells can specifically respond to each of these differently. Potentially, this could explain how seemingly different tissues could respond widely differently and adapt to different mechanical stimuli.

The study on the response of integrin-mediated adhesions was fundamentally conducted on isolated single cells. However, ours results show how a protein typically constrained to cell-cell junctions also affects integrin-mediated adhesions to the extracellular matrix. This leaves the open question whether the response observed in integrin-mediated adhesions is also valid for cell-cell adhesions. The fact is that the response is dependant on the molecular binding/unbinding and folding/unfolding characteristics of the molecular

components, as I introduced previously. Cell -cell adhesions are also composed of different proteins forming the adhesion, with different molecular characteristics. Therefore, the same response could in principle apply to cell-cell adhesions. Interestingly, the fact that the molecules bind or unbind as catch bonds, or that they unfold as slip bonds is not a requirement for the behaviour to be exhibited. In fact, it is the existence of the crossover point between the different components what in the ends determines the response of the system.

Chapter 6. Conclusions

The general aim of this thesis was to study the mechanical response of integrin-mediated cell adhesions, in response to both integrin binding partners and force loading rates. In chapter 4 I studied the integrin response by a binding partner, and in chapter 5 I studied the mechanical response of cells to force loading rates. Here I present a summary of the conclusions for each chapter.

Binding of ZO-1 to α5β1 integrins regulates the mechanical properties of α5β1–fibronectin links

1. ZO-1 forms a complex with α5β1 at the edge of monolayers that affects cell motility

2. Disruption of the α5β1/ZO-1 complex increases α5β1-fn link resistance to forces only at the edge of monolayers

3. Disruption of the α5β1/ZO-1 complex decreases α5β1-fn recruitment at the edge of monolayers

4. Disruption of the α5β1/ZO-1 complex leads to a higher number of smaller nascent adhesions

The Force loading rate drives cell mechanosensing

1. The rate of cell stretch drives adhesion growth and YAP nuclear translocation in a biphasic manner, first increasing as the rate of stretch increases and then decreasing for very high stretch rates.

2. The loading rate of force application to single adhesions drives their maturation

3. The force loading rate induces mechanosensing, but is limited by cytoskeletal fluidization at high deformation rates

4. Increasing rates of lung ventilation in vivo induce YAP nuclear localization

Appendix A. Funding

This work was supported by the Spanish Ministry of Science and Innovation (BFU2016-79916-P and BFU2014-52586-REDT), a Career Integration Grant within the Seventh European Community Framework Programme (PCIG10-GA-2011-303848), the European Commission (Grant Agreement SEP-210342844 and H2020-FETPROACT-01-2016-731957), the Generalitat de Catalunya (2017-SGR-1602), the prize “ICREA Academia” for excellence in research to P.R-C., Obra Social “La Caixa” and Fundació la Marató de TV3 (project 20133330). S.H and T.B. were supported by the German Science Foundation (EXC 1003 CiM, Cells in Motion), the European Research Council (Consolidator Grants 771201, PolarizeMe) and the Human Frontier Science Program (HFSP grant RGP0018/2017).

I was supported by a Severo Ochoa Grant (Spanish Ministry of Economy and Competitiveness).

Appendix B: A note on statistics

Statistics is a topic that in my opinion several people really understand well. I personally think that my statistics knowledge is very limited. When quantifying data, most of the people strive to find a central tendency figure of merit. After obtaining it, people then ask the question whether if there is a difference between groups. The theory that was taught to me says that you want to apply a parametric test in order to have the maximum statistical power possible. However, this is only possible if all datasets comply with certain assumptions. One of the assumptions is that the dataset must be normal, or close to normal. That is, the distribution of the data must be close to a gaussian function. In order to know this, one must perform a normality test. There are several normality tests, and I would like to briefly comment on three of them.

Kolmogorov-Smirnov

The Kolmogorov-Smirnov was the first normality test ever developed. While it was good at the time, it has a main drawback. It computes the p-value with 1 sample. The sample that shows the highest difference between two distributions. This is not very reliable (306). Given a high enough sample number, everything will show normality, since there will be extreme values and those will be the ones used. I therefore did not use this test, ever, to decide if a distribution was normal.

Shapiro-Wilk

The Shapiro-Wilk test has been proven to be the normality test that has the highest statistical power for a significance value of all known normality tests (307). However, it is hard to understand. It uses a series of coefficients, a vector, a vector norm, it computes a covariance matrix and finally computes a p-value. I do not understand it even after reading about it. Therefore, I computed it, but did not base my decision around it in order to decide if a dataset was normal.

D’Agostino-Pearson omnibus K2

This test is one of the series of tests developed by Ralph B. D’agostino (308). It first computes the skewness and kurtosis of the dataset. It then computes how far these values compare with a gaussian distribution. Finally, it computes a p-value based on the sum of these differences. It is easy to understand, and it has a very good statistical power compared to other tests. Therefore, I used this test to decide if a distribution was normal.

Appendix C: Detailed protocols

C.1 Script used to extract data from the Optical Tweezers setup

```
% 16 matrix (binned file) structure

%1 AOD x
%2 AOD y
%3 AOD sum
%4 Lunam x
%5 SD Lunam x
%6 Lunam y
%7 SD Lunam y
%8 Lunam sum
%9 SD lunam sum
%10 Photodiode
%11 SD Photodiode
%12 Detection Laser x
%13 SD Detection Laser x
%14 Detection Laser y
%15 SD Detection Laser Y
%16 Detection Laser sum

%Force_x =  4.68*10^-11*lunamX;  Value depends on specific lunam
%Force_y =  4.85*10^-11*lunamY;  Value depends on specific lunam
%multiply values for 4.41 due to ratio between OD20 and OD30 filters

%dispX = abs(data(1,:)) / A.cal(5) * 10^-6 -1/
(A.xy_slope(1)*10^6)*lunamX;
%dispY = abs(data(2,:)) / A.cal(6) * 10^-6 -1/
(A.xy_slope(2)*10^6)*lunamY;

clear all
close all

%set path to load data
folder =
['\Upload\reference_tweezers_force\response_function_set_1016\'];

%loads data
for ii =0:1:5 %0:1:5

    pathName = strcat(['C:'...
        folder ...
        '100' num2str(ii)...
        '_100deformation_response.mat']); %loads data
    parameters = load(pathName); %loads data
    dataUnsqueezed = parameters.data; %extracts data
    if ii ==0
        data=squeeze(dataUnsqueezed);
        sf = parameters.s_eff; %extracts sampling rate in Hz
        dt= 1/sf; %sampling time in s
    else
```

```
        data=horzcat(data,squeeze(dataUnsqueezed)); %squeezes data
since there is only 1 trap
    end
    disp(pathName);
end


t=0:dt:((length(data)-1)*dt); %generates time vector

lunamX= (data(4,:)); %extracts x force data abs
lunamY= (data(6,:)); %extracts y force data

forceX = ( 4.68*10^-11*lunamX  ); %scales force to Newton
forceY = ( 4.85*10^-11*lunamY  ); %scales force to Newton

d2 = designfilt('lowpassiir','FilterOrder',8, ...
    'HalfPowerFrequency',0.001,'DesignMethod','butter');

forceX_trend = filtfilt(d2,forceX); %calculates force trend
forceY_trend = filtfilt(d2,forceY); %calculates force trend

forceX_detrended = forceX-forceX_trend; %detrends force
forceY_detrended = forceY-forceY_trend; %detrends force

forceX_detrended_reflected = -1*forceX_detrended; %reflects
forceY_detrended_reflected = -1*forceY_detrended; %reflects

forceX_inv = forceX_detrended_reflected + forceX_trend; %adds trend
forceY_inv = forceY_detrended_reflected + forceY_trend; %adds trend

forceX_rec = -1*forceX_inv; %backreflects
forceY_rec = -1*forceY_inv; %backreflects

forceXY = sqrt(forceX_rec.^2+forceY_rec.^2); %XY calc

dispX   = (data(1,:)) / parameters.cal(5) * 10^-6 -1/
(parameters.xy_slope(1)*10^6)*lunamX; %calc disp x
dispY   = (data(2,:)) / parameters.cal(6) * 10^-6 -1/
(parameters.xy_slope(2)*10^6)*lunamY; %calc disp y
dispXY  = sqrt(dispX.^2+dispY.^2); %disp in xy

plotyy(t,dispXY,t,forceXY);

% figure, plot(dispX,'-'),hold on, plot(dispY,'-'),plot(dispXY,'-');
% yyaxis right ,plot(forceX_rec,'-','color',[0.4660, 0.6740,
0.1880]),hold on, plot(forceY_rec,'-','color',[0.3010, 0.7450,
0.9330]),plot(forceXY_rec,'-');
% legend('dispX','dispY','dispXY','forceX','forceY','forceXY');
%
% figure, plot(t,dispXY), hold on, yyaxis right,plot(t,forceXY);
% legend('dispXY','forceXY');

%%

forceXY_trend = filtfilt(d2,forceXY); %calculates force trend
dispXY_trend = filtfilt(d2,dispXY); %calculates force trend
```

```
dispXY_det = dispXY-dispXY_trend; %detrends disp XY
forceXY_det = forceXY-forceXY_trend; %detrends force XY

ti = 32; % Time interval for stiffness calculation in s
n = fix(ti*sf); %chunk size
freq=1; %frequency in hertz


    i = 1;
    for i = 1:floor(length(forceXY)./n); %runs along chunk sizes

        dispChunk = dispXY_det(1+n*(i-1):n*i); %Gets displacement
chunk
        forceChunk = forceXY_det(1+n*(i-1):n*i); %Gets force chunk

        [Gi freq2] = tfestimate(dispChunk,forceChunk,[],[],n,sf);
%calculates tfe
        gammai     = mscohere(dispChunk,forceChunk,[],[],n,sf);
%calculates coherence
        [trash val] = min(abs(freq2-freq)); %gets value at correct
frequency

        Gphasei = Gi(val);
        gammaphasei = gammai(val);

        [trash val] = max(gammaphasei);
        G(i) = Gphasei(val);
        gammа(i) = gammaphasei(val);
    end

    K = abs(G);
    figure,plot (K,'.-');
    legend('K');
    figure, plot(gamma); legend('gamma');

    clear acor
    clear lag
    clear ~
    clear I
    clear timeDiff
    clear Gi
    clear freq2
    clear gammai
    clear trash
    clear val
    clear Gphasei
    clear gammaphasei
    clear G
    clear gamma
```

C.2 Coating of cantilevers for their use in single cell force spectroscopy

1. Place the AFM tips in a glass container, fill it with H_2SO_4 1M, leave for 1h
2. Clean with MQH_2O
3. Place tips on a glass slide and Plasma clean at max power for 3'
4. Place tips in 50 ul droplets of 0.5 mg/ml biotin-BSA
5. Leave in a humid chamber at 37ºC overnight
6. Wash by submerging tips 3x in PBS
7. Place tips in 50 ul droplets of 0.5 mg/ml Streptavidin
8. Leave at RT in a humid chamber 30'
9. Wash by submerging tips 3x in PBS
10. Place tips in 50 ul droplets of 0.4 mg/ml biotin-ConA
11. Leave at RT in a humid chamber 30'
12. Wash by submerging tips 3x in PBS
13. Store them submerged in a Petri dish containing 10 ml PBS

Notes:

- Cantilevers can be reused by redoing all steps from step number 1.
- Plasma cleaning on glass (not plastic!) works better.
- After plasma cleaning, tips can be easily handled by placing them on top of PDMS.

Appendix D: Publications and conferences

D.1 Original research articles

5. Molecular reshaping of the plasma membrane subjected to mechanical stress
   Anabel-Lise Le Roux, Caterina Tozzi, Nikhil Walani, Xarxa Quiroga, Victor González-Tarragó, Margarita Staykova, Marino Arroyo, Pere Roca-Cusachs
   (In preparation)

4. The force loading rate drives cell mechanosensing
   González-Tarragó V, Falcones B, Andreu I, Hurst S, Chahare N, Quiroga X, Leroux AL, Trepat X, Farré R, Betz T, Almendros I, Roca-Cusachs P
   (Submitted, 2019)

3. Binding of ZO-1 to α5β1 integrins regulates the mechanical properties of α5β1-fibronectin links
   González-Tarragó V, Elosegui-Artola A, Bazellières E, Oria R, Pérez-González C, Roca-Cusachs P
   Molecular Biology of the Cell (2017) 28(14):1847-1852

2. A mechanically active heterotypic E-cadherin/N-cadherin adhesion enables fibroblasts to drive cancer cell invasion
   Labernadie A, Kato T, Brugués A, Serra-Picamal X, Derzsi S, Arwert E, Weston A, González-Tarragó V, Elosegui-Artola A, Albertazzi L, Alcaraz J, Roca-Cusachs P, Sahai E, Trepat X
   Nature Cell Biology (2017) 19(3):224-237

1. Physical principles of membrane remodelling during cell mechanoadaptation

Kosmalska AJ, Casares L, Elosegui-Artola A, Thottacherry JJ, Moreno-Vicente R, González-Tarragó V, del Pozo MÁ, Mayor S, Arroyo M, Navajas D, Trepat X, Gauthier NC, Roca-Cusachs P.
Nature Communications (2015) 15;6:7292.

D.2 Conference posters and presentations (selection)

10. Víctor González-Tarragó, Bryan Falcones, Anabel-Lise Leroux, Ramon Farré, Isaac Almendros, Pere Roca-Cusachs, Control of integrin-mediated mechanorresponse by force loading rates, presented at Gordon Research Conference on Signaling by adhesion receptors, 2018, Maine, USA (Poster presentation)

9. Víctor González-Tarragó, Bryan Falcones, Anabel-Lise Leroux, Ramon Farré, Isaac Almendros, Pere Roca-Cusachs, Control of integrin-mediated mechanorresponse by force loading rates, presented at 6th Jornada d'Investigadors Predoctorals Interdisciplinària (JIPI), 2018, Barcelona, Spain (Poster presentation)

8. Víctor González-Tarragó, Alberto Elosegui-Artola, Elsa Bazellières, Roger Oria, Carlos Pérez-González, Pere Roca-Cusachs, Binding of ZO-1 to α5β1 integrins regulates the mechanical properties of α5β1-fibronectin links, presented at 19th International Union of Pure and Applied Biophysics (IUPAB) and 11th European Biophysical Societies' Association (EBSA) Congress, 2017, Edinburgh, UK (Oral and poster presentation)

7. 2nd Biomed phD day, 2017, Barcelona, Spain (Conference organizer)

6. Víctor González-Tarragó, Alberto Elosegui-Artola, Elsa Bazellières, Roger Oria, Carlos Pérez-González, Pere Roca-Cusachs, Unveiling the mechanical interaction between α5β1 and ZO-1, presented at 10th IBEC Symposium on Bioengineering for Future Medicine, 2017, Barcelona, Spain (Poster presentation)

5. Víctor González-Tarragó, Alberto Elosegui-Artola, Elsa Bazellières, Roger Oria, Carlos Pérez-González, Pere Roca-Cusachs, Unveiling the mechanical interaction between α5β1 and ZO-1, presented at Mechanobiology across networks, 2016, Barcelona, Spain (Poster presentation)

4. Víctor González-Tarragó, Alberto Elosegui-Artola, Elsa Bazellières, Roger Oria, Carlos Pérez-González, Pere Roca-Cusachs, Unveiling the mechanical interaction between α5β1 and ZO-1, presented at 1st Biomed phD day, 2016, Barcelona, Spain (Talk)

3. Víctor González-Tarragó, Alberto Elosegui-Artola, Elsa Bazellières, Roger Oria, Carlos Pérez-González, Pere Roca-Cusachs, Unveiling the mechanical interaction between α5β1 and ZO-1, presented at 9th IBEC Symposium on Bioengineering and Nanomedicine, 2016, Barcelona, Spain (Poster presentation)

2. Víctor González-Tarragó, Alberto Elosegui-Artola, Elsa Bazellières, Roger Oria, Carlos Pérez-González, Pere Roca-Cusachs, Unveiling the mechanical interaction between α5β1 and ZO-1, presented at XXXII Congreso Anual de la Sociedad Española de Ingeniería Biomédica, CASEIB, 2014, Barcelona, Spain, (Poster presentation)

1. Víctor González-Tarragó, Alberto Elosegui-Artola, Elsa Bazellières, Roger Oria, Carlos Pérez-González, Pere Roca-Cusachs, Unveiling the mechanical interaction between α5β1 and ZO-1, presented at 7th IBEC Symposium on Bioengineering and Nanomedicine, 2014, Barcelona, Spain, (Talk and poster presentation)

List of abbreviations

ECM	Extracellular matrix
FN	Fibronectin
RGD	Argining-Glycin-Asparagin sequence
MLC	Myosin light chain
pMLC	Phospho-myosin light chain
TFM (TM)	Traction Force Microscopy
pAAg (PA)	Polyacrylamide gel
PDMS	Polydimethylsiloxane
PIV	Particle Image velocimetry
MCF10A	Mammary cystic fibrous disease epithelial cell line
DMEM	Dulbecco’s modified Eagle’s medium
siRNA	Small interfering ribonucleic acid
BSA	Bovine serum albumin
FLAG	DYKDDDDK peptide sequence
GAPDH	Glyceraldehyde-3-phosphate dehydrogenase
ANOVA	Analysis of variance
DNA	Deoxyribonucleic acid
LINC	Linker of Nucleoskeleton and Cytoskeleton
SUN	Sad1 and UNC-88 proteins
KASH	Klarsicht, ANC-1 and Syne/Nesprin homology
NPC	Nuclear Pore Complex
IF	Intermediate Filament
CAM	Cell-adhesion molecule
ZO	Zona occludens
ICAP1	Integrin cytoplasmic domain-associated protein-1
FAK	Focal adhesion kinase

Figure list

References

1. González-Tarragó V, et al. (2017) Binding of ZO-1 to α5β1 integrins regulates the mechanical properties of α5β1-fibronectin links. *Mol Biol Cell* 28(14):1847–1852.
2. Rosowski K (2013) Introduction to Cell Mechanics and Mechanobiology. *Yale J Biol Med* 86(3):436.
3. Spill F, Reynolds DS, Kamm RD, Zaman MH (2016) Impact of the physical microenvironment on tumor progression and metastasis. *Curr Opin Biotechnol* 40:41–48.
4. Jang I, Beningo KA, Jang I, Beningo KA (2019) Integrins, CAFs and Mechanical Forces in the Progression of Cancer. *Cancers (Basel)* 11(5):721.
5. Katsumi A, Orr AW, Tzima E, Schwartz MA (2004) Integrins in mechanotransduction. *J Biol Chem* 279(13):12001–4.
6. Alberts B, et al. (2007) *Molecular Biology of the Cell*. 5th Ed.
7. Fletcher DA, Mullins RD (2010) Cell mechanics and the cytoskeleton. *Nature* 463(7280).
8. Wickstead B, Gull K (2011) The evolution of the cytoskeleton. *J Cell Biol* 194(4):513–525.
9. Hämälistö S, et al. (2013) A ZO-1/α5β1-integrin complex regulates cytokinesis downstream of PKCε in NCI-H460 cells plated on fibronectin. *PLoS One* 8(8):e70696.
10. Geli MI, Riezman H (1998) Endocytic internalization in yeast and animal cells: similar and different. *J Cell Sci* 111 (Pt 8):1031–7.
11. Henderson CA, Gomez CG, Novak SM, Mi-Mi L, Gregorio CC (2017) Overview of the Muscle Cytoskeleton. *Comprehensive Physiology* (John Wiley & Sons, Inc., Hoboken, NJ, USA), pp 891–944.
12. Gardel ML, Kasza KE, Brangwynne CP, Liu J, Weitz DA (2008) Chapter 19: Mechanical response of cytoskeletal networks. *Methods Cell Biol*

89:487–519.

13. Alcaraz J, et al. (2003) Microrheology of human lung epithelial cells measured by atomic force microscopy. *Biophys J* 84(3):2071–9.

14. Kwiatkowska M, Popłońska K, Stepiński D, Hejnowicz Z (2006) Microtubules with different diameter, protofilament number and protofilament spacing in Ornithogalum umbellatum ovary epidermis cells. *Folia Histochem Cytobiol* 44(2):133–8.

15. Letourneau PC (1982) Analysis of microtubule number and length in cytoskeletons of cultured chick sensory neurons. *J Neurosci* 2(6):806–14.

16. Weisenberg RC (1972) Microtubule formation in vitro in solutions containing low calcium concentrations. *Science* 177(4054):1104–5.

17. Walker RA, et al. (1988) Dynamic instability of individual microtubules analyzed by video light microscopy: rate constants and transition frequencies. *J Cell Biol* 107(4):1437–1448.

18. Gierke S, Kumar P, Wittmann T (2010) Analysis of microtubule polymerization dynamics in live cells. *Methods Cell Biol* 97:15–33.

19. Mitchison T, Kirschner M (1984) Dynamic instability of microtubule growth. *Nature* 312(5991):237–242.

20. Mandelkow E, Mandelkow EM (1995) Microtubules and microtubule-associated proteins. *Curr Opin Cell Biol* 7(1):72–81.

21. Janke C, Chloë Bulinski J (2011) Post-translational regulation of the microtubule cytoskeleton: mechanisms and functions. *Nat Rev Mol Cell Biol* 12(12):773–786.

22. Manning JA, Shalini S, Risk JM, Day CL, Kumar S (2010) A Direct Interaction with NEDD1 Regulates γ-Tubulin Recruitment to the Centrosome. *PLoS One* 5(3):e9618.

23. Aldaz H, Rice LM, Stearns T, Agard DA (2005) Insights into microtubule nucleation from the crystal structure of human γ-tubulin. *Nature* 435(7041):523–527.

24. Vale RD (2003) The molecular motor toolbox for intracellular transport. *Cell*

112(4):467–80.

25. Meunier S, Vernos I (2012) Microtubule assembly during mitosis – from distinct origins to distinct functions? *J Cell Sci* 125(12):2805–2814.

26. Bardy SL, Ng SYM, Jarrell KF (2003) Prokaryotic motility structures. *Microbiology* 149(2):295–304.

27. McGrath JL (2006) Microtubule Mechanics: A Little Flexibility Goes a Long Way. *Curr Biol* 16(18):R800–R802.

28. Goldmann WH (2018) Intermediate filaments and cellular mechanics. *Cell Biol Int* 42(2):132–138.

29. Cooper GM, Hausman RE (2013) *The cell : a molecular approach* (Sinauer Associates).

30. Herrmann H, Bär H, Kreplak L, Strelkov S V., Aebi U (2007) Intermediate filaments: from cell architecture to nanomechanics. *Nat Rev Mol Cell Biol* 8(7):562–573.

31. Sharma P, et al. (2019) Intermediate Filaments as Effectors of Cancer Development and Metastasis: A Focus on Keratins, Vimentin, and Nestin. *Cells* 8(5):497.

32. Moll R, Divo M, Langbein L (2008) The human keratins: biology and pathology. *Histochem Cell Biol* 129(6):705–733.

33. Novel functions of vimentin in cell adhesion, migration, and signaling (2007) *Exp Cell Res* 313(10):2050–2062.

34. Lammerding J, et al. (2006) Lamins A and C but Not Lamin B1 Regulate Nuclear Mechanics. *J Biol Chem* 281(35):25768–25780.

35. Lammerding J, et al. (2004) Lamin A/C deficiency causes defective nuclear mechanics and mechanotransduction. *J Clin Invest* 113(3):370–378.

36. Bar H, et al. (2005) Severe muscle disease-causing desmin mutations interfere with in vitro filament assembly at distinct stages. *Proc Natl Acad Sci* 102(42):15099–15104.

37. Dominguez R, Holmes KC (2011) Actin structure and function. *Annu Rev Biophys* 40:169–86.

38. Pollard TD (2016) Actin and Actin-Binding Proteins. *Cold Spring Harb Perspect Biol* 8(8). doi:10.1101/cshperspect.a018226.

39. Hanson J, Lowy J (1963) The structure of F-actin and of actin filaments isolated from muscle. *J Mol Biol* 6(1):46-IN5.

40. Rottner K, Faix J, Bogdan S, Linder S, Kerkhoff E (2017) Actin assembly mechanisms at a glance. *J Cell Sci* 130(20):3427–3435.

41. Pollard TD (Thomas D, Earnshaw WC, Lippincott-Schwartz J, Johnson GT *Cell biology*.

42. Sept D, McCammon JA (2001) Thermodynamics and Kinetics of Actin Filament Nucleation. *Biophys J* 81(2):667–674.

43. Dominguez R (2016) The WH2 Domain and Actin Nucleation: Necessary but Insufficient. *Trends Biochem Sci* 41(6):478–490.

44. Machesky LM, Insall RH Scar1 and the related Wiskott-Aldrich syndrome protein, WASP, regulate the actin cytoskeleton through the Arp2/3 complex. *Curr Biol* 8(25):1347–56.

45. Graceffa P, Dominguez R (2003) Crystal Structure of Monomeric Actin in the ATP State. *J Biol Chem* 278(36):34172–34180.

46. Holmes KC, Popp D, Gebhard W, Kabsch W (1990) Atomic model of the actin filament. *Nature* 347(6288):44–49.

47. Kassianidou E, Kumar S (2015) A biomechanical perspective on stress fiber structure and function. *Biochim Biophys Acta - Mol Cell Res* 1853(11):3065–3074.

48. Cramer LP (1997) Molecular mechanism of actin-dependent retrograde flow in lamellipodia of motile cells. *Front Biosci* 2:d260-70.

49. Pollard TD, Cooper JA (2009) Actin, a Central Player in Cell Shape and Movement. *Science (80-)* 326(5957):1208–1212.

50. Crisp M, et al. (2006) Coupling of the nucleus and cytoplasm: role of the LINC complex. *J Cell Biol* 172(1):41–53.

51. Tapley EC, Starr DA (2013) Connecting the nucleus to the cytoskeleton by SUN-KASH bridges across the nuclear envelope. *Curr Opin Cell Biol*

25(1):57–62.

52. Uzer G, et al. (2015) Cell Mechanosensitivity to Extremely Low-Magnitude Signals Is Enabled by a LINCed Nucleus. *Stem Cells* 33(6):2063–76.

53. Bachir AI, Horwitz AR, Nelson WJ, Bianchini JM (2017) Actin-Based Adhesion Modules Mediate Cell Interactions with the Extracellular Matrix and Neighboring Cells. *Cold Spring Harb Perspect Biol* 9(7). doi:10.1101/cshperspect.a023234.

54. Kristó I, Bajusz I, Bajusz C, Borkúti P, Vilmos P (2016) Actin, actin-binding proteins, and actin-related proteins in the nucleus. *Histochem Cell Biol* 145(4):373–388.

55. Wesolowska N, Lénárt P (2015) Nuclear roles for actin. *Chromosoma* 124(4):481–489.

56. Lombard J (2014) Once upon a time the cell membranes: 175 years of cell boundary research. *Biol Direct* 9:32.

57. Singer SJ, Nicolson GL (1972) The fluid mosaic model of the structure of cell membranes. *Science* 175(4023):720–31.

58. Haswell ES, Phillips R, Rees DC (2011) Mechanosensitive channels: what can they do and how do they do it? *Structure* 19(10):1356–69.

59. Wu C (2007) Focal adhesion: a focal point in current cell biology and molecular medicine. *Cell Adh Migr* 1(1):13–8.

60. Pethő Z, Najder K, Bulk E, Schwab A (2019) Mechanosensitive ion channels push cancer progression. *Cell Calcium* 80:79–90.

61. Frantz C, Stewart KM, Weaver VM (2010) The extracellular matrix at a glance. *J Cell Sci* 123(Pt 24):4195–200.

62. Hynes RO, Naba A (2012) Overview of the Matrisome--An Inventory of Extracellular Matrix Constituents and Functions. *Cold Spring Harb Perspect Biol* 4(1):a004903–a004903.

63. Rye C, et al. *Biology.*

64. Yue B (2014) Biology of the extracellular matrix: an overview. *J Glaucoma* 23(8 Suppl 1):S20-3.

65. Lindahl U, Couchman J, Kimata K, Esko JD (2015) *Proteoglycans and Sulfated Glycosaminoglycans* (Cold Spring Harbor Laboratory Press) doi:10.1101/GLYCOBIOLOGY.3E.017.

66. Mecham RP (1998) Overview of Extracellular Matrix. *Curr Protoc Cell Biol* 00(1):10.1.1-10.1.14.

67. Durbeej M (2010) Laminins. *Cell Tissue Res* 339(1):259–268.

68. Ricard-Blum S (2011) The Collagen Family. *Cold Spring Harb Perspect Biol* 3(1):a004978–a004978.

69. Coussen F, Choquet D, Sheetz MP, Erickson HP (2002) Trimers of the fibronectin cell adhesion domain localize to actin filament bundles and undergo rearward translocation. *J Cell Sci* 115(12):2581–2590.

70. Hattori A, et al. (2009) Sequence specificity of the PHSRN peptide from fibronectin on corneal epithelial migration. *Biochem Biophys Res Commun* 379(2):346–350.

71. Zhong C, et al. (1998) Rho-mediated Contractility Exposes a Cryptic Site in Fibronectin and Induces Fibronectin Matrix Assembly. *J Cell Biol* 141(2):539–551.

72. Hynes RO (1986) Fibronectins. *Sci Am* 254(6):42–51.

73. Schwarzbauer JE, DeSimone DW (2011) Fibronectins, Their Fibrillogenesis, and In Vivo Functions. *Cold Spring Harb Perspect Biol* 3(7):a005041–a005041.

74. Pankov R, Yamada KM (2002) Fibronectin at a glance. *J Cell Sci* 115(20):3861–3863.

75. Dallas SL, Chen Q, Sivakumar P (2006) Dynamics of Assembly and Reorganization of Extracellular Matrix Proteins. *Current Topics in Developmental Biology*, pp 1–24.

76. Singh P, Schwarzbauer JE (2012) Fibronectin and stem cell differentiation - lessons from chondrogenesis. *J Cell Sci* 125(16):3703–3712.

77. Kubow KE, et al. (2015) Mechanical forces regulate the interactions of fibronectin and collagen I in extracellular matrix. *Nat Commun* 6(1):8026.

78. Gattazzo F, Urciuolo A, Bonaldo P (2014) Extracellular matrix: A dynamic microenvironment for stem cell niche. *Biochim Biophys Acta - Gen Subj* 1840(8):2506–2519.

79. Pope SD, Medzhitov R (2018) Emerging Principles of Gene Expression Programs and Their Regulation. *Mol Cell* 71(3):389–397.

80. Andersson R, Sandelin A, Danko CG (2015) A unified architecture of transcriptional regulatory elements. *Trends Genet* 31(8):426–433.

81. Heinz S, Romanoski CE, Benner C, Glass CK (2015) The selection and function of cell type-specific enhancers. *Nat Rev Mol Cell Biol* 16(3):144–154.

82. Pombo A, Dillon N (2015) Three-dimensional genome architecture: players and mechanisms. *Nat Rev Mol Cell Biol* 16(4):245–257.

83. Brivanlou AH (2002) Signal Transduction and the Control of Gene Expression. *Science (80-)* 295(5556):813–818.

84. Latchman DS (1993) Transcription factors: an overview. *Int J Exp Pathol* 74(5):417–22.

85. Wang JH-C, Thampatty BP, Lin J-S, Im H-J (2007) Mechanoregulation of gene expression in fibroblasts. *Gene* 391(1–2):1–15.

86. Matsui H, et al. (2014) The Expression of Fn14 via Mechanical Stress-activated JNK Contributes to Apoptosis Induction in Osteoblasts. 289(10). Available at: http://www.ncbi.nlm.nih.gov/pubmed/24446436 [Accessed May 15, 2019].

87. Pomiès L, Decourteix M, Franchel J, Moulia B, Leblanc-Fournier N (2017) Poplar stem transcriptome is massively remodelled in response to single or repeated mechanical stimuli. *BMC Genomics* 18(1):300.

88. Rysä J, Tokola H, Ruskoaho H (2018) Mechanical stretch induced transcriptomic profiles in cardiac myocytes. *Sci Rep* 8(1):4733.

89. Thiel CS, et al. (2017) Dynamic gene expression response to altered gravity in human T cells. *Sci Rep* 7(1):5204.

90. Szczesny SE, Mauck RL (2017) The Nuclear Option: Evidence Implicating

the Cell Nucleus in Mechanotransduction. *J Biomech Eng* 139(2):0210061.

91. Lammerding J, et al. (2005) Abnormal nuclear shape and impaired mechanotransduction in emerin-deficient cells. *J Cell Biol* 170(5):781–791.

92. Zwerger M, et al. (2013) Myopathic lamin mutations impair nuclear stability in cells and tissue and disrupt nucleo-cytoskeletal coupling. *Hum Mol Genet* 22(12):2335–2349.

93. Elosegui-Artola A, et al. (2017) Force Triggers YAP Nuclear Entry by Regulating Transport across Nuclear Pores. *Cell* 171(6):1397-1410.e14.

94. Codelia VA, Sun G, Irvine KD (2014) Regulation of YAP by Mechanical Strain through Jnk and Hippo Signaling. *Curr Biol* 24(17):2012–2017.

95. Cui Y, et al. (2015) Cyclic stretching of soft substrates induces spreading and growth. *Nat Commun* 6(1):6333.

96. Montel L, Sotiropoulos A, Hénon S (2019) The nature and intensity of mechanical stimulation drive different dynamics of MRTF-A nuclear redistribution after actin remodeling in myoblasts. *PLoS One* 14(3):e0214385.

97. Fedorchak GR, Kaminski A, Lammerding J (2014) Cellular mechanosensing: Getting to the nucleus of it all. *Prog Biophys Mol Biol* 115(2–3):76–92.

98. Starr DA, Fridolfsson HN (2010) Interactions Between Nuclei and the Cytoskeleton Are Mediated by SUN-KASH Nuclear-Envelope Bridges. *Annu Rev Cell Dev Biol* 26(1):421–444.

99. Razafsky D, Hodzic D (2009) Bringing KASH under the SUN: the many faces of nucleo-cytoskeletal connections. *J Cell Biol* 186(4):461–472.

100. Burke B, Roux KJ (2009) Nuclei Take a Position: Managing Nuclear Location. *Dev Cell* 17(5):587–597.

101. Lee YL, Burke B (2018) LINC complexes and nuclear positioning. *Semin Cell Dev Biol* 82:67–76.

102. Elosegui-Artola A, Trepat X, Roca-Cusachs P (2018) Control of Mechanotransduction by Molecular Clutch Dynamics. *Trends Cell Biol*

28(5):356–367.

103. Abedin M, King N (2010) Diverse evolutionary paths to cell adhesion. *Trends Cell Biol* 20(12):734–742.

104. Bayas M V., Leung A, Evans E, Leckband D (2006) Lifetime Measurements Reveal Kinetic Differences between Homophilic Cadherin Bonds. *Biophys J* 90(4):1385–1395.

105. Volk T, Cohen O, Geiger B (1987) Formation of heterotypic adherens-type junctions between L-CAM-containing liver cells and A-CAM-containing lens cells. *Cell* 50(6):987–94.

106. Niessen CM, Gumbiner BM (2002) Cadherin-mediated cell sorting not determined by binding or adhesion specificity. *J Cell Biol* 156(2):389–400.

107. Wheelock MJ, Johnson KR (2003) Cadherins as Modulators of Cellular Phenotype. *Annu Rev Cell Dev Biol* 19(1):207–235.

108. Delva E, Tucker DK, Kowalczyk AP (2009) The desmosome. *Cold Spring Harb Perspect Biol* 1(2):a002543.

109. Kottke MD, Delva E, Kowalczyk AP (2006) The desmosome: cell science lessons from human diseases. *J Cell Sci* 119(5):797–806.

110. Amagai M, Klaus-Kovtun V, Stanley JR (1991) Autoantibodies against a novel epithelial cadherin in pemphigus vulgaris, a disease of cell adhesion. *Cell* 67(5):869–77.

111. Mertens C, Kuhn C, Franke WW (1996) Plakophilins 2a and 2b: constitutive proteins of dual location in the karyoplasm and the desmosomal plaque. *J Cell Biol* 135(4):1009–25.

112. Elias PM, et al. (2001) Desmoglein isoform distribution affects stratum corneum structure and function. *J Cell Biol* 153(2):243–9.

113. Koch PJ, et al. (1997) Targeted Disruption of the Pemphigus Vulgaris Antigen (Desmoglein 3) Gene in Mice Causes Loss of Keratinocyte Cell Adhesion with a Phenotype Similar to Pemphigus Vulgaris. *J Cell Biol* 137(5):1091–1102.

114. Yonemura S (2017) Actin filament association at adherens junctions. *J Med*

Investig 64(1.2):14–19.

115. Kobielak A, Fuchs E (2004) α-catenin: at the junction of intercellular adhesion and actin dynamics. *Nat Rev Mol Cell Biol* 5(8):614–625.

116. Gumbiner BM (2005) Regulation of cadherin-mediated adhesion in morphogenesis. *Nat Rev Mol Cell Biol* 6(8):622–634.

117. Meng W, Takeichi M (2009) Adherens junction: molecular architecture and regulation. *Cold Spring Harb Perspect Biol* 1(6):a002899.

118. Cavey M, Lecuit T (2009) Molecular Bases of Cell-Cell Junctions Stability and Dynamics. *Cold Spring Harb Perspect Biol* 1(5):a002998–a002998.

119. Ziegler WH, Liddington RC, Critchley DR (2006) The structure and regulation of vinculin. *Trends Cell Biol* 16(9):453–460.

120. Geiger B, Spatz JP, Bershadsky AD (2009) Environmental sensing through focal adhesions. *Nat Rev Mol Cell Biol* 10(1):21–33.

121. Huveneers S, et al. (2012) Vinculin associates with endothelial VE-cadherin junctions to control force-dependent remodeling. *J Cell Biol* 196(5):641–52.

122. Itoh M, et al. (1993) The 220-kD protein colocalizing with cadherins in non-epithelial cells is identical to ZO-1, a tight junction-associated protein in epithelial cells: cDNA cloning and immunoelectron microscopy. *J Cell Biol* 121(3):491–502.

123. Ikenouchi J, Umeda K, Tsukita S, Furuse M, Tsukita S (2007) Requirement of ZO-1 for the formation of belt-like adherens junctions during epithelial cell polarization. *J Cell Biol* 176(6):779–86.

124. Imamura Y, Itoh M, Maeno Y, Tsukita S, Nagafuchi A (1999) Functional domains of alpha-catenin required for the strong state of cadherin-based cell adhesion. *J Cell Biol* 144(6):1311–22.

125. Sheikh F, et al. (2006) α-E-Catenin Inactivation Disrupts the Cardiomyocyte Adherens Junction, Resulting in Cardiomyopathy and Susceptibility to Wall Rupture. *Circulation* 114(10):1046–1055.

126. Yonemura S (2011) Cadherin–actin interactions at adherens junctions.

Curr Opin Cell Biol 23(5):515–522.

127. Buckley CD, et al. (2014) The minimal cadherin-catenin complex binds to actin filaments under force. *Science (80-)* 346(6209):1254211–1254211.

128. Cereijido M, Contreras RG, Shoshani L, Flores-Benitez D, Larre I (2008) Tight junction and polarity interaction in the transporting epithelial phenotype. *Biochim Biophys Acta - Biomembr* 1778(3):770–793.

129. Balda MS, Matter K (2008) Tight junctions at a glance. *J Cell Sci* 121(22):3677–3682.

130. Runkle EA, Mu D (2013) Tight junction proteins: from barrier to tumorigenesis. *Cancer Lett* 337(1):41–8.

131. Förster C (2008) Tight junctions and the modulation of barrier function in disease. *Histochem Cell Biol* 130(1):55–70.

132. Furuse M, Sasaki H, Fujimoto K, Tsukita S (1998) A Single Gene Product, Claudin-1 or -2, Reconstitutes Tight Junction Strands and Recruits Occludin in Fibroblasts. *J Cell Biol* 143(2):391–401.

133. Furuse M, Sasaki H, Tsukita S (1999) Manner of Interaction of Heterogeneous Claudin Species within and between Tight Junction Strands. *J Cell Biol* 147(4):891–903.

134. Günzel D, Yu ASL (2013) Claudins and the modulation of tight junction permeability. *Physiol Rev* 93(2):525–69.

135. Amasheh S, et al. (2002) Claudin-2 expression induces cation-selective channels in tight junctions of epithelial cells. *J Cell Sci* 115(Pt 24):4969–76.

136. Itoh M, et al. (1999) Direct Binding of Three Tight Junction-Associated Maguks, Zo-1, Zo-2, and Zo-3, with the Cooh Termini of Claudins. *J Cell Biol* 147(6):1351–1363.

137. Aijaz S, Sanchez-Heras E, Balda MS, Matter K (2007) Regulation of tight junction assembly and epithelial morphogenesis by the heat shock protein Apg-2. *BMC Cell Biol* 8:49.

138. Umeda K, et al. (2006) ZO-1 and ZO-2 Independently Determine Where Claudins Are Polymerized in Tight-Junction Strand Formation. *Cell*

126(4):741–754.

139. Matter K, Balda MS (2007) Epithelial tight junctions, gene expression and nucleo-junctional interplay. *J Cell Sci* 120(9):1505–1511.

140. Meyer TN, Schwesinger C, Denker BM (2002) Zonula occludens-1 is a scaffolding protein for signaling molecules. Galpha(12) directly binds to the Src homology 3 domain and regulates paracellular permeability in epithelial cells. *J Biol Chem* 277(28):24855–8.

141. Singh D, Solan JL, Taffet SM, Javier R, Lampe PD (2005) Connexin 43 Interacts with Zona Occludens-1 and -2 Proteins in a Cell Cycle Stage-specific Manner. *J Biol Chem* 280(34):30416–30421.

142. Kausalya PJ, Reichert M, Hunziker W (2001) Connexin45 directly binds to ZO-1 and localizes to the tight junction region in epithelial MDCK cells. *FEBS Lett* 505(1):92–6.

143. Taliana L, Benezra M, Greenberg RS, Masur SK, Bernstein AM (2005) ZO-1: lamellipodial localization in a corneal fibroblast wound model. *Invest Ophthalmol Vis Sci* 46(1):96–103.

144. Tuomi S, et al. (2009) PKCepsilon regulation of an alpha5 integrin-ZO-1 complex controls lamellae formation in migrating cancer cells. *Sci Signal* 2(77):ra32.

145. Paris L, Tonutti L, Vannini C, Bazzoni G (2008) Structural organization of the tight junctions. *Biochim Biophys Acta - Biomembr* 1778(3):646–659.

146. Polette M, et al. (2007) β-Catenin and ZO-1: Shuttle Molecules Involved in Tumor Invasion-Associated Epithelial-Mesenchymal Transition Processes. *Cells Tissues Organs* 185(1–3):61–65.

147. Katsube T, et al. (1998) Cortactin Associates with the Cell-Cell Junction Protein ZO-1 in both *Drosophila* and Mouse. *J Biol Chem* 273(45):29672–29677.

148. D'Atri F, Nadalutti F, Citi S (2002) Evidence for a Functional Interaction between Cingulin and ZO-1 in Cultured Cells. *J Biol Chem* 277(31):27757–27764.

149. Etournay R, et al. (2007) Shroom2, a myosin-VIIa- and actin-binding protein, directly interacts with ZO-1 at tight junctions. *J Cell Sci* 120(16):2838–2850.

150. Citi S (1992) Protein kinase inhibitors prevent junction dissociation induced by low extracellular calcium in MDCK epithelial cells. *J Cell Biol* 117(1):169–78.

151. Bazellières E, et al. (2015) Control of cell-cell forces and collective cell dynamics by the intercellular adhesome. *Nat Cell Biol* 17(4):409–20.

152. Soroka V, Kasper C, Poulsen FM (2008) Structural Biology of NCAM. *Neurochem Res*:1.

153. Wai Wong C, Dye DE, Coombe DR (2012) The Role of Immunoglobulin Superfamily Cell Adhesion Molecules in Cancer Metastasis. *Int J Cell Biol* 2012. doi:10.1155/2012/340296.

154. Barclay AN (2003) Membrane proteins with immunoglobulin-like domains—a master superfamily of interaction molecules. *Semin Immunol* 15(4):215–223.

155. Nicholson BJ (2003) Gap junctions - from cell to molecule. *J Cell Sci* 116(Pt 22):4479–81.

156. Connors BW, Long MA (2004) ELECTRICAL SYNAPSES IN THE MAMMALIAN BRAIN. *Annu Rev Neurosci* 27(1):393–418.

157. Pogoda K, Kameritsch P (2019) Molecular regulation of myoendothelial gap junctions. *Curr Opin Pharmacol* 45:16–22.

158. McEver RP (2015) Selectins: initiators of leucocyte adhesion and signalling at the vascular wall. *Cardiovasc Res* 107(3):331–9.

159. Ganot P, et al. (2015) Structural Molecular Components of Septate Junctions in Cnidarians Point to the Origin of Epithelial Junctions in Eukaryotes. *Mol Biol Evol* 32(1):44–62.

160. Pastan I, Willingham M, Markovic I, Walther P, Gerdes H-H (1981) Journey to the center of the cell: role of the receptosome. *Science (80-)* 214(4520):504–509.

161. Gerdes H-H, Rustom A, Wang X (2013) Tunneling nanotubes, an emerging intercellular communication route in development. *Mech Dev* 130(6–8):381–387.

162. Vicente-Manzanares M, Horwitz AR (2011) Adhesion dynamics at a glance. *J Cell Sci* 124(23):3923–3927.

163. Gupta M, Doss B, Lim CT, Voituriez R, Ladoux B (2016) Single cell rigidity sensing: A complex relationship between focal adhesion dynamics and large-scale actin cytoskeleton remodeling. *Cell Adh Migr* 10(5):554–567.

164. Elosegui-Artola A, et al. (2014) Rigidity sensing and adaptation through regulation of integrin types. *Nat Mater* 13(6):631–7.

165. Deeg JA, et al. (2011) Impact of local versus global ligand density on cellular adhesion. *Nano Lett* 11(4):1469–76.

166. Oria R, et al. (2017) Force loading explains spatial sensing of ligands by cells. *Nature* 552(7684):219–224.

167. Bennett M, et al. (2018) Molecular clutch drives cell response to surface viscosity. *Proc Natl Acad Sci* 115(6):1192–1197.

168. Zaidel-Bar R, et al. (2003) Early molecular events in the assembly of matrix adhesions at the leading edge of migrating cells. *J Cell Sci* 116(22):4605–4613.

169. Cramer LP, Siebert M, Mitchison TJ (1997) Identification of Novel Graded Polarity Actin Filament Bundles in Locomoting Heart Fibroblasts: Implications for the Generation of Motile Force. *J Cell Biol* 136(6):1287–1305.

170. Berginski ME, Vitriol EA, Hahn KM, Gomez SM (2011) High-resolution quantification of focal adhesion spatiotemporal dynamics in living cells. *PLoS One* 6(7):e22025.

171. Choi CK, et al. (2008) Actin and alpha-actinin orchestrate the assembly and maturation of nascent adhesions in a myosin II motor-independent manner. *Nat Cell Biol* 10(9):1039–50.

172. Burnette DT, et al. (2011) A role for actin arcs in the leading-edge advance

of migrating cells. *Nat Cell Biol* 13(4):371–382.

173. Roca-Cusachs P, et al. (2013) Integrin-dependent force transmission to the extracellular matrix by α-actinin triggers adhesion maturation. *Proc Natl Acad Sci U S A* 110(15):E1361-70.

174. Webb DJ, et al. (2004) FAK–Src signalling through paxillin, ERK and MLCK regulates adhesion disassembly. *Nat Cell Biol* 6(2):154–161.

175. Vicente-Manzanares M, Ma X, Adelstein R, Horwitz A Non-muscle myosin II takes centre stage in cell adhesion and migration. *Nat Rev Mol Cell Biol* 10(11):778–790.

176. Zamir E, Geiger B (2001) Molecular complexity and dynamics of cell-matrix adhesions. *J Cell Sci* 114(Pt 20):3583–90.

177. Chrzanowska-Wodnicka M, Burridge K (1996) Rho-stimulated contractility drives the formation of stress fibers and focal adhesions. *J Cell Biol* 133(6):1403–1415.

178. Kaverina I, Krylyshkina O, Small JV (1999) Microtubule Targeting of Substrate Contacts Promotes Their Relaxation and Dissociation. *J Cell Biol* 146(5):1033–1044.

179. Franco SJ, et al. (2004) Calpain-mediated proteolysis of talin regulates adhesion dynamics. *Nat Cell Biol* 6(10):977–983.

180. Srivastava J, et al. (2008) Structural model and functional significance of pH-dependent talin-actin binding for focal adhesion remodeling. *Proc Natl Acad Sci* 105(38):14436–14441.

181. Barczyk M, Carracedo S, Gullberg D (2010) Integrins. *Cell Tissue Res* 339(1):269–280.

182. Hynes RO (2002) Integrins: bidirectional, allosteric signaling machines. *Cell* 110(6):673–87.

183. Campbell ID, Humphries MJ (2011) Integrin structure, activation, and interactions. *Cold Spring Harb Perspect Biol* 3(3). doi:10.1101/cshperspect.a004994.

184. Wegener KL, Campbell ID (2008) Transmembrane and cytoplasmic

domains in integrin activation and protein-protein interactions (Review). *Mol Membr Biol* 25(5):376–387.

185. Askari JA, Buckley PA, Mould AP, Humphries MJ (2009) Linking integrin conformation to function. *J Cell Sci* 122(2):165–170.

186. Das M, Subbayya Ithychanda S, Qin J, Plow EF (2014) Mechanisms of talin-dependent integrin signaling and crosstalk. *Biochim Biophys Acta* 1838(2):579–88.

187. Kong F, García AJ, Mould AP, Humphries MJ, Zhu C (2009) Demonstration of catch bonds between an integrin and its ligand. *J Cell Biol* 185(7):1275–1284.

188. Millon-Frémillon A, et al. (2008) Cell adaptive response to extracellular matrix density is controlled by ICAP-1–dependent β1-integrin affinity. *J Cell Biol* 180(2):427.

189. Humphries JD, Paul NR, Humphries MJ, Morgan MR (2015) Emerging properties of adhesion complexes: what are they and what do they do? *Trends Cell Biol* 25(7):388–97.

190. Goult BT, et al. (2010) Structure of a double ubiquitin-like domain in the talin head: a role in integrin activation. *EMBO J* 29(6):1069–1080.

191. Calderwood DA, Campbell ID, Critchley DR (2013) Talins and kindlins: partners in integrin-mediated adhesion. *Nat Rev Mol Cell Biol* 14(8):503–517.

192. Hemmings L, et al. (1996) Talin contains three actin-binding sites each of which is adjacent to a vinculin-binding site. *J Cell Sci* 109 (Pt 11):2715–26.

193. Klapholz B, Brown NH (2017) Talin – the master of integrin adhesions. *J Cell Sci* 130(15):2435–2446.

194. Atherton P, et al. (2015) Vinculin controls talin engagement with the actomyosin machinery. *Nat Commun* 6(1):10038.

195. Gingras AR, et al. (2008) The structure of the C-terminal actin-binding domain of talin. *EMBO J* 27(2):458–469.

196. Rodius S, et al. (2008) The talin rod IBS2 alpha-helix interacts with the beta3 integrin cytoplasmic tail membrane-proximal helix by establishing charge complementary salt bridges. *J Biol Chem* 283(35):24212–23.

197. Gingras AR, et al. (2005) Mapping and consensus sequence identification for multiple vinculin binding sites within the talin rod. *J Biol Chem* 280(44):37217–24.

198. Humphries JD, et al. (2007) Vinculin controls focal adhesion formation by direct interactions with talin and actin. 179(5). doi:10.1083/jcb.200703036.

199. del Rio A, et al. (2009) Stretching single talin rod molecules activates vinculin binding. *Science* 323(5914):638–41.

200. Comrie WA, Babich A, Burkhardt JK (2015) F-actin flow drives affinity maturation and spatial organization of LFA-1 at the immunological synapse. *J Cell Biol* 208(4):475–491.

201. Yao M, et al. (2015) Mechanical activation of vinculin binding to talin locks talin in an unfolded conformation. *Sci Rep* 4(1):4610.

202. Bouvard D, et al. (2003) Disruption of focal adhesions by integrin cytoplasmic domain-associated protein-1 alpha. *J Biol Chem* 278(8):6567–74.

203. Liu W, Draheim KM, Zhang R, Calderwood DA, Boggon TJ (2013) Mechanism for KRIT1 Release of ICAP1-Mediated Suppression of Integrin Activation. *Mol Cell* 49(4):719–729.

204. Gough RE, Goult BT (2018) The tale of two talins – two isoforms to fine-tune integrin signalling. *Febs Lett* 592(12):2108.

205. Bays JL, DeMali KA (2017) Vinculin in cell-cell and cell-matrix adhesions. *Cell Mol Life Sci* 74(16):2999–3009.

206. Carisey A, Ballestrem C (2011) Vinculin, an adapter protein in control of cell adhesion signalling. *Eur J Cell Biol* 90(2–3):157–163.

207. Borgon RA, Vonrhein C, Bricogne G, Bois PRJ, Izard T (2004) Crystal Structure of Human Vinculin. *Structure* 12(7):1189–1197.

208. Chen H, Cohen DM, Choudhury DM, Kioka N, Craig SW (2005) Spatial

distribution and functional significance of activated vinculin in living cells. *J Cell Biol* 169(3):459–470.

209. Golji J, Mofrad MRK (2010) A Molecular Dynamics Investigation of Vinculin Activation. *Biophys J* 99(4):1073–1081.

210. Golji J, Lam J, Mofrad MRK (2011) Vinculin Activation Is Necessary for Complete Talin Binding. *Biophys J* 100(2):332–340.

211. Izard T, et al. (2004) Vinculin activation by talin through helical bundle conversion. *Nature* 427(6970):171–175.

212. Moese S, et al. (2007) The Helicobacter pylori CagA protein disrupts matrix adhesion of gastric epithelial cells by dephosphorylation of vinculin. *Cell Microbiol* 9(5):1148–1161.

213. Cohen DM, Kutscher B, Chen H, Murphy DB, Craig SW (2006) A Conformational Switch in Vinculin Drives Formation and Dynamics of a Talin-Vinculin Complex at Focal Adhesions. *J Biol Chem* 281(23):16006–16015.

214. Thievessen I, et al. (2013) Vinculin–actin interaction couples actin retrograde flow to focal adhesions, but is dispensable for focal adhesion growth. *J Cell Biol* 202(1):163–177.

215. Sjöblom B, Salmazo A, Djinović-Carugo K (2008) α-Actinin structure and regulation. *Cell Mol Life Sci* 65(17):2688–2701.

216. López-Colomé AM, Lee-Rivera I, Benavides-Hidalgo R, López E (2017) Paxillin: a crossroad in pathological cell migration. *J Hematol Oncol* 10(1):50.

217. Brown MC, Perrotta JA, Turner CE (1996) Identification of LIM3 as the principal determinant of paxillin focal adhesion localization and characterization of a novel motif on paxillin directing vinculin and focal adhesion kinase binding. *J Cell Biol* 135(4):1109–1123.

218. Huang W, Sakamoto N, Miyazawa R, Sato M (2012) Role of paxillin in the early phase of orientation of the vascular endothelial cells exposed to cyclic stretching. *Biochem Biophys Res Commun* 418(4):708–713.

219. Kloeker S, et al. (2004) The Kindler Syndrome Protein Is Regulated by Transforming Growth Factor-β and Involved in Integrin-mediated Adhesion. *J Biol Chem* 279(8):6824–6833.

220. Lefort CT, et al. (2012) Distinct roles for talin-1 and kindlin-3 in LFA-1 extension and affinity regulation. *Blood* 119(18):4275–82.

221. Lai-Cheong JE, Ussar S, Arita K, Hart IR, McGrath JA (2008) Colocalization of Kindlin-1, Kindlin-2, and Migfilin at Keratinocyte Focal Adhesion and Relevance to the Pathophysiology of Kindler Syndrome. *J Invest Dermatol* 128(9):2156–2165.

222. Horowitz JC (2017) Releasing Tensin. *Am J Respir Cell Mol Biol* 56(4):417–418.

223. Bernau K, et al. (2017) Tensin 1 Is Essential for Myofibroblast Differentiation and Extracellular Matrix Formation. *Am J Respir Cell Mol Biol* 56(4):465–476.

224. Kotb A, Hyndman ME, Patel TR (2018) The role of zyxin in regulation of malignancies. *Heliyon* 4(7):e00695.

225. Chang DD, Hoang BQ, Liu J, Springer TA (2002) Molecular basis for interaction between Icap1 alpha PTB domain and beta 1 integrin. *J Biol Chem* 277(10):8140–5.

226. Bouvard D, Block MR (1998) Calcium/Calmodulin-Dependent Protein Kinase II Controls Integrin α5β1-Mediated Cell Adhesion through the Integrin Cytoplasmic Domain Associated Protein-1α. *Biochem Biophys Res Commun* 252(1):46–50.

227. Bouin A-P, et al. (2017) ICAP-1 monoubiquitylation coordinates matrix density and rigidity sensing for cell migration through ROCK2–MRCKα balance. *J Cell Sci* 130(3):626–636.

228. Paszek MJ, et al. (2005) Tensional homeostasis and the malignant phenotype. *Cancer Cell* 8(3):241–54.

229. Krishnan R, et al. (2009) Reinforcement versus fluidization in cytoskeletal mechanoresponsiveness. *PLoS One* 4(5):e5486.

230. Hytönen VP, Wehrle-Haller B (2015) Mechanosensing in cell-matrix adhesions - Converting tension into chemical signals. *Exp Cell Res* 343(1):35–41.

231. Humphrey JD, Schwartz MA, Tellides G, Milewicz DM (2015) Role of Mechanotransduction in Vascular Biology. *Circ Res* 116(8):1448–1461.

232. DuFort CC, Paszek MJ, Weaver VM (2011) Balancing forces: architectural control of mechanotransduction. *Nat Rev Mol Cell Biol* 12(5):308–319.

233. Schedin P, Keely PJ (2011) Mammary gland ECM remodeling, stiffness, and mechanosignaling in normal development and tumor progression. *Cold Spring Harb Perspect Biol* 3(1):a003228.

234. Weickenmeier J, et al. (2016) Brain stiffness increases with myelin content. *Acta Biomater* 42:265–272.

235. Zioupos P, Currey JD (1998) Changes in the stiffness, strength, and toughness of human cortical bone with age. *Bone* 22(1):57–66.

236. Thompson AJ, et al. (2019) Rapid changes in tissue mechanics regulate cell behaviour in the developing embryonic brain. *Elife* 8. doi:10.7554/eLife.39356.

237. Chu G, et al. (2019) Substrate stiffness- and topography-dependent differentiation of annulus fibrosus-derived stem cells is regulated by Yes-associated protein. *Acta Biomater*. doi:10.1016/j.actbio.2019.05.013.

238. Dupont S, et al. (2011) Role of YAP/TAZ in mechanotransduction. *Nature* 474(7350):179–183.

239. Huang J, Wu S, Barrera J, Matthews K, Pan D (2005) The Hippo Signaling Pathway Coordinately Regulates Cell Proliferation and Apoptosis by Inactivating Yorkie, the Drosophila Homolog of YAP. *Cell* 122(3):421–434.

240. Kim M-K, Jang J-W, Bae S-C (2018) DNA binding partners of YAP/TAZ. *BMB Rep* 51(3):126–133.

241. Rozengurt E, Sinnett-Smith J, Eibl G (2018) Yes-associated protein (YAP) in pancreatic cancer: at the epicenter of a targetable signaling network associated with patient survival. *Signal Transduct Target Ther* 3(1):11.

242. Lo Sardo F, Strano S, Blandino G (2018) YAP and TAZ in Lung Cancer: Oncogenic Role and Clinical Targeting. *Cancers (Basel)* 10(5). doi:10.3390/cancers10050137.

243. Elosegui-Artola A, et al. (2016) Mechanical regulation of a molecular clutch defines force transmission and transduction in response to matrix rigidity. *Nat Cell Biol*. doi:10.1038/ncb3336.

244. Chan CE, Odde DJ (2008) Traction dynamics of filopodia on compliant substrates. *Science* 322(5908):1687–91.

245. Lin CH, Forscher P (1995) Growth cone advance is inversely proportional to retrograde F-actin flow. *Neuron* 14(4):763–71.

246. Mitchison T, Kirschner M (1988) Cytoskeletal dynamics and nerve growth. *Neuron* 1(9):761–72.

247. Gardel ML, et al. (2008) Traction stress in focal adhesions correlates biphasically with actin retrograde flow speed. *J Cell Biol* 183(6):999–1005.

248. Craig EM, Stricker J, Gardel M, Mogilner A (2015) Model for adhesion clutch explains biphasic relationship between actin flow and traction at the cell leading edge. *Phys Biol* 12(3):035002.

249. Bell G, Odde DJ (1978) Models for the specific adhesion of cells to cells. *Science (80-)* 200(4342):618–627.

250. Dudko OK, Hummer G, Szabo A (2008) Theory, analysis, and interpretation of single-molecule force spectroscopy experiments. *Proc Natl Acad Sci* 105(41):15755–15760.

251. Evans E, Ritchie K (1997) Dynamic strength of molecular adhesion bonds. *Biophys J* 72(4):1541–1555.

252. Jiang L, et al. (2016) Cells Sensing Mechanical Cues: Stiffness Influences the Lifetime of Cell–Extracellular Matrix Interactions by Affecting the Loading Rate. *ACS Nano* 10(1):207–217.

253. Rief M, Gautel M, Oesterhelt F, Fernandez JM, Gaub HE (1997) Reversible unfolding of individual titin immunoglobulin domains by AFM. *Science* 276(5315):1109–12.

254. Saez A, Buguin A, Silberzan P, Ladoux B (2005) Is the mechanical activity of epithelial cells controlled by deformations or forces? *Biophys J* 89(6):L52-4.

255. Ghassemi S, et al. (2012) Cells test substrate rigidity by local contractions on submicrometer pillars. *Proc Natl Acad Sci U S A* 109(14):5328–33.

256. Yip AK, et al. (2013) Cellular Response to Substrate Rigidity Is Governed by Either Stress or Strain. *Biophys J* 104(1):19–29.

257. Plotnikov SV, Pasapera AM, Sabass B, Waterman CM (2012) Force Fluctuations within Focal Adhesions Mediate ECM-Rigidity Sensing to Guide Directed Cell Migration. *Cell* 151(7):1513–1527.

258. Kosmalska AJ, et al. (2015) Physical principles of membrane remodelling during cell mechanoadaptation. *Nat Commun* 6:7292.

259. Ahmed WW, et al. (2018) Active Mechanics Reveal Molecular-Scale Force Kinetics in Living Oocytes. *Biophys J* 114(7):1667–1679.

260. Vries A De (2004) High force magnetic tweezers for molecular manipulation.

261. Sunyer R, et al. (2016) Collective cell durotaxis emerges from long-range intercellular force transmission. *Science* 353(6304):1157–61.

262. Lerche M, et al. (2019) Integrin binding dynamics modulate ligand-specific mechanosensing in mammary gland fibroblasts. *bioRxiv*:570721.

263. Georg Simon Ohm (2006) *Die galvanische Kette, mathematisch bearbeitet* (University of Applied Sciences Library Nuremberg).

264. Kollmannsberger P, Fabry B (2007) High-force magnetic tweezers with force feedback for biological applications. *Rev Sci Instrum* 78(11):114301.

265. Casares L, et al. (2015) Hydraulic fracture during epithelial stretching. *Nat Mater* 14(3):343–351.

266. Galbraith CG, Yamada KM, Sheetz MP (2002) The relationship between force and focal complex development. *J Cell Biol* 159(4):695–705.

267. Strohmeyer N, Bharadwaj M, Costell M, Fässler R, Müller DJ (2017) Fibronectin-bound α5β1 integrins sense load and signal to reinforce

adhesion in less than a second. *Nat Mater* 16(12):1262–1270.

268. An SS, et al. (2009) Cell stiffness, contractile stress and the role of extracellular matrix. *Biochem Biophys Res Commun* 382(4):697–703.

269. Calderwood DA (2004) Integrin activation. *J Cell Sci* 117(Pt 5):657–66.

270. Roca-Cusachs P, Iskratsch T, Sheetz MP (2012) Finding the weakest link: exploring integrin-mediated mechanical molecular pathways. *J Cell Sci* 125(Pt 13):3025–38.

271. Ghatak S, Morgner J, Wickström SA (2013) ILK: a pseudokinase with a unique function in the integrin-actin linkage. *Biochem Soc Trans* 41(4):995–1001.

272. Ciobanasu C, Faivre B, Le Clainche C (2013) Integrating actin dynamics, mechanotransduction and integrin activation: the multiple functions of actin binding proteins in focal adhesions. *Eur J Cell Biol* 92(10–11):339–48.

273. Goldmann WH, Auernheimer V, Thievessen I, Fabry B (2013) Vinculin, cell mechanics and tumour cell invasion. *Cell Biol Int* 37(5):397–405.

274. Fanning AS (1998) The Tight Junction Protein ZO-1 Establishes a Link between the Transmembrane Protein Occludin and the Actin Cytoskeleton. *J Biol Chem* 273(45):29745–29753.

275. González-Mariscal L, Tapia R, Chamorro D (2008) Crosstalk of tight junction components with signaling pathways. *Biochim Biophys Acta* 1778(3):729–56.

276. Roman J, Ritzenthaler JD, Roser-Page S, Sun X, Han S (2010) alpha5beta1-integrin expression is essential for tumor progression in experimental lung cancer. *Am J Respir Cell Mol Biol* 43(6):684–91.

277. Ni S, et al. (2013) Increased ZO-1 expression predicts valuable prognosis in non-small cell lung cancer. *Int J Clin Exp Pathol* 6(12):2887–95.

278. Roca-Cusachs P, Gauthier N, Del Rio A, Sheetz M (2009) Clustering of alpha(5)beta(1) integrins determines adhesion strength whereas alpha(v)beta(3) and talin enable mechanotransduction. *Proc Natl Acad Sci U S A* 106(38):16245–50.

279. Fanning AS, Van Itallie CM, Anderson JM (2012) Zonula occludens-1 and -2 regulate apical cell structure and the zonula adherens cytoskeleton in polarized epithelia. *Mol Biol Cell* 23(4):577–90.

280. Tornavaca O, et al. (2015) ZO-1 controls endothelial adherens junctions, cell-cell tension, angiogenesis, and barrier formation. *J Cell Biol* 208(6):821–38.

281. Choi W, et al. (2016) Remodeling the zonula adherens in response to tension and the role of afadin in this response. *J Cell Biol* 213(2):243–60.

282. Mierke CT, et al. (2008) Mechano-coupling and regulation of contractility by the vinculin tail domain. *Biophys J* 94(2):661–70.

283. Bolte S, Cordelières FP (2006) A guided tour into subcellular colocalization analysis in light microscopy. *J Microsc* 224(3):213–232.

284. Kandow CE, Georges PC, Janmey PA, Beningo KA (2007) Polyacrylamide hydrogels for cell mechanics: steps toward optimization and alternative uses. *Methods Cell Biol* 83:29–46.

285. Trepat X, et al. (2009) Physical forces during collective cell migration. *Nat Phys* 5(6):426–430.

286. Serra-Picamal X, et al. (2012) Mechanical waves during tissue expansion. *Nat Phys* 8(8):628–634.

287. Waters CM, Roan E, Navajas D (2012) Mechanobiology in Lung Epithelial Cells: Measurements, Perturbations, and Responses. *Comprehensive Physiology* (John Wiley & Sons, Inc., Hoboken, NJ, USA), pp 1–29.

288. De R, Zemel A, Safran SA (2008) Do Cells Sense Stress or Strain? Measurement of Cellular Orientation Can Provide a Clue. *Biophys J* 94(5):L29–L31.

289. Wolfenson H, et al. (2016) Tropomyosin controls sarcomere-like contractions for rigidity sensing and suppressing growth on soft matrices. *Nat Cell Biol* 18(1):33–42.

290. Kaunas R, Nguyen P, Usami S, Chien S (2005) From The Cover: Cooperative effects of Rho and mechanical stretch on stress fiber

organization. *Proc Natl Acad Sci* 102(44):15895–15900.

291. Riveline D, et al. (2001) Focal Contacts as Mechanosensors. *J Cell Biol* 153(6):1175–1186.

292. Galbraith C, Yamada K, Sheetz M The relationship between force and focal complex development. *J Cell Biol* 159. doi:10.1083/jcb.200204153.

293. Trepat X, et al. (2007) Universal physical responses to stretch in the living cell. *Nature* 447(7144):592–5.

294. Semmrich C, et al. (2007) Glass transition and rheological redundancy in F-actin solutions. *Proc Natl Acad Sci U S A* 104(51):20199–203.

295. Wyss HM, et al. (2007) Strain-Rate Frequency Superposition: A Rheological Probe of Structural Relaxation in Soft Materials. *Phys Rev Lett* 98(23):238303.

296. Peng GE, Wilson SR, Weiner OD (2011) A pharmacological cocktail for arresting actin dynamics in living cells. *Mol Biol Cell* 22(21):3986–3994.

297. Almendros I, Gutierrez PT, Closa D, Navajas D, Farre R (2008) One-lung overventilation does not induce inflammation in the normally ventilated contralateral lung. *Respir Physiol Neurobiol* 162(1):100–2.

298. Li H, et al. (2018) Hypoxia promotes maintenance of the chondrogenic phenotype in rat growth plate chondrocytes through the HIF-1α/YAP signaling pathway. *Int J Mol Med* 42(6):3181–3192.

299. Zhang X, et al. (2018) Yes-associated protein (YAP) binds to HIF-1α and sustains HIF-1α protein stability to promote hepatocellular carcinoma cell glycolysis under hypoxic stress. *J Exp Clin Cancer Res* 37(1):216.

300. Greenhough A, et al. (2018) Cancer cell adaptation to hypoxia involves a HIF-GPRC5A-YAP axis. *EMBO Mol Med* 10(11):e8699.

301. Dion GR, et al. (2016) Functional assessment of the ex vivo vocal folds through biomechanical testing: A review. *Mater Sci Eng C* 64:444–453.

302. Zhang X, et al. (2008) Talin depletion reveals independence of initial cell spreading from integrin activation and traction. *Nat Cell Biol* 10(9):1062–8.

303. De Pascalis C, et al. (2018) Intermediate filaments control collective

migration by restricting traction forces and sustaining cell-cell contacts. *J Cell Biol* 217(9):3031–3044.

304. Lakins JN, Chin AR, Weaver VM (2012) Exploring the Link Between Human Embryonic Stem Cell Organization and Fate Using Tension-Calibrated Extracellular Matrix Functionalized Polyacrylamide Gels. *Methods in Molecular Biology (Clifton, N.J.)*, pp 317–350.

305. Friedrichs J, Helenius J, Muller DJ (2010) Quantifying cellular adhesion to extracellular matrix components by single-cell force spectroscopy. *Nat Protoc* 5(7):1353–1361.

306. Koziol JA, D'Agostino RB, Stephens MA (1987) Goodness-of-Fit Techniques. *J Educ Stat* 12(4):412.

307. Razali NM, Wah YB (2011) Power comparisons of Shapiro-Wilk , Kolmogorov-Smirnov , Lilliefors and Anderson-Darling tests. Available at: https://www.semanticscholar.org/paper/Power-comparisons-of-Shapiro-Wilk-%2C-%2C-Lilliefors-Razali-Wah/dcdc0a0be7d65257c4e6a9117f69e246fb227423 [Accessed May 31, 2019].

308. D'agostino RB, Belanger A, D'agostino Jr R, D'agostino RB (1990) A Suggestion for Using Powerful and Informative Tests of Normality. *Am Stat* 44(4):316–321.

¿Qué es la vida? ***Un frenesí****.*
¿Qué es la vida? Una ilusión,
una sombra, una ficción,
y el mayor bien es pequeño:
que toda la vida es sueño,
y los sueños, sueños son.

Pedro Calderón de la Barca